

UC San Diego

UC San Diego Electronic Theses and Dissertations

Title

Exploring Cellular Modifications of Guanine Using Fluorescent, Isomorphous, and Isofunctional Nucleobase Analogs

Permalink

<https://escholarship.org/uc/item/4gq7w9c3>

Author

Bucardo, Marcela Sotelo

Publication Date

2023

Peer reviewed|Thesis/dissertation

UNIVERSITY OF CALIFORNIA SAN DIEGO

Exploring Cellular Modifications of Guanine Using Fluorescent, Isomorphous and Isofunctional Nucleobase Analogs

A Dissertation submitted in partial satisfaction of the requirements
for the degree Doctor of Philosophy

in

Chemistry

by

Marcela Sotelo Bucardo

Committee in charge:

Professor Yitzhak Tor, Chair
Professor Susan Ackerman
Professor Tadeusz Molinski
Professor Dionicio Siegel

2023

Copyright

Marcela Sotelo Bucardo, 2023

All rights reserved.

The dissertation of Marcela Bucardo is approved, and it is acceptable in quality and form for publication on microfilm and electronically.

University of California San Diego

2023

DEDICATION

*To my parents, Jesus and Josefina,
and my best friends, Alexia and Paloma,
for their endless support.*

EPIGRAPH

It doesn't matter what the cause necessarily. This is your path, and you will pursue it with excellence. You face your fear because your goal demands it. That is the warrior spirit.

Alex Honnold

TABLE OF CONTENTS

DISSERTATION APPROVAL PAGE	iii
DEDICATION	iv
EPIGRAPH.....	v
TABLE OF CONTENTS.....	vi
LIST OF FIGURES	ix
LIST OF SCHEMES	xi
LIST OF TABLES.....	xii
ACKNOWLEDGEMENTS	xiii
VITA.....	xvi
PUBLICATIONS.....	xvi
ABSTRACT OF THE DISSERTATION	xvii
CHAPTER 1: Introduction	1
1.1 Introduction to the central dogma and nucleoside building blocks	1
1.2 The beginnings of fluorescent nucleoside analogs	4
1.2 Chemical and electronic criterion	5
1.3 Desirable photophysical properties.....	6
1.4 Development of fluorescent nucleoside alphabets by the Tor lab	8
1.5 References.....	15
CHAPTER 2: Real-Time Monitoring of Human Guanine Deaminase Activity by an Emissive Guanine Analog	19
2.1 Abstract.....	19
2.2 Introduction.....	20
2.3 Results and Discussion	23
2.4 Conclusion	31
2.5 Methods.....	32
2.5.1 Expression and Purification of GDA	32
2.5.2 Synthetic Procedures.....	33
2.5.3 Photophysical Properties: General Methods.....	33
2.5.4 Quantum Yield Measurements	34
2.5.5 Sensitivity to pH	34
2.5.6 Sensitivity to Polarity.....	34

2.5.7 Enzymatic Deamination: General Methods	35
2.5.8 Real-Time Monitoring of GDA via Absorption and Emission.....	35
2.5.9 Steady State Absorption Measurements in the Presence of GDA	36
2.5.10 HPLC analysis of Enzymatic Conversion of Native G to X and $^{13}\text{C}_N\text{G}$ to $^{13}\text{C}_N\text{X}$	36
2.5.11 Inhibition Studies	38
2.5.12 Docking of Guanine, Xanthine, and Analogs in GDA	38
2.6 Acknowledgements.....	39
2.7 Supporting Information.....	40
2.7.1 Synthetic procedures	40
2.7.2 X-Ray Crystal structures.....	42
2.7.3 Absorption and emission spectroscopy.....	47
2.7.4 Real-time monitoring of GDA reactions.....	50
2.7.5 MOE docking results	52
2.7.6 Real-time monitoring of GDA and tzG with inhibitors.....	54
2.7.8 Supplementary references	55
2.8 References.....	56
CHAPTER 3: Fluorescent Probes for O^6 -Alkylguanine-DNA-Transferase Activity and Microscopy in Living Cells	60
3.1 Abstract.....	60
3.2 Introduction.....	60
3.3 Results and Discussion	63
3.4 Conclusion	73
3.5 Methods.....	74
3.5.1 Synthetic Procedures.....	74
3.5.2 Photophysical Properties: General Methods	78
3.5.3 Quantum Yield Measurements	78
3.5.4 Protein Reaction: Real-Time monitoring of hAGT and SNAP-Tag reactions via Emission.....	79
3.5.5 Mammalian cell culture	80
3.5.6 Live Cell Imaging	80
3.5.7 Working concentrations determination.....	80
3.5.8 Confocal microscopy	81
3.5.9 Fluorescence Real-time monitoring of O^6 -Bn- $^{13}\text{C}_N\text{G}$ and O^6 -Bn- $^{13}\text{C}_N\text{X}$ in live cells	81

3.6 Acknowledgements.....	82
3.7 Supplemental Information	83
3.8 References.....	85
CHAPTER 4: Reflections and Future Directions	89
4.1 Reflections and Dissertation Summary.....	89
4.2 Future synthetic directions and activity investigation of hAGT	90
4.2.1 Project shortcomings and further possible experimentation	90
4.2.2 Synthesis of O6-alkyl $\mathbf{d}^{\text{th}}\mathbf{G}_N$ and $\mathbf{d}^{\text{tz}}\mathbf{G}_N$ nucleosides	91
4.2.3 Preliminary data of O6-alkyl $\mathbf{d}^{\text{th}}\mathbf{G}_N$ with SNAP-Tag protein reactions	92
4.3 Future of nucleobase-based probes	92
4.4 References.....	94

LIST OF FIGURES

Figure 1.1 Canonical Nucleosides.....	2
Figure 1.2 Classes of Emissive Nucleoside Analogs.....	4
Figure 1.3 Watson-Crick Base Pairing in RNA	6
Figure 1.4 Hoosteen Base Pairing in RNA	6
Figure 1.5 Xanthine and Uridine Analogs Based on thieno[3,2-d]pyrimidine.....	9
Figure 1.6 th U Based on thieno[3,4-d]pyrimidine core	9
Figure 1.7 RNA Alphabet Based on thieno[3,4-d]pyrimidine core (th N).	10
Figure 1.8 RNA Alphabet Based on isothiazole[4,3-d]pyrimidine (^{tz} N)	11
Figure 1.9 Guanine and Relevant Isomorphous Guanine Analogs.....	11
Figure 1.10 RNA Alphabet Based on methylthieno[3,4-d]pyrimidine (^{mth} N).	11
Figure 1.11 Guanine Nucleobase and Relevant Emissive Isomorphous Analogs.....	12
Figure 2.0 Abstract Figure: Heterocyclic Core Evolution and Guanine Deaminase Reaction.....	19
Figure 2.1 Heterocyclic Core Evolution, ADA Reaction, and GDA Reaction.....	22
Figure 2.2 Nucleobase Structures and Photophysical.....	24
Figure 2.3 X-ray Crystal Structures of Nucleobases and MOE Docking.....	25
Figure 2.4 Enzymatic Guanine Deaminase Reactions.....	27
Figure 2.5 Guanine Deaminase Inhibitor Study.....	31
Figure 2.S1 Nucleobase absorption and emission traces in water:dioxane mixtures.....	48
Figure 2.S2 Nucleobase absorption and emission traces in buffer solution at varying pH.....	49
Figure 2.S3 GDA-mediated deamination analysis by HPLC.....	50
Figure 2.S4 Steady state absorption of guanine and analogs by GDA.....	51
Figure 2.S5 MOE docking of xanthine and analogs in GDA active site.....	52

Figure 2.S6 MOE docking of guanine and analogs in GDA active site.....	53
Figure 2.S7 Kinetics of AICA, ATCA, and ICA as GDA inhibitors.....	54
Figure 3.1 Structures of guanine, th G _N , and ^{tz} G _N . GDA and hAGT reactions.....	63
Figure 3.2 th G _N , ^{tz} G _N , and alkylated derivative structures and spectra.....	67
Figure 3.3 Tracking hAGT and SNAP-Tag reactions via emission change.....	69
Figure 3.4 Live Cell Imaging of O⁶-BnthG_N , O⁶-MethG_N , O⁶-Bn^{tz}G_N , and O⁶-Me^{tz}G_N	72
Figure 3.5 Real-time fluorescence monitoring of O⁶-Bn^{tz}G_N and O⁶-BnthG_N in live cells.....	73
Figure 3.S1 HPLC traces of stock solutions for compounds.....	83
Figure 3.S2 Fluorescence change control for microscopy experiments.....	84
Figure 4.1 Preliminary data for fluorescence intensity change tracked for O⁶-BndthG and O⁶-MedthG reaction with SNAP-Tag protein.....	92
Figure 4.2 Theoretical further evolution of emissive nucleobase analogs.....	93

LIST OF SCHEMES

Scheme 2.S1 Synthesis of thienopyrimidine-based analogs, ${}^{\text{th}}\text{G}_N$ and ${}^{\text{th}}\text{X}_N$	40
Scheme 2.S2 Synthesis of isothiazolepyrimidine precursor methyl 4-aminothiazole 3-carboxylate hydrochloride (1).....	40
Scheme 2.S3 Synthesis of isothiazolo-pyrimidine-based analogs, ${}^{\text{tz}}\text{G}_N$ and ${}^{\text{tz}}\text{X}_N$, from precursor 4.....	41
Scheme 2.S4 Synthesis of 4-aminoisothiazole-3-carboxamide 2, (ATCA).....	41
Scheme 3.1 Synthesis of O ⁶ -benzyl thieno- and isothiazolo-guanine analogs.....	64
Scheme 3.2 Synthesis of O ⁶ -alkylguanine analogs $\text{O}^6\text{-Bn}{}^{\text{th}}\text{G}_N$ and $\text{O}^6\text{-Me}{}^{\text{th}}\text{G}_N$	74
Scheme 3.3 Synthesis ${}^{\text{tz}}\text{G}_N$ and O ⁶ -alkylguanine analogs $\text{O}^6\text{-Bn}{}^{\text{tz}}\text{G}_N$ and $\text{O}^6\text{-Me}{}^{\text{tz}}\text{G}_N$	75
Scheme 4.1 Synthesis of $\text{O}^6\text{-Bnd}{}^{\text{th}}\text{G}$ and $\text{O}^6\text{-Med}{}^{\text{th}}\text{G}$	91
Scheme 4.2 Synthesis of $\text{O}^6\text{-Med}{}^{\text{tz}}\text{G}$	91

LIST OF TABLES

Table 1.1 Photophysical data for Previously Published Emissive RNA Alphabets.....	13
Table 2.1 Photophysical data for nucleobase analogs.....	26
Table 2.2 GDA reaction rates.....	28
Table 2.S1 Crystal data and structure refinement for th G _N	43
Table 2.S2 Crystal data and structure refinement for th X _N	44
Table 2.S3 Crystal data and structure refinement for ^{tz} G _N	45
Table 2.S4 Crystal data and structure refinement for ^{tz} X _N	46
Table 2.S5 Complete photophysical properties of nucleobases.....	47
Table 2.S6 E _T (30) experimental values for water:dioxane mixtures.....	47
Table 3.1 Photophysical data of nucleobase analogs in water.....	65
Table 3.2 AGT and SNAP-Tag reaction rates.....	68

ACKNOWLEDGEMENTS

First and foremost, I would like to thank my research advisor, Professor Yitzhak Tor. Yitzhak's lab was a place where I was able to grow in confidence as a scientist and individual. Yitzhak imparted me with the aptitude to approach life with curiosity and pursue a scholarly attitude. I will carry what I learned in his lab for the rest of my life and career.

I would also like to thank my committee members, Professor Susan Ackerman, Professor Partho Ghosh, Professor Tadeusz Molinski, and Professor Dionicio Siegel for their time and valuable insight.

I would like to thank all past and present members of the Tor lab, especially: Dr. Paul T. Ludford, Dr. Kaivin Hadidi, Dr. Kfir Steinbuch, Dr. Phil Bartels, Dr. Yao Li, Dr. Yusuke Kawamoto, Jamie Lam, Deyuan Cong, Shenghua Yang, Darlene Woodward, Benjamin Huang, and Ruby Wu.

I would like to acknowledge my undergraduate professors and mentors who guided *en voyage* to graduate school, especially Dr. David Lingner, who got me hooked on chemistry and persuaded me to change my major to Chemistry; Dr. Matthieu Rouffet, who instilled in me an enthusiasm for organic chemistry and has been a constant support system and mentor through every step of my academic journey; and Dr. Dale Shellhamer, my first research advisor; Dr. Katherine Maloney; Dr. Ken Martin; Dr. Ariane Jansma; Dr. Marc Perry; and Dr. Sarah Choung. If it was not for their inspiration, careful instruction, encouragement, and humor I would not have pursued graduate school.

I would like to thank Dr. Bruce Ito, who truly embodies compassion and devotion to his craft.

I would like to acknowledge the professors at the University of California, Irvine who cultivated my interest in chemical biology and encouraged me to continue my studies, Dr. Robert Spitale, Dr. John Chaput, and Dr. Andrej Luptak. I would especially like to thank my peer and mentor Dr. Samantha Beasley, who, through example taught me what resilience and growth looked like in graduate school.

Most importantly, I would like to express my deepest thanks to my parents, Jesus and Josefina. They always have supported every academic aspiration and random hobby I pursue. Thank you for your endless support and grace at every step of the way, whether it be in going through the everyday motions of life or life defining events. Words cannot begin to express my gratitude and love.

I would be remiss in not acknowledging my best friends. I would like to thank, Alexia Guzman, Paloma Polanco, and Corynne Swafford, for their continuous support at every stage of life we've shared. Thanks to Abbey Liu, Belinda Nguyen, and Jasmine Mikesell for always being down to climb and for inspiring me to be better and stronger than before. Also, thanks to Dr. Sergio Sandoval for showing me what it looks like to shoot for the Moon (and Mars).

Chapter 2, in full, is a reprint of the material from: Marcela S. Bucardo, You Wu, Paul T. Ludford, Yao Li, Andrea Fin, and Yitzhak Tor. "Real-Time Monitoring of Human Guanine Deaminase Activity by an Emissive Guanine Analog." *ACS Chem Biol.* **2021**; 16 (7): 1208-1214. doi: 10.1021/acscchembio.1c00232. Permission to use the materials from this manuscript was obtained by the American Chemical Society. The dissertation author was the primary researcher and author of this paper.

Chapter 3, in part, is adapted from work currently being prepared for submission of the material: "Fluorescent Probes for O⁶-Alkylguanine-DNA-Transferase Activity and Microscopy in

Living Cells” *in preparation*. Permission to use materials from the manuscript was also obtained from co-authors, Kfir Steinbuch and Yitzhak Tor. The dissertation author was the primary researcher and author of this paper.

VITA

- 2016 Bachelor of Science in Chemistry, Point Loma Nazarene University
- 2018 Master of Science in Pharmaceutical Sciences, University of California Irvine
- 2023 Doctor of Philosophy in Chemistry, University of California San Diego

PUBLICATIONS

Ludford, P. T.; Yang, S.; Bucardo, M. S.; Tor, Y. A New Variant of Emissive RNA Alphabets. *Chem. Eur. J.* **2022**, *18*, e202104472.

Bucardo, M. S.; Wu, Y.; Ludford, P. T.; Fin, A.; Tor, Y. Real-time Monitoring of Human Guanine Deaminase Activity by an Emissive Guanine Analog. *ACS Chem. Biol.* **2021**, *16*, 1208–1214.

Garcia, R. A.; Ito, B. R.; Lupisella, J.; Carson, N.; Hsu, M.; Fernando, G.; Heroux, M.; Bouvier, M.; Dierks, E.; Kick, E.; Gordon, D.; Chen, J.; Mintier, G.; Carrier, M.; St-Onge, S.; Shah, H.; Towne, J.; Bucardo, M. S.; Ma, X.; Ryan, C. S.; Wurtz, N. R.; Ostrowski, J.; Villarreal, F. J. Preservations of Post-Infarction Cardiac Structure and Function via Long-Term Oral Formyl Peptide Receptor Agonist Treatment. *JACC Basic Transl Sci.* **2019**, *4* (8), 905-20.

Shellhamer, D. F.; Beavis, Z. J.; Brady, D. L.; Bucardo, M. S.; Elwin, S. L.; Fiorella, N.; Gomez, L.; Van Horne, S.; Perry, M. C. NMR line-broadening and transverse relaxation time measurements support a di-radical intermediate for the reaction of chlorosulfonyl isocyanate with electron-rich alkenes. *Results in Chemistry.* **2019**.

Shellhamer, D.; Alexander, K.; Beavis, Z.; Bucardo, M.; Elwin, S.; Gomez, L.; Licata, C.; Home, S.; Perry, M. Comparing Neat vs. Solution Reactions of Chlorosulfonyl Isocyanate with Alkenes. *Trends in Organic Chemistry.* **2016**.

ABSTRACT OF THE DISSERTATION

Exploring Cellular Modifications of Guanine Using Fluorescent, Isomorphous, and Isofunctional Nucleobase Analogs

by

Marcela Sotelo Bucardo

Doctor of Philosophy in Chemistry

University of California San Diego, 2023

Professor Yitzhak Tor, Chair

Nucleosides are the essential building blocks of DNA and RNA. Given that the chromophoric region of the canonical nucleosides is nonemissive, their biophysical examination is difficult. To circumvent this, illumination of these molecules has been accomplished using fluorescent nucleoside analogs. One challenge in the design of emissive nucleoside analogs is maintaining isomorphism while retaining isofunctionality. The Tor lab has designed and

implemented the use of a series of RNA alphabets that resemble the native nucleosides but have enhanced photophysical features. These alphabets are based on thieno[3,4-*d*]pyrimidine (thN), isothiazole[4,3-*d*]pyrimidine (^{tz}N), and methylthieno[3,4-*d*]pyrimidine (^{mth}N) cores. One area that remained unexplored using the nucleoside analog alphabets developed by the Tor lab was the isofunctionality of the nucleobase cores to study proteins acting on purines. These structures naturally do not contain the large contact forming sugar moiety which aid with biochemical recognition. Herein, the use of guanine based emissive analogs based on the thN and ^{tz}N cores are used for the evaluation of cellular modifications.

Guanine deaminase converts guanine to xanthine. The study of human guanine deaminase remains limited compared to other metabolic deaminases and as a result its substrate and inhibitor repertoire are limited. Additionally, recent observations have shown it is implicated in neuronal morphology, traumatic brain injury, memory dysfunction, and psychiatric diseases. In this work, we explore two emissive heterocyclic cores, based on thN and ^{tz}N, as surrogate guanine deaminase substrates. We demonstrate that the isothiazolo guanine surrogate, ^{tz}G_N, does undergo effective enzymatic deamination by guanine deaminase to the isothiazolo xanthine analog, ^{tz}X_N, while the thiophene guanine analog, thG_N, does not. Further, we showcase the potential of this fluorescent nucleobase surrogate to provide a visible spectral window for a real-time study of guanine deaminase and its inhibition.

*O*⁶-Alkylguanine-DNA-transferase is a repair protein that provides protection from mutagenic events caused by *O*⁶-alkylguanine lesions. The activity of human *O*⁶-alkylguanine-DNA-transferase is tissue specific, indicative of tumor status, and correlated to chemotherapeutic success. For this reason, tracking its activity could prove informative for disease diagnosis and therapy. We explore two families of emissive *O*⁶-methyl- and *O*⁶-benzylguanine analogs based on

${}^{\text{th}}\text{G}_N$ and ${}^{\text{tz}}\text{G}_N$ as potential surrogates. We establish that the O^6 -benzylated ${}^{\text{th}}\text{G}_N$ and ${}^{\text{tz}}\text{G}_N$ derivatives provide a spectral window to optically monitor human O^6 -alkylguanine-DNA-transferase activity, can be used as substrates for the widely used SNAP-Tag delivery system, and are sufficiently bright for visualization in mammalian cells using fluorescence microscopy.

CHAPTER 1: Introduction

As this chapter was being written, the 2023 Nobel Prize in Physiology or Medicine was awarded to Katalin Karikó and Drew Weissman. During the worst pandemic in over a century, their discovery provided the basis for a vaccine response to the COVID-19 virus. The vaccine was administered to billions of individuals worldwide to protect them from one of the most contagious viruses in modern history.¹

Karikó and Weissman discovered that replacement of uridine with pseudouridine, an analog of the nucleoside, in mRNA removes the strong inflammation response while still delivering the chemical script for a specific and protective immune response.² Pseudouridine is one example of hundreds of nucleoside analogs characterized by scientists. Whether nucleoside analogs are naturally occurring or designed synthetically, they have served as tools to propel the field of chemical biology beyond the molecular biology of the central dogma originally proposed by Crick in the 1950s.

1.1 Introduction to the central dogma and nucleoside building blocks

After the discovery of the DNA double helix, the original central dogma of molecular biology was proposed by Francis Crick. This dogma postulated a unidirectional information flow from DNA, to RNA, to proteins. It suggested no feedback facilitated from proteins or RNA, which we now understand to be incorrect.³⁻⁴ In addition to the comprehensive study of DNA, the human genome project provided the scientific community with the significant discovery that only 2% of the genome encodes for protein encoding genes. The other 98% of the genome encodes for

noncoding RNA.⁵⁻⁶ The cellular function of RNA goes far beyond an intermediary role between DNA and proteins.⁷

Nucleosides are the essential building blocks of both DNA and RNA (Figure 1.1). In DNA, the four deoxyribonucleosides are adenosine (dA), guanosine (dG), cytosine (dC), and thymidine (dT), while in RNA the four ribonucleosides are adenosine (A), guanosine (G), cytosine (C), and uridine (U). These canonical building blocks are composed of N-glycosides of sugars, 2-deoxy-D-Ribose or D-ribose, linked to heterocyclic nitrogenous bases at the anomeric carbon. The nitrogenous base heterocycles are either purine, two-ring, or pyrimidine, single ring, units. dA, dG, A and G are the purine containing nucleosides and dC, dT, C, and U are the pyrimidine containing nucleosides. Two key differences between DNA and RNA are (1) the 2' hydroxyl moiety of the sugar and (2) the substitution of U for dT that contribute to each of their unique reactivities (and susceptibilities to hydrolysis or oxidation).^{3-4,7-9} Moreover, nucleosides not only constitute DNA and RNA as their essential building blocks but are also the core structures of many of cellular cofactors, modified nucleosides, and secondary messengers.¹⁰

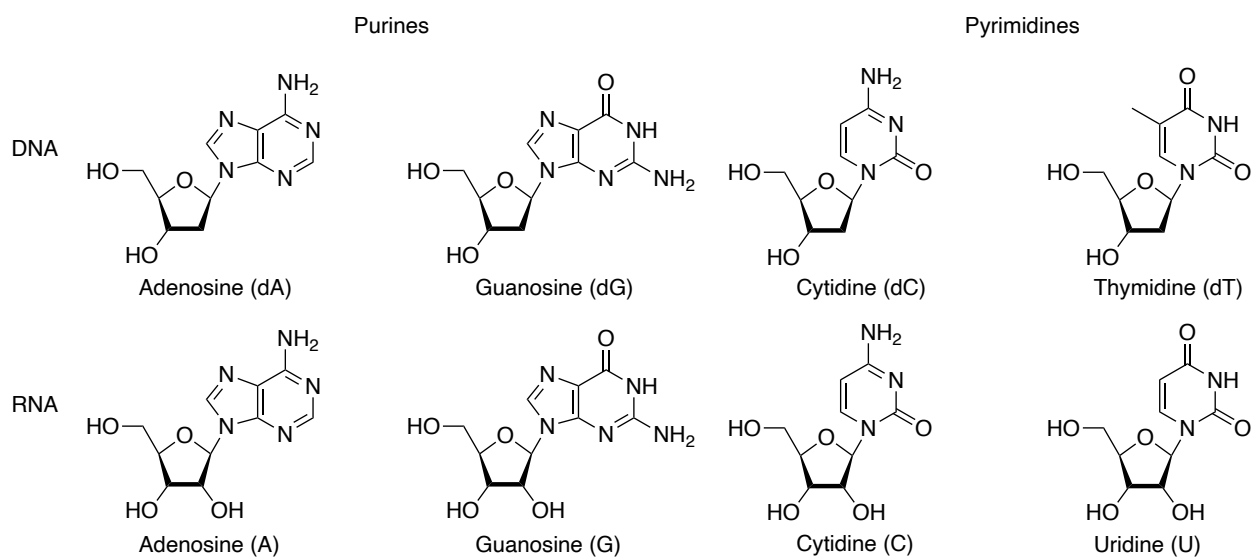


Figure 1.1 Canonical Nucleosides

As nucleosides are essential to a plethora of cellular processes, many techniques have been developed to observe them and detect modifications to their structures. The techniques used include, but are not limited to, nuclear magnetic resonance (NMR), X-ray crystallography, ultraviolet-visible (UV-Vis) spectroscopy, fluorescence, and radiolabeling. However, when it comes to real-time monitoring of processes where the time window associated with structural modifications is very narrow, for example enzymatic transformations, most of these techniques fall short. UV-Vis and fluorescence spectroscopy provide the means to observe nucleosides in real-time during narrow time windows. However, the canonical nucleosides do not have desirable photophysical properties in water.¹¹⁻¹²

The chromophoric unit of the canonical nucleosides are the purine or pyrimidine nitrogenous bases. These heterocycles absorb near the 260 nm region, which is especially crowded by other cellular components, especially peptides. While absorbance measurements may be useful for tracking modifications of nucleosides in an in vitro context where other biological macromolecules do not interfere, enzymatic analysis of proteins in a cellular context or with purified proteins containing high tryptophan content would not be feasible. In the context of fluorescence, the canonical nucleosides are essentially dark. Although this is advantageous from an evolutionary perspective, by facilitating the stability of genetic information when excitation of these species does occur, the biophysical examination of native nucleoside activity proves difficult.

To circumvent this, chemical biologists have designed, synthesized, and applied modified nucleoside analogs with improved spectroscopic properties to those of the canonical nucleosides. Understanding and illuminating the intricacies of RNA remains a fundamental objective in chemical biology. Therefore, a demand remains for developing tools that showcase RNA activity.

1.2 The beginnings of fluorescent nucleoside analogs

It is difficult to have a conversation regarding the evolution of fluorescent nucleoside analogs that does not begin with the pioneering discoveries of 2-aminopurine (2-AP) by Stryer in 1969 and ethenoadenosine (ϵ -A) by Leonard in 1972.¹³⁻¹⁴ Both 2-AP and ϵ -A are landmark emissive nucleoside analogs in the field that have served as powerful tools in nucleic acid discoveries and have been applied extensively. Later, in the 1990s, the classes of these probes quickly evolved with the discoveries of McLaughlin's m5K cytidine analog, Hawkin's pteridine nucleosides, Kool's pyrene nucleoside (the first emissive c-glycoside), Moreau's expanded nucleosides, and Hocek's extended nucleosides.¹⁵⁻¹⁹ Then, in 2007, Tor introduced thiophene-pyrimidine fused analogs. Since then, the families of small molecule nucleoside alphabets, best described as isomorphic, have continued to expand (Figure 1.2).²⁰

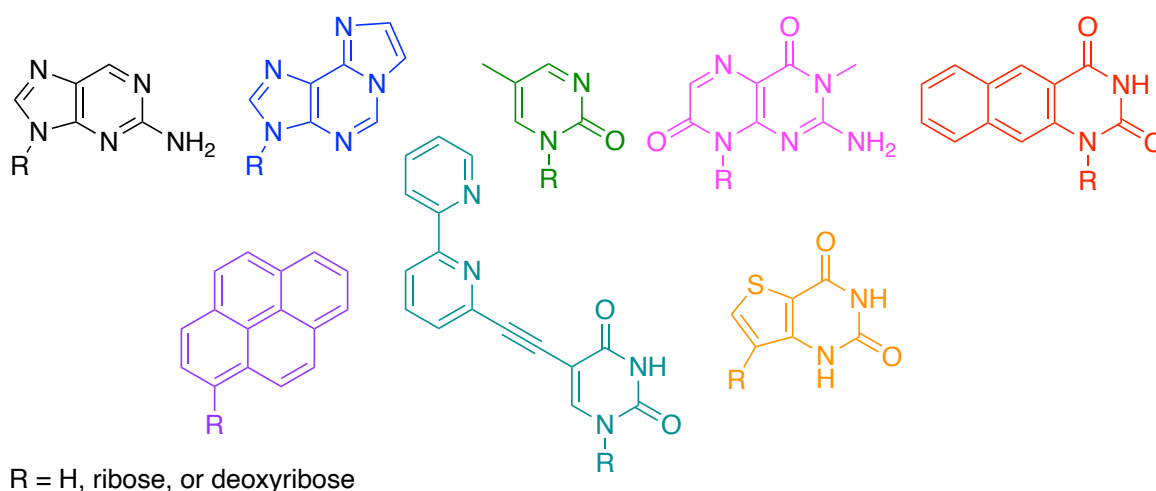


Figure 1.2 Classes of Emissive Nucleoside Analogs

Nucleoside structures of 2-aminopurine (black), ethenoadenosine (blue), m5K cytidine analog (green), 3-MI pteridine analog (magenta), pyrene C-glycosidic nucleoside (purple), ring fused BgQ (red), nucleoside analog with extended conjugation (teal), isomorphic thienopyrimidine xanthine analog (orange).

1.2 Chemical and electronic criterion

While many scaffolds of fluorescent nucleoside analogs have been designed and characterized, two qualities that make a surrogate especially useful are having (1) morphology and (2) functionality analogous to the native counterpart they represent. The Tor lab has coined two terms to describe these properties in the context of nucleosides. When the structure and dimensions of the analogs preserves likeness to the native counterpart, it is defined as “isomorphic.” If a nucleoside surrogate retains the chemical and biological activity executed by its native counterpart, it is described as “isofunctional.”²¹

Maintaining isomorphic and isofunctional character will diminish steric hindrance and provide the means for electrical interactions like those of native nucleosides. It is key that nucleoside analogs retain hydrogen bonding and pi stacking capabilities. These features are particularly relevant for oligonucleotide 3-dimensional structure and protein active site recognition.

Nucleosides have hydrogen bonding capabilities that promote base pairing between purine and pyrimidines. Two common modes of base pairing are Watson-Crick base pairing and Hoogsteen base pairing. Watson-Crick base pairing is referred to as “complementary” base pairing as it results in a particular complementary pattern of hydrogen bonding (Figure 1.3). Specifically in RNA, A hydrogen-bonds to U through two hydrogen bonds and G hydrogen bonds to C through three hydrogen bonds. In DNA, A hydrogen bonds to T and G hydrogen bonds to C, through the same hydrogen bonding patterns. In DNA, the double helix formed from these interactions is greatly important for the stability of the cellular genetic code and for proper DNA replication.³⁻⁴ Hoogsteen base pairing is a less common base pairing system, that includes a different face of the nucleoside with additional hydrogen bonding points of contact.²² This type of base pairing

contributes to RNA secondary and tertiary structure and gives rise to more complex functional structures. Therefore, retaining the hydrogen bonding character is important when designing a nucleoside analog.

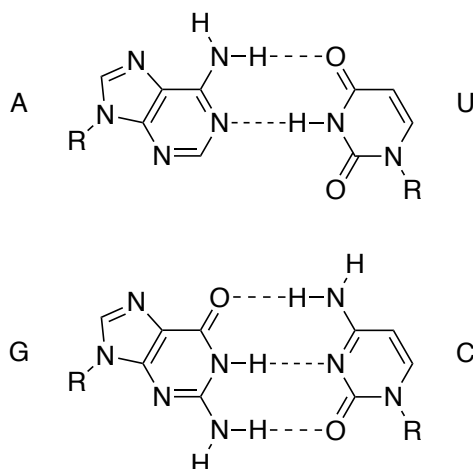


Figure 1.3 Watson-Crick Base Pairing in RNA

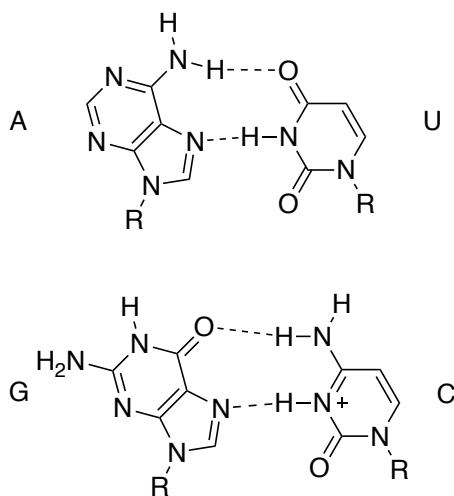


Figure 1.4 Hoosteen Base Pairing in RNA

1.3 Desirable photophysical properties

When designing a small molecule fluorophore, the inability to accurately predict spectroscopic qualities proves difficult, especially when pursuing favorable improvements

compared to past nucleoside surrogates. However, to quantitatively describe what favorable spectroscopic qualities are, their values must be described.

Absorbance (A), or the optical density, of a sample in solution can be measured experimentally using the Beer-Lambert Law:

$$\ln \frac{I_0}{I} = A = \epsilon b c \quad (1.1)$$

where I_0 is incident light, I is the detected light that has passed through the sample, ϵ is the extinction coefficient, b is the pathlength of the cuvette used, and c is the solution concentration. This equation forms a linear relationship between A and sample concentration if the path length remains constant, so solving for the extinction coefficient can experimentally be done. The extinction coefficient is thus a measure of the ability of a chromophore to absorb a photon.

After a photon of light is absorbed, it resides in the excited state. The deactivation of this process will occur through the most rapid path. If the photon relaxes to the ground state through non radiative process (vibrational relaxation or internal conversion) the compound can be described as dark. However, if the photon relaxes radiatively, a fluorescent signal will be observed. The quantum yield (ϕ) of a chromophore is a ratio of the photons emitted and the photons absorbed, or the radiative processes over the total processes of the excited state. Experimentally, a relative quantum yield can be calculated through mathematical comparison to a fluorophore standard with an established quantum yield by using:

$$\phi = \phi_{STD} \frac{I}{I_{STD}} \frac{OD_{STD}}{OD} \frac{n^2}{n_{STD}^2} \quad (1.2)$$

where ϕ_{STD} is the fluorescence quantum yield of the standard, I and I_{STD} are the integrated area of the emission band of the sample and the standard respectively, OD and OD_{STD} are the optical density at the excitation wavelength for the sample and standard respectively, and n and n_{STD} are the solvent refractive index of the sample and the standard solutions.²³

The product of the molar absorptivity (the probability of a species to absorb a photon of light) and the quantum efficiency (the probability of a species to emit a photon of light based on the) is defined as the brightness of a fluorophore. The brightness is relevant in a biological context, especially when imaging studies in cells or in vivo are relevant.

Photophysical properties relevant to this work are absorption and emission wavelength maxima, molar absorptivity, emission quantum yield, and brightness. Favorable photophysical properties can therefore be described as follows. Absorption maxima for a nucleoside fluorophore should have absorption maxima and emission maxima with bathochromic shifts away from the 260 to 280 nm region where other biological macromolecules absorb.¹¹ Although quantum yields as low as 1% can provide a means for analysis, the closer to 100% a fluorophore is probability of bearing sufficient brightness for detection and experiment sensitivity the more desirable it will be. Additionally, it is important to note that although the building blocks of DNA and RNA macromolecular structures do not have inherent emissive properties, the building blocks of proteins, amino acids, do have species that provide a fluorescent signal. Tryptophan, an amino acid, absorbs at around 270 nm and when excited at that wavelength emits near 350 nm with a 12% quantum yield. Deconvolution of fluorescence signals would prove difficult during enzymatic analysis of proteins containing high tryptophan content if the emissive nucleoside analog did not have emission red-shifted past 350 nm and a quantum yield sufficiently above 12%.²⁴

1.4 Development of fluorescent nucleoside alphabets by the Tor lab

For over 15 years, the Tor lab has pursued the design of isomorphous and isofunctional pyrimidine-based fluorescent nucleosides. The design of analogs based on a thieno[3,2-*d*]pyrimidine core by Tor et al. in 2007, provided the first photophysical data for compounds of

their kind. From a synthetic standpoint, they come from a convergent approach, in that either c-glycosylation or n-glycosylation of the nucleobase or a precursor, can yield either xanthine or uridine (Figure 1.4).²⁰ While these compounds show promise of improved spectroscopic signatures compared to the canonical nucleosides, with wavelength absorption and emission maxima at 300 nm and 350 nm respectively, these analogs had very low quantum yields of 4% and 6%, for xanthine and uridine respectively.

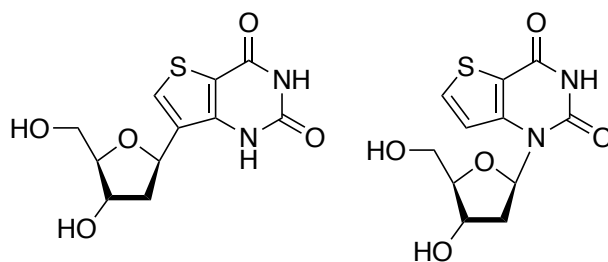


Figure 1.5 Xanthine and Uridine Analogs Based on thieno[3,2-d]pyrimidine

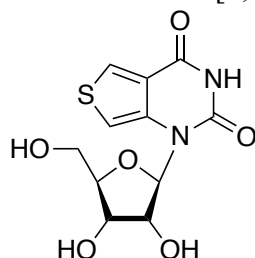


Figure 1.6 thU Based on thieno[3,4-d]pyrimidine core

A slight design change by Srivatsan et al. in 2008 changed the electronics of the molecules sufficiently to provide very desirable fluorescent properties. By altering the fusion points of the rings to a thieno[3,4-*d*]pyrimidine core, the new uridine analog (Figure 1.5), thU, showed absorption maximum at 304 nm, emission maximum with a substantial bathochromic-shift to 412 nm, and the quantum yield increased 10 fold to 48%.²⁵ This inspired the development of the first complete emissive RNA nucleoside alphabet, with the same thieno[3,4-*d*]pyrimidine core (thN) by Shin et al in 2011 (Figure 1.6). In water, these probes display absorption maxima from 304 to 341 nm, emission maxima from 409 to 453 nm, and quantum efficiencies ranging from 21% to 46%.²⁶

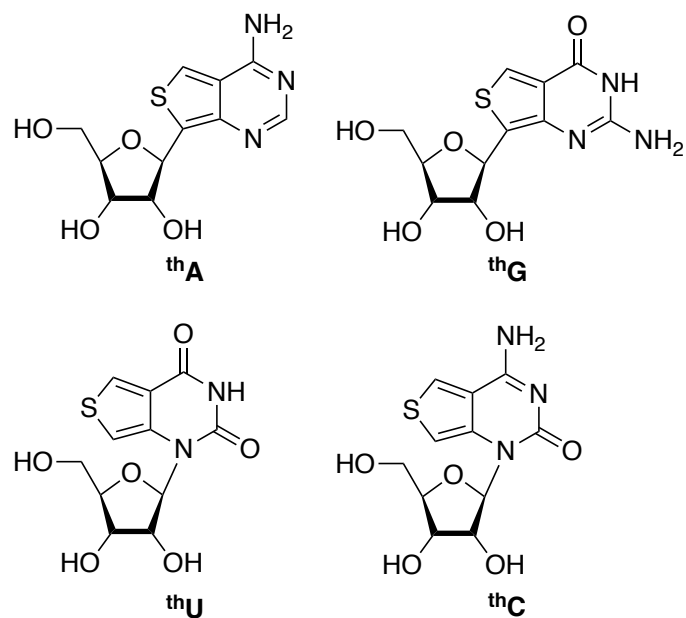


Figure 1.7 RNA Alphabet Based on thieno[3,4-*d*]pyrimidine core (thN)

In 2015, Rovira et al further evolved these probes to the second generation RNA alphabet with a isothiazole[4,3-*d*]pyrimidine core (^{tz}N) (Figure 1.7). These isothiazolepyrimidine nucleosides reinstate the nitrogen at the position equivalent to the N7 basic site in purines. This significantly improves their isofunctional architecture as the N7 restores the Hoogsteen face and the hydrogen bonding capabilities of that position. In water, these probes display absorption maxima from 312 to 338 nm, emission maxima from 377 to 459 nm, and quantum yields from 1% to 25%. While this structural enhancement provided a means for more accurate biophysical probing of RNA and nucleoside processes, the quantum efficiencies were reduced.²⁷⁻²⁸ Through the evolution of these alphabets and the modifications of these probes at the atom level, we have been able to make conclusions about biology unapproachable by other means of real-time and highly sensitive tools. Figure 1.9 shows the reinstating of the nitrogen at the N7 position of the guanosine analog when compared to numbering of the native nucleosides.

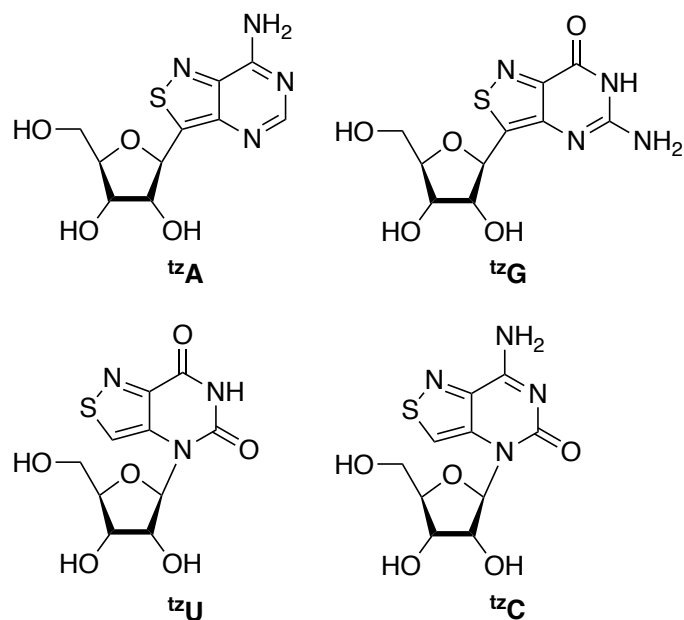


Figure 1.8 RNA Alphabet Based on isothiazole[4,3-d]pyrimidine (tzN)

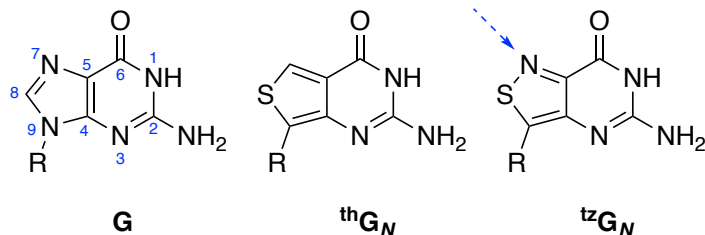


Figure 1.9 Guanine and Relevant Isomorphous Guanine Analogs

Guanine with conventional purine numbering that will be used throughout this work (G), thiophene guanine analog (thG_N), and isothiazole guanine analog (^{tz}G_N) with nitrogen at 7 position reinstated.

The repertoire of alphabet toolkits was again expanded with the development of the methylthieno[3,4-*d*]pyrimidine (^{mth}N) alphabet by Ludford et al in 2022 (Figure 1.9). This alphabet was pursued with the understanding that while isofunctional and isomorphous considerations may suffer, more robust photophysical properties may be displayed from the addition of a nonpolar moiety by changing the electronics of the nucleobase core. In water, these

probes display absorption maxima from 306 to 353 nm, emission maxima from 414 to 467, and quantum yields from 21% to 56%.²⁹

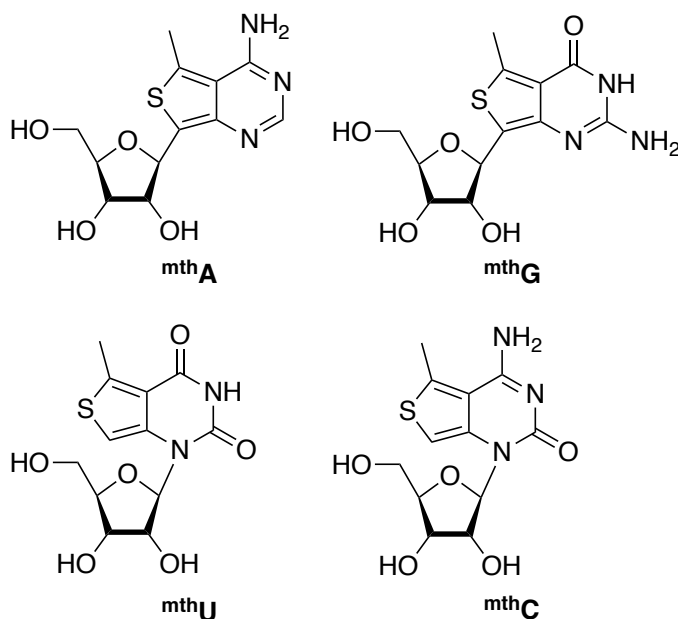


Figure 1.10 RNA Alphabet Based on methylthieno[3,4-d]pyrimidine (^{mth}N)

The RNA nucleoside alphabets thN, ^{tz}N, and ^{mth}N all are retained, to different extents, isomorphous and isofunctional features. The three generations of analogs preserve the Watson-Crick hydrogen bonding face and small two ring architecture. Compared to other classes of emissive nucleoside analogs, they do not require an expanded number of rings, embellishments extending from the nucleobase, or bulky fluorophores that take the place of the nucleobase entirely. Not only do these compounds structurally and biologically resemble their native counterparts, but they also provide a real-time optical window with high sensitivity to their microenvironments.

Table 1.1 Photophysical data for Previously Published Emissive RNA Alphabets

	$\lambda_{\text{abs,max}}^{\text{a}}$	ϵ^{b}	$\lambda_{\text{em,max}}^{\text{a}}$	ϕ
th G, ^{tz} G, ^{mth} G	321, 333, 327	4.15, 4.87, 3.5	463, 459, 456	0.46, 0.25, 0.42
th A, ^{tz} A, ^{mth} A	341, 338, 353	7.44, 7.8, 5.8	420, 338, 467	0.21, 0.50, 0.21
th C, ^{tz} C, ^{mth} C	320, 325, 323	4.53, 5.4, 3.4	429, 411, 455	0.41, 0.05, 0.24
th U, ^{tz} U, ^{mth} U	304, 312, 306	3.16, 5.17, 2.6	409, 392, 427	0.41, 0.01, 0.30

^a λ_{mntr} in nm. ^b ϵ is in $10^3 \text{ M}^{-1} \text{ cm}^{-1}$.

Through the years, the core of these emissive nucleoside analogs have been applied extensively in the context of both oligonucleotides and nucleoside based small-molecules. These applications include but are not limited to the monitoring of translation-related events, enzymatic purine and pyrimidine metabolism by deaminases, hammerhead ribozyme cleavage, cofactor transformations, secondary messengers, depurinations mechanisms, and antibiotic activity.³⁰⁻⁴² Each of the alphabets had a role in the exploration and illumination in the aforementioned processes. It is important to recognize that there is no single universal solutions for fluorescent nucleoside probes, but their utility remains in the context of the specific experiment pursued.

One area that remained unexplored was that of using the developed nucleobase cores without their sugar moiety as nucleobase surrogates. In this work, the use of guanine (G) based emissive analogs based on the thienopyrimidine (thG_N) and isothiazolepyrimidine (^{tz}G_N) cores are used for the evaluation of metabolic and epigenetic cellular modifications (Figure 1.11).

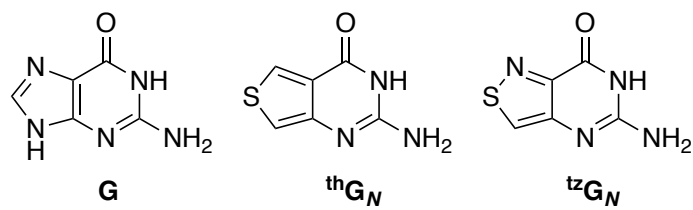


Figure 1.11 Guanine Nucleobase and Relevant Emissive Isomorphous Analogs

Guanine nucleobase and emissive guanine analogs based on previously published nucleoside analogs thieno[3,4-d]pyrimidine and isothiazolo[4,3-d]pyrimidine cores that are investigated in this work.

1.5 References

1. Callaway, E.; Naddaf, M. Pioneers of mRNA COVID vaccines win Nobel. *Nature*. **2023**, *622*, 228–229.
2. Kariko, K.; Buckstein, M.; Ni, H.; Weissman, D. Suppression of RNA recognition by Toll-like receptors: the impact of nucleoside modification and the evolutionary origin of RNA. *Immunity*. **2005**, *23*, 165–175.
3. Crick, F. On Protein Synthesis, The biological Replication of Macromolecules. *Symp. Soc. Exp. Biol.*, **1958**, *12*, 138–163.
4. Crick, F. Central Dogma of Molecular Biology. *Nature* **1970**, *227*, 561-563.
5. International Human Genome Sequencing Consortium. *Nature* **2004**, *431*, 931–945.
6. The ENCODE Project Consortium. *Nature* **2021**, *489*, 57–74.
7. Morris, K. V.; Mattick, J. The rise of regulatory RNA. *S. Nat. Rev. Genet.* **2014**, *15*, 423–437
8. Weeks, K. M. Review toward all RNA structures, concisely. *Biopolymers*. **2015**, *103* (8), 438–448.
9. Watson, J. D.; Crick, F. H. C.; Molecular Structure of Nucleic Acids. *Nature*. **1953**, *171*, 737–738.
10. Westhof, E.; Fritch, V. RNA folding: beyond Watson-Crick pairs. *Structure* **2000**, *8* (3), 55–65.
11. Sinkldam, R. W.; Greco, N.; Tor, Y. Fluorescent Analogs of Biomolecular building blocks. *Chem. Rev.* **2010**, *110* (5), 2579–2619.
12. Tanpure, A.; Pawar, M. G.; Srivatsan, S. G.; Fluorescent Nucleoside Analogs: Probes for Investigating Nucleic Acid Structure and Function. *Isr. J. Chem.* **2013**, *53* (6), 366–378.
13. Ward, D. C.; Reich, E.; Stryer, L. Fluorescence studies of nucleotides and polynucleotides: I. Formycin, 2-Aminopurine Riboside, 2,6-Diaminopurine Riboside, and their Derivatives. *J. Biol. Chem.* **1969**, *244*, 1228–1237.
14. Secrist, J. A.; Barrio, J. R.; Leonard, N. J. A Fluorescent Modification of Adenosine Triphosphate with Activity in Enzyme Systems: 1, N⁶-Ethenoadenosine Triphosphate. *Science*. **1972**, *175*, 646–647.

15. Wu, P.; Nordlund, T. M.; Gildea, B.; McLaughlin, L. W. Base Stacking and Unstacking as Determined from a DNA Decamer Containing Fluorescent Base. *Biochemistry* **1990**, *29*, 6508–6514.
16. Hawkins, M. E.; Pleiderer, W.; Mazumder, A.; Pommier, Y. G.; Balis, F. M. Incorporation of a fluorescent guanosine analog into oligonucleotides and its application to a real time assay for the HIV-1 integrase 3'-processing reaction. *Nucleic Acids Res.* **1995**, *24*, 2872–2880.
17. Ren, R. X.; Chaudhuri, N. C.; Paris, P. L.; Rumney, S.; Kool, E. T. Napthalene, Phenanthrene, and Pyrene as DNA Base Analogues: Synthesis, Structure, and Fluorescence in DNA. *J. Am. Chem. Soc.* **1996**, *118*, 7671–7678.
18. Godde, F.; Toulme, J. J.; Moreau, S. Benzoquinazoline derivatives as substitutes for thymine in nucleic acid complexes. Use of fluorescence emission of benzoquinazoline-2,4-(1H,3H)-dione in probing duplex and triplex formation. *Biochemistry* **1998**, *37*, 13765–13775.
19. Vrabel, M.; Horakova, P.; Pivonkova, H.; Kalachova, L.; Cernocka, H.; Cahova, H.; Pohl, R.; Sebest, P.; Havran, L.; Hocek, M.; Fojita, M. Base-Modified DNA Labeled by [Ru(bpy)₃]²⁺ and [Os(bpy)₃]²⁺ Complexes: Construction by Polymerase Incorporation of Modified Nucleoside Triphosphates, Electrochemical and Luminescent Properties, and Applications. *Chem. Euro. J.* **2009**, *15*, 1144–1154.
20. Tor, Y.; Del Valle, S.; Jaramillo, D.; Srivatsan, S. G.; Rios, A.; Weizman, H. Designing New Isomorphous Fluorescent Nucleobase Analogues: The Thieno[3,2-*d*]pyrimidine Core. *Tetrahedron* **2007**, *63* (17), 3608–3614.
21. Rovira, A. R.; Fin, A.; Tor, Y. Chemical Mutagenesis of an Emissive RNA Alphabet. *J. Am. Chem. Soc.* **2015**, *137* (46), 14602–14605.
22. Sundaralingam, M. Non-Watson-Crick Base-Pairs in Ribonucleic-Acids. *Int. J. Quantum Chem.* **1977**, 11–23.
23. Lakowicz, J. R. Principles of fluorescent spectroscopy. Second Ed. New York: Kluwer Academic/Plenum, 1999.
24. Chen, R. F. Measurements of Absolute Values in Biochemical Fluorescence Spectroscopy. *J. Res. Natl. Bur. Stand. A. Phys. Chem.* **1972**, *76* (6), 593–606.
25. Srivatsan, S. G.; Weizman, H.; Tor, Y. A highly fluorescent nucleoside analog based on thieno[3,4-*d*]pyrimidine senses mismatched pairing. *Org. Biomol. Chem.* **2008**, *6* (8), 1334–1338.
26. Shin, D.; Sinkeldam, R. W.; Tor, Y. Emissive RNA Alphabet. *J. Am. Chem. Soc.* **2011**, *133* (38), 14912–14915.

27. Rovira, A. R.; Fin, A.; Tor, Y. Chemical Mutagenesis of an Emissive RNA Alphabet. *J. Am. Chem. Soc.* **2015**, *137*, 14602–14605.
28. Rovira, A. R.; Fin, A.; Tor, Y. Expanding a Fluorescent Alphabet. *Chem. Sci.* **2017**, *8*, 2983–2993.
29. Ludford, P. T.; Yang, S.; Bucardo, M. S.; Tor, Y. A New Variant of Emissive RNA Alphabets. *Chem. Euro. J.* **2022**, *28* (13), e202104472.
30. Liu, W.; Shin, D.; Tor, Y. Monitoring translation with modified mRNAs strategically labeled with isomorphic fluorescent guanosine mimetics. *ACS Chem. Biol.* **2013**, *8* (9), 2017–2023.
31. Sinkeldam, R. W.; McCoy, L. S.; Shin, D.; Tor, Y. Enzymatic Interconversion of Isomorphic Fluorescent Nucleosides: Adenosine Deaminase Transforms thA to thI, Two Distinct Fluorophores. *Angew. Chem. Int. Ed.* **2013**, *52*, 14026–14030.
32. Mizrahi, R. A.; Shin, D.; Sinkeldam, R. W.; Phelps, K. J.; Fin, A.; Tantillo, D. J.; Tor, Y.; Beal, P. A. A Fluorescent Adenosine Analogue as a Substrate for A-to-I RNA Editing Enzyme. *Angew. Chem. Int. Ed.* **2015**, *54*, 8713–8716.
33. Vranken, C.; Fin, A.; Tufar, P.; Hofkens, J.; Burkhart, M.; Tor, Y. Chemoenzymatic Synthesis and Utilization of a SAM Analog with an Isomorphic Nucleobase. *J. Org. Chem.* **2016**, *81*, 4530–4539.
34. Li, Y.; Fin, A.; McCoy, L. S.; Tor, Y. Polymerase-Mediated Site-Specific Incorporation of a Synthetic Fluorescent Isomorphic G Surrogate into RNA. *Angew. Chem. Int. Ed.* **2017**, *56*, 1303–1307.
35. Rovira, A. R.; Fin, A.; Tor, Y. Emissive Synthetic Cofactors: An Isomorphic, Isofunctional, and Responsive NAD⁺ Analogue. *J. Am. Chem. Soc.* **2017**, *139*, 15556–15559.
36. Halle, F.; Fin, A.; Rovira, A. R.; Tor, Y. Emissive synthetic cofactors interconversions of ^{tz}A analogues of ATP, NAD⁺, NADH, NADP⁺, AND NADPH. *Angew. Chem. Int. Ed.* **2017**, *57*, 1087–1090.
37. Li, Y.; Ludford, P. T.; Fin, A.; Rovira, A. R.; Tor, Y. Enzymatic Synthesis and Applications of Fluorescent Cyclic Dinucleotides. *Chem. Euro. J.* **2020**, *26*, 6076–6084.
38. Li, Y.; Fin, A.; Rovira, A. R.; Su, Y.; Dippel, A. B.; Valderrama, J. A.; Riestra, A.; Nizet, V.; Hammond, M. C.; Tor, Y. Tuning the innate immune response to cyclic dinucleotides using atomic mutagenesis. *ChemBioChem* **2020**, *21* (18), 2595–2598.

39. Adamek, R. N.; Ludford, P. T.; Duggan, S. M.; Tor, Y.; Cohen, S. M. Identification of Adenosine Deaminase Inhibitors by Metal-binding Pharmacophore Screening. *ChemMedChem* **2020**, *22*, 2151–2156.
40. Ludford, P. T.; Li, Y.; Yang, S.; Tor, Y. Cytidine deaminase can deaminate fused pyrimidine ribonucleosides. *Org. Biol. Chem.* **2021**, *19*, 6237–6243.
41. Cong, D.; Li, Y.; Ludford, P. T.; Tor, Y. Isomorphic Fluorescent Nucleosides Facilitate Real-Time Monitoring of RNA Depurination by Ribosome Inactivating Proteins. *Chem. Euro. J.* **2022**, *28*, e202200994.
42. Hadidi, K. Steinbuch, K. B.; Dozier, L. E.; Patrick, G. N.; Tor, Y. Inherently Emissive Puromycin Analogues for Live Cell Labelling. *Angew. Chem. Int. Ed. Engl.* **2023**, *62* (23), e202216784.

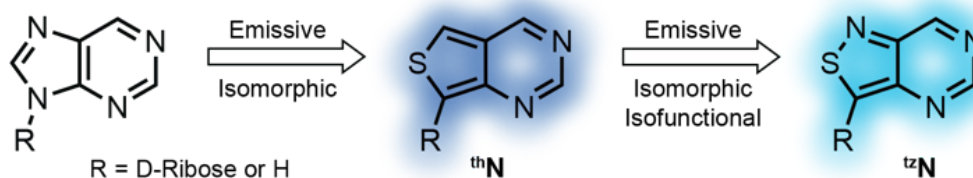
CHAPTER 2: Real-Time Monitoring of Human Guanine Deaminase

Activity by an Emissive Guanine Analog

2.1 Abstract

Guanine deaminase (GDA) deaminates guanine to xanthine. Despite its significance, the study of human GDA remains limited compared to other metabolic deaminases. As a result, its substrate and inhibitor repertoire are limited, and effective real-time activity, inhibitory, and discovery assays are missing. Herein, we explore two emissive heterocyclic cores, based on thieno[3,4-*d*]pyrimidine (thN) and isothiazole[4,3-*d*]pyrimidine (^{tz}N), as surrogate GDA substrates. We demonstrate that, unlike the thieno analog, thG_N, the isothiazolo guanine surrogate, ^{tz}G_N, does undergo effective enzymatic deamination by GDA and yields the spectroscopically distinct xanthine analog, ^{tz}X_N. Further, we showcase the potential of this fluorescent nucleobase surrogate to provide a visible spectral window for a real-time study of GDA and its inhibition.

Heterocyclic Core Evolution



Guanine Deaminase Reaction

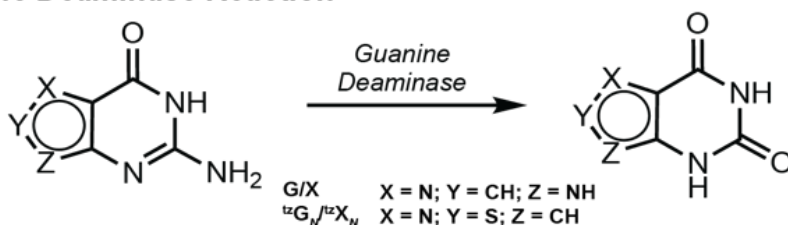


Figure 2.0 Abstract Figure: Heterocyclic Core Evolution and Guanine Deaminase Reaction

2.2 Introduction

Nucleobase and nucleoside deaminases play key roles in cellular pathways. Being responsible for the cellular levels of purine- and pyrimidine-based heterocycles, their over (or under) expression is frequently related to pathological conditions.¹⁻⁴ Additionally, differences between human and bacterial enzymes provide intriguing opportunities for new therapeutic approaches, exploiting their distinct fidelity and inherent activities.¹

Guanine deaminase (GDA), a hydrolytic zinc-based enzyme, converts guanine to xanthine.^{5,6} Recent observations have shown it impacts neuronal morphology^{7,8} and have implicated GDA in traumatic brain injury,⁹ memory dysfunction and psychiatric diseases.¹⁰ The study of human GDA, from the aminohydrolase superfamily, has remained somewhat sparse compared to other deaminases, including adenosine deaminase (ADA)^{11,12} and cytidine deaminase (CDA),¹³ which convert adenosine to inosine and cytidine to uridine, respectively. As a result, real-time activity and inhibitory assays for GDA, especially the human isoform, have yet to be advanced, and its substrate scope remains somewhat elusive.¹⁴

Diverse methods have been utilized for assessing the enzymatic activity and inhibition of deaminases. Most protocols capable of directly measuring GDA activity rely on the distinct chromatographic behavior or the UV absorption signature of the substrate/product pair.¹⁵ The former techniques are accurate but can be time-consuming, while the latter tools frequently suffer from spectral interference as many inhibitors share similar chromophoric properties with the substrate or product. To facilitate the biochemical study of deaminases, define their substrate scope, and identify inhibitors, innovative methods for monitoring their activity are needed. Although fluorescence spectroscopy might *a priori* appear most attractive due to its high

sensitivity, it cannot be applied in such contexts due to the lack of any useful emissive features of the native purine nucleobases.

Over the past two decades our laboratory has designed, synthesized, and implemented minimally perturbing and responsive fluorescent nucleoside analogs.^{15–29} The guiding criterion for their design has been the diminution of structural and functional perturbations, which are inevitable consequences of modifying any native building block. Nucleosides that fulfill such critical constraints are thus coined isomorphic. If they function identically to their native counterparts, we define them as being isofunctional. We have advanced two emissive RNA alphabets, based on thieno[3,4-*d*]pyrimidine (1st generation; thN)³⁰ and isothiazole[4,3-*d*]pyrimidine (2nd generation; ^{tz}N)³¹ heterocyclic cores (Figure 1a). The emissive adenosine analogs have been successfully used to advance real-time activity and inhibition assays of adenosine deaminase, exploiting the distinct emission profiles of the substrates (thA and ^{tz}A), and their corresponding deamination products (thI and ^{tz}I, respectively), with the latter (^{tz}A) being essentially isofunctional (Figure 2.1b).^{32,33} The red-shifted absorption and visible-range emission of such fluorescent substrate surrogates opens a spectral window not accessible by other means, which facilitates the real-time monitoring of these reactions even in the presence of potentially interfering chromophores.³⁴

Applying such approaches to nucleobase-processing enzymes such as human GDA represents, however, a minimally explored territory, as highly emissive nucleobase analogs have not been broadly tested and scrutinized as substrates.^{6,13} The lack of the rather large and contact forming D-ribose residue presents the challenge of altering guanine without disturbing contacts at the active site of such a potentially fastidious nucleobase-processing enzyme.³⁵ We therefore set out to investigate two emissive nucleobase analogs, thieno[3,4-*d*]pyrimidine (thG_N) and isothiazole[4,3-*d*]pyrimidine (^{tz}G_N) (Figure 2.1c), and demonstrate that while the former is not a

viable substrate, ${}^{\text{tz}}\text{G}_\text{N}$ does undergo facile GDA-mediated deamination to yield the fluorescently distinct xanthine analog, ${}^{\text{tz}}\text{X}_\text{N}$. The spectral differences displayed by the substrate and product are exploited for a real-time monitoring of the enzymatic reaction. Moreover, the potential of ${}^{\text{tz}}\text{G}_\text{N}$ as a tool for GDA screenings is showcased by measuring GDA inhibition by a previously reported inhibitor and identifying two new inhibitors. Taken together, these findings highlight the necessity of the N7 for substrate recognition by GDA and provide information regarding its substrate and inhibitor scope.

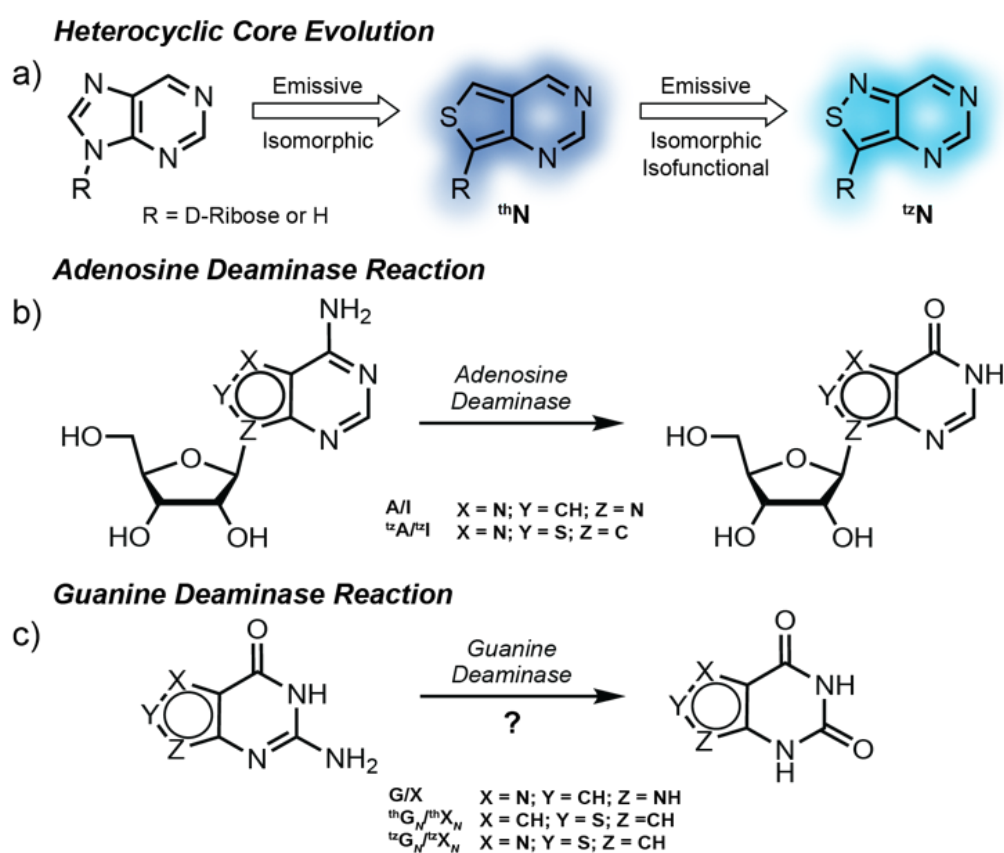


Figure 2.1 Heterocyclic Core Evolution, ADA Reaction, and GDA Reaction

a) Heterocycle evolution pertaining to this study starting from the native purine core to ${}^{\text{th}}\text{N}$ to ${}^{\text{tz}}\text{N}$. b) Adenosine deaminase conversion of A to I and isofunctional nucleoside analog ${}^{\text{tz}}\text{A}$ to ${}^{\text{tz}}\text{I}$. c) Guanine deaminase conversion of G to X, isomorphic nucleobase analog ${}^{\text{th}}\text{G}_\text{N}$ to ${}^{\text{th}}\text{X}_\text{N}$, and isofunctional nucleobase analog ${}^{\text{tz}}\text{G}_\text{N}$ to ${}^{\text{tz}}\text{X}_\text{N}$.

2.3 Results and Discussion

The four nucleobases, containing either a thienopyrimidine-core, ${}^{\text{th}}\mathbf{G}_N$ and ${}^{\text{th}}\mathbf{X}_N$, or an isothiazolepyrimidine-core, ${}^{\text{tz}}\mathbf{G}_N$ and ${}^{\text{tz}}\mathbf{X}_N$, were prepared according to established procedures (Figure 2.2a, Schemes 2.S1-S3).^{30,31,35,36} Briefly, treatment of commercially available methyl 4-aminothiophene 3-carboxylate hydrochloride with chloroformamidine hydrochloride in DMSO₂ at 125°C yields ${}^{\text{th}}\mathbf{G}_N$ in one step. The corresponding xanthine analog, ${}^{\text{th}}\mathbf{X}_N$, was synthesized in two steps by treating the same starting material with KOCN to yield the corresponding urea, which was then cyclized under basic conditions with sodium methoxide in methanol (Scheme 2.S1). For the isothiazole-based nucleobases ${}^{\text{tz}}\mathbf{G}_N$ and ${}^{\text{tz}}\mathbf{X}_N$, methyl 4-aminothiazole 3-carboxylate hydrochloride, a key precursor, was prepared from methyl thioglycolate and N-tosylated Oxyma, followed by decarboxylation and esterification (Scheme 2.S2).³⁷ Conversion of the isothiazole-based precursor to ${}^{\text{tz}}\mathbf{G}_N$ and ${}^{\text{tz}}\mathbf{X}_N$ followed the same cyclization procedures described above for the thiophene derivatives (Scheme 2.S3). Crystal structures have been determined for all nucleobases (Figure 2.3a-d, Tables 2.S1-S4).

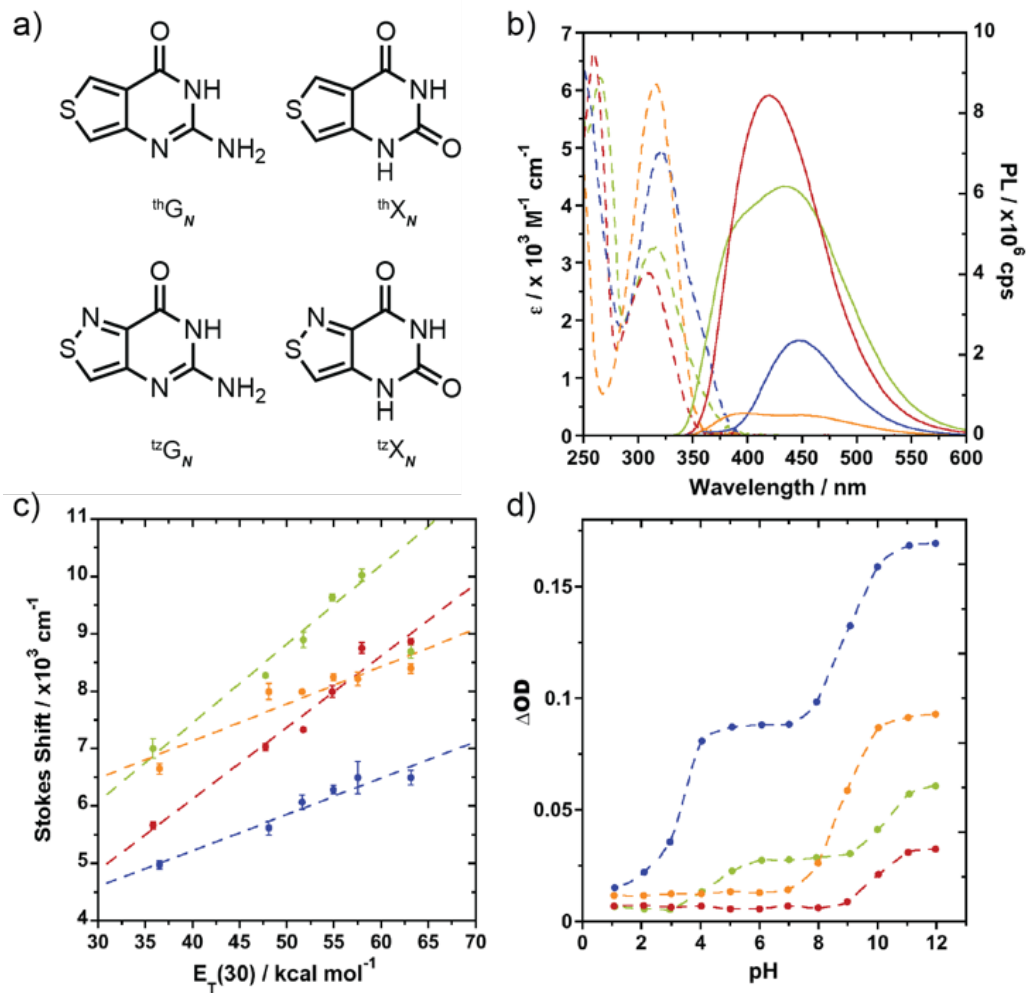


Figure 2.2 Nucleobase Structures and Photophysical Properties

a) Structure of ${}^{\text{th}}\text{G}_N$, ${}^{\text{th}}\text{X}_N$, ${}^{\text{tz}}\text{G}_N$, and ${}^{\text{tz}}\text{X}_N$ nucleobases. b) Absorption (dashed lines) and emission (solid lines) of ${}^{\text{th}}\text{G}_N$ (green), ${}^{\text{th}}\text{X}_N$ (red), ${}^{\text{tz}}\text{G}_N$ (blue), and ${}^{\text{tz}}\text{X}_N$ (orange) in water. c) Stokes shift correlations versus solvent polarity [$E_T(30)$ of water/dioxane mixtures] for ${}^{\text{th}}\text{G}_N$ (green), ${}^{\text{th}}\text{X}_N$ (red), ${}^{\text{tz}}\text{G}_N$ (blue), and ${}^{\text{tz}}\text{X}_N$ (orange). d) Change in optical density versus pH for ${}^{\text{th}}\text{G}_N$ (green), ${}^{\text{th}}\text{X}_N$ (red), ${}^{\text{tz}}\text{G}_N$ (blue), and ${}^{\text{tz}}\text{X}_N$ (orange).

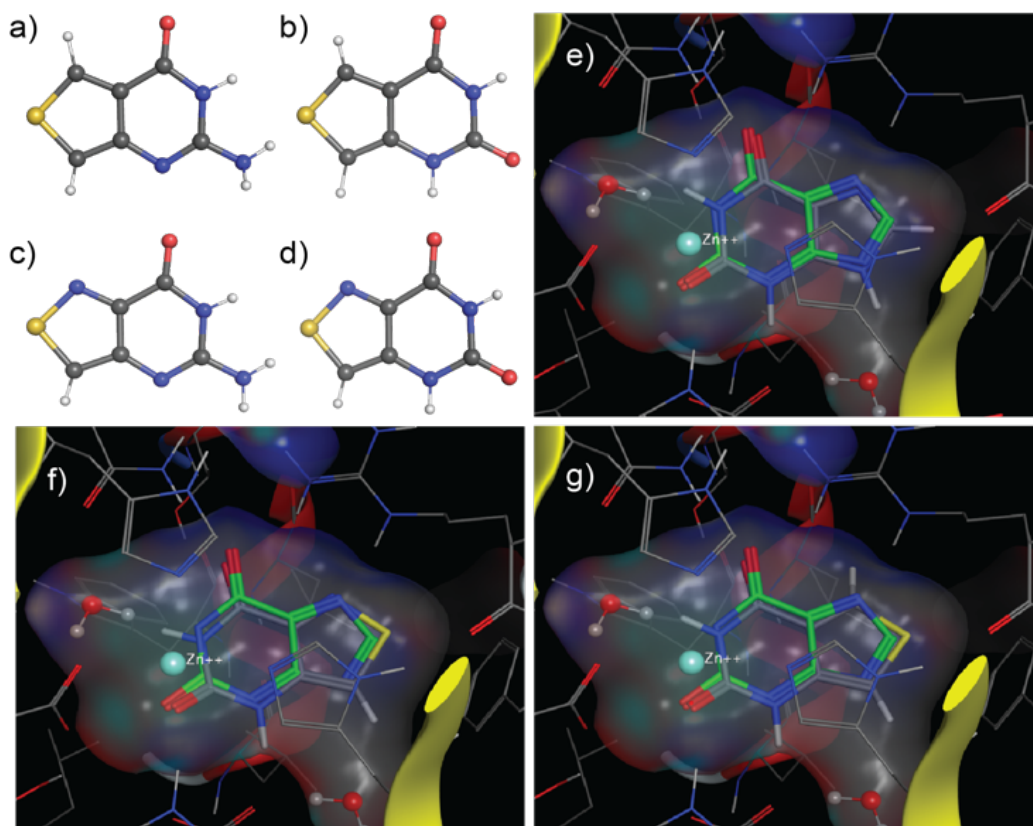


Figure 2.3 X-ray Crystal Structures of Nucleobases and MOE Docking

a) ${}^{\text{th}}\text{G}_N$, b) ${}^{\text{th}}\text{X}_N$, c) ${}^{\text{tz}}\text{G}_N$, d) and ${}^{\text{tz}}\text{X}_N$. MOE docking of e) xanthine as reference ($\Delta\Delta G$ 0), f) ${}^{\text{tz}}\text{X}_N$ ($\Delta\Delta G$ 0.28), g) and ${}^{\text{th}}\text{X}_N$ ($\Delta\Delta G$ 1.89) in GDA active site (PDB ID 2UZ9, see methods).

To assess the likelihood of spectroscopically distinguishing between the substrates and their corresponding products, the fundamental spectroscopic properties of the nucleobases were determined (Tables 2.1 and 2.S5). Absorption spectra in water displayed red-shifted maxima of the nucleobase analogs compared to their native counterparts, showing maxima at 315, 308, 320 and 315 nm for ${}^{\text{th}}\text{G}_N$, ${}^{\text{th}}\text{X}_N$, ${}^{\text{tz}}\text{G}_N$ and ${}^{\text{tz}}\text{X}_N$, respectively. Excitation at their absorption maxima gave rise to visible emission, which peaked at 439, 420, 446 and 394 nm for ${}^{\text{th}}\text{G}_N$, ${}^{\text{th}}\text{X}_N$, ${}^{\text{tz}}\text{G}_N$ and ${}^{\text{tz}}\text{X}_N$, respectively (Figure 2.2b). As expected, the emission quantum yields of the thiophene analogs, ${}^{\text{th}}\text{G}_N$ and ${}^{\text{th}}\text{X}_N$ (0.40 and 0.46, respectively) were higher than their isothiazole counterparts, ${}^{\text{tz}}\text{G}_N$ and ${}^{\text{tz}}\text{X}_N$ (0.07 and 0.02, respectively.)

Table 2.1 Photophysical data for nucleobase analogs

	$\lambda_{\text{abs,max}}^{\text{a}}$	ϵ^{b}	$\lambda_{\text{em,max}}^{\text{a}}$	ϕ
th G _N	315	3.0	439	0.40
th X _N	308	3.2	420	0.46
^{tz} G _N	320	5.4	446	0.07
^{tz} X _N	315	6.1	394	0.02

^a λ_{mnr} in nm. ^b ϵ is in 10³ M⁻¹ cm⁻¹. Experiments done in triplicate.

Additionally, the sensitivity of photophysical parameters to environmental polarity was evaluated and spectroscopically derived pK_a values were determined (Table 2.S5). The absorption and emission parameters of each nucleobase were measured in dioxane, water and mixtures thereof. By linearly correlating the calculated Stokes shift against the solvent polarity of each sample, the chromophore's responsiveness was defined. The four nucleobases showed differing levels of sensitivity to polarity, with the thiophene derivatives showing substantial impact on Stokes shift compared to the isothiazole derivatives (Figure 2.2c, Figure 2.S1). The nucleobases also showed responsiveness to pH changes. pK_a values were extrapolated by plotting the absorption maxima versus pH (Figure 2.2d, Figure 2.S2). The guanine derivatives, thG_N and ^{tz}G_N, show two pK_a values (pK_a = 4.41, 10.19 and pK_a = 3.28, 8.96, respectively), while the xanthine derivatives, thX_N and ^{tz}X_N, show one pK_a value (pK_a = 9.92 and pK_a = 8.8, respectively), as expected.^{31,38,39}

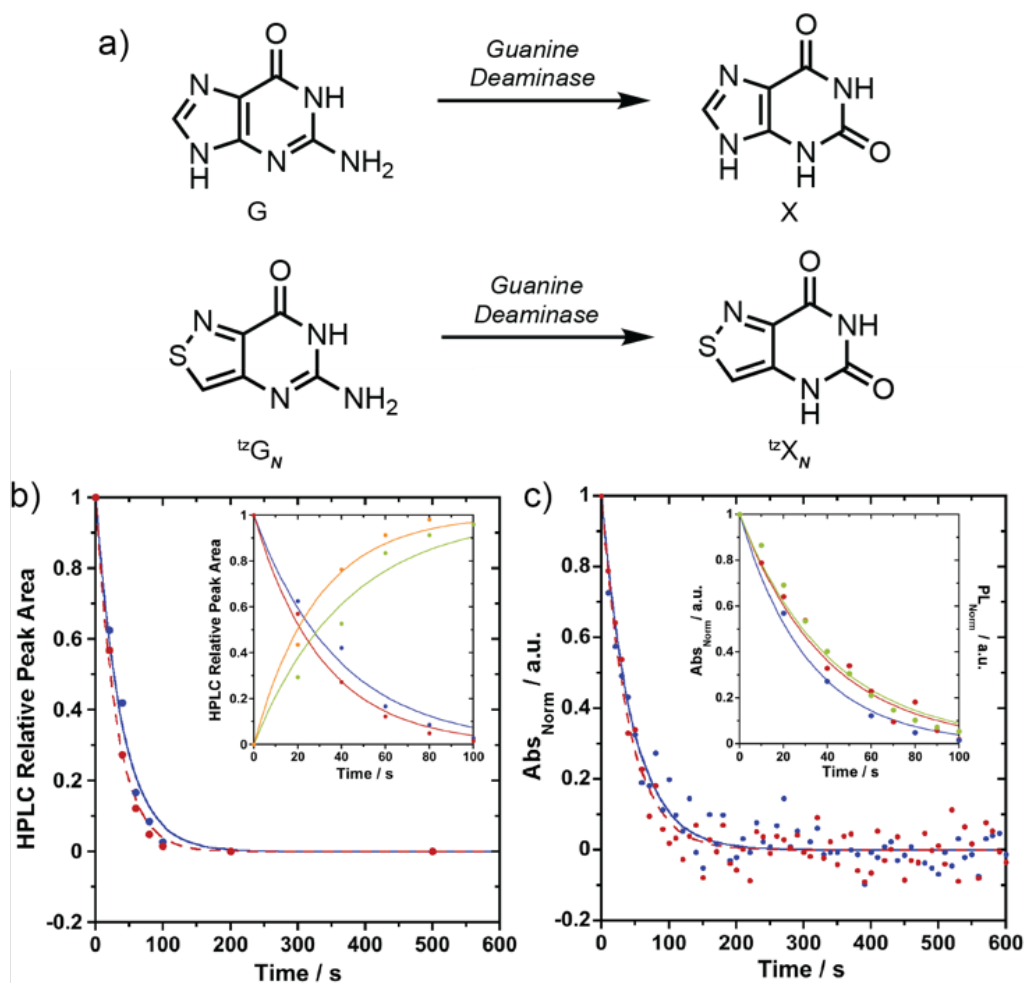


Figure 2.4 Enzymatic Guanine Deaminase Reactions

a) Conversion of guanine to xanthine and conversion of isofunctional ${}^t\text{zG}_N$ to ${}^t\text{zX}_N$ by GDA. b) HPLC relative peak area versus time for consumption of guanine to xanthine at 260 nm (blue) and consumption of ${}^t\text{zG}_N$ to ${}^t\text{zX}_N$ at 320 nm (red). Inset: HPLC relative peak area versus time for the consumption of guanine (blue) and formation of xanthine (green) at 260 nm and the consumption of ${}^t\text{zG}_N$ (red) and formation of ${}^t\text{zX}_N$ (orange) at 320 nm from 0 to 100 second. c) Absorption changes upon enzymatic deamination of guanine to xanthine at 270 nm (blue) and ${}^t\text{zG}_N$ to ${}^t\text{zX}_N$ at 355 nm (red). Inset: Enzymatic deamination of ${}^t\text{zG}_N$ to ${}^t\text{zX}_N$ monitored by absorbance (at 355 nm, red), fluorescence (450 nm, excitation at 328 nm, green), and HPLC relative peak area over time (at 320 nm, blue).

To compare the susceptibility of ${}^{\text{th}}\text{G}_N$ and ${}^t\text{zG}_N$ to GDA-mediated deamination, enzymatic reactions were first analyzed by HPLC and then monitored in real-time by absorption and emission spectroscopy. HPLC analysis confirmed the complete transformation of native guanine to xanthine by GDA within 500 seconds (Figure 2.4a and 2.S3a). The reaction of ${}^t\text{zG}_N$ with GDA showed

conversion to the corresponding product, $^{13}\text{X}_N$ (Figures 2.4a and 2.S3b). However, the reaction of $^{14}\text{G}_N$ showed no conversion of substrate across all time point studied (Figure 2.S3c). By plotting the area under the curve at different reaction times (Figure 2.4b), comparable reaction half-life values for guanine deamination ($\text{G } t_{1/2} = 27 \text{ s}$) and $^{13}\text{G}_N$ deamination ($^{13}\text{G}_N t_{1/2} = 21 \text{ s}$) were calculated assuming pseudo-first order reaction conditions (Table 2.2). Kinetic parameters were also calculated by fitting HPLC-monitored deamination reactions to a set of ordinary differential equations consistent with Michaelis–Menten kinetics (see Methods). Similar values were obtained for guanine ($K_M = 12 \pm 9 \mu\text{M}$; $k_2 = 36 \pm 27 \text{ s}^{-1}$; $k_2/K_M = 3.0 \pm 0.3 \mu\text{M}^{-1} \text{ s}^{-1}$) and its isothiazolo analog $^{13}\text{G}_N$ ($K_M = 8 \pm 3 \mu\text{M}$; $k_2 = 32 \pm 7 \text{ s}^{-1}$; $k_2/K_M = 4.2 \pm 1.0 \mu\text{M}^{-1} \text{ s}^{-1}$; see Table 2.2). We note that the K_M value obtained for the deamination of guanine is comparable to previously published figures for rabbit liver GDA (K_M of $12.5 \mu\text{M}$)⁴⁰ and the k_2/K_M is comparable to $k_1/[\text{GDA}]$ ($\text{G } k_1/[\text{GDA}] = 2.6 \mu\text{M}^{-1} \text{ s}^{-1}$) from the pseudo-first order kinetic curves (Table 2.2).

Table 2.2 GDA reaction rates

	HPLC						Absorbance			Emission		
	$\lambda_{\text{mnr}}^{\text{a}}$	k_1^{b}	$t_{1/2}^{\text{c}}$	K_M^{d}	k_2^{d}	k_2/K_M^{d}	$\lambda_{\text{mnr}}^{\text{a}}$	k_1^{b}	$t_{1/2}^{\text{c}}$	$\lambda_{\text{mnr}}^{\text{a}}$	k_1^{b}	$t_{1/2}^{\text{c}}$
G to X	260	26 ± 2	27	12 ± 9	36 ± 27	3.0 ± 0.3	270	22 ± 1	31	-	-	-
$^{14}\text{G}_N$ to $^{14}\text{X}_N$	320	NR	NR	NR	NR	NR	355	NR	NR	450	NR	NR
$^{13}\text{G}_N$ to $^{13}\text{X}_N$	260	32 ± 1	21	8 ± 3	32 ± 7	4.2 ± 1.0	355	25 ± 1	27	450	24 ± 1	29

^a λ_{mnr} in nm and represent the monitored and excitation wavelengths respectively in each experiment. ^b Pseudo first order reaction kinetics slope of the exponential approximation in 10^{-3} s^{-1} . ^c $t_{1/2}$ is reaction half-life calculated assuming pseudo-first order kinetics. K_M , k_2 , and k_2/K_M are reported in μM , s^{-1} , and $10^6 \text{ M}^{-1} \text{ s}^{-1}$ respectively. At 360 nm for $^{14}\text{G}_N$ reactions. At 328 nm for $^{13}\text{G}_N$ reactions. Experiments done in triplicate.

Rewordingly, spectroscopic analyses agree with the chromatographic analysis (Figure 4c). When monitoring the enzymatic deamination of $^{13}\text{G}_N$ spectroscopically, an increase in absorbance at 355 nm and an emission decrease at 450 nm when exciting at 328 nm, the isosbestic point, were

observed. The reaction half-life for ${}^{\text{tz}}\text{G}_N$ was calculated using the same assumptions mentioned previously (${}^{\text{tz}}\text{G}_N$ abs $t_{1/2} = 27$ s; $t_{1/2}$ em = 29 s) and was found to be comparable to the native substrate (G abs $t_{1/2} = 31$ s), as shown in Table 2.2. The transformation of both native guanine to xanthine and ${}^{\text{tz}}\text{G}_N$ to ${}^{\text{tz}}\text{X}_N$ by GDA is also illustrated by the absorption maxima shift (Figure 2.S4). Thienopyrimidine ${}^{\text{th}}\text{G}_N$ showed no change in absorption or emission in the presence of GDA over 500 seconds.

Reactions monitored by HPLC as well as real-time absorption and emission spectroscopy suggest that ${}^{\text{tz}}\text{G}_N$, the isothiazolepyrimidine substrate, is equally susceptible to GDA-mediated deamination as native guanine. Intriguingly, ${}^{\text{th}}\text{G}_N$, the thienopyrimidine guanine analog, is unreactive and does not undergo GDA-mediated deamination. These findings showcase the functionality and increased isomorphism of the isothiazolepyrimidine-based nucleobase alphabet, which reinstated the N7 moiety, compared to the thienopyrimidine-based nucleobases, even without the large and contact forming D-ribose residue the nucleoside counterparts possess. Further support is obtained by Molecular Operating Environment (MOE) molecular docking experiments (Figures 2.3e–g, Figures 2.S5 and 2.S6) using the published crystallographic data for xanthine-bound human GDA (PDB ID 2UZ9). The enzyme recognition preferences for ${}^{\text{tz}}\text{X}_N$ over ${}^{\text{th}}\text{X}_N$ are illustrated by the markedly higher positive $\Delta\Delta G$ values obtained for the latter vs. the former ($\Delta\Delta G$ 1.89 and 0.28, respectively). A similar trend was observed for the substrates (Figure 2.S6). Docking also shows a plausible structure deformation induced by Arg235, which is projected towards the N7 position at the native substrate. This basic site, present in native G/X and the isothiazolo analogs, ${}^{\text{tz}}\text{G}_N/{}^{\text{tz}}\text{X}_N$, likely hydrogen bonds to Arg235. Clashing of this arginine side chain with the CH group of ${}^{\text{th}}\text{G}_N$ at the same position, likely renders the thiophenopyrimidine-based substrate unrecognizable by GDA.

As stated, the presence of the nitrogen at a position equivalent to N7 in the purine skeleton endows ${}^t\mathbf{G}_N$, the isothiazole purine surrogate, with substrate recognition features that appear lacking in ${}^h\mathbf{G}_N$. While comprehensive investigations of GDA substrate scope have not been pursued, previous substrate and inhibitor analyses of aminohydrolase isoforms suggest that the O6, N3, and N7 points of contact are important for substrate recognition.^{6,17,40,41} Intriguingly, while ${}^t\mathbf{G}_N$ retains these contact points, it is lacking the NH group found in the purine's 9 position. Previously reported inhibitors, such as valciclovir and derivatives of azepinomycin, containing substituents at the N9 position suggest GDA can tolerate diverse groups at that position, which may explain the high tolerance and the native deamination rate displayed by ${}^t\mathbf{G}_N$.^{14,42}

The change in emission signal intensity upon GDA-mediated deamination of ${}^t\mathbf{G}_N$ to ${}^t\mathbf{X}_N$, facilitates real-time monitoring of the enzymatic reaction and its inhibition. To demonstrate its potential, three inhibitors were tested, 5-aminoimidazole-4-carboxamide (AICA), 4-aminoisothiazole-3-carboxamide (ATCA) and 4-imidazolecarboxylic acid (ICA, Figure 5a). AICA is an established competitive inhibitor of GDA.⁴⁰ ATCA, the isothiazole counterpart, we synthesized (Scheme 2.S4). Reaction conditions used for previous experiments were sustained with the exception of inhibitor addition at various concentrations. Percent inhibition plots were fitted with sigmoidal Hill curves to obtain IC_{50} values of the tested inhibitors. AICA ($IC_{50} = 100 \mu\text{M}$) showed comparable inhibition to ATCA ($IC_{50} = 80 \mu\text{M}$), while ICA is comparatively a less potent inhibitor ($IC_{50} = 2 \text{ mM}$, Figure 2.5b).

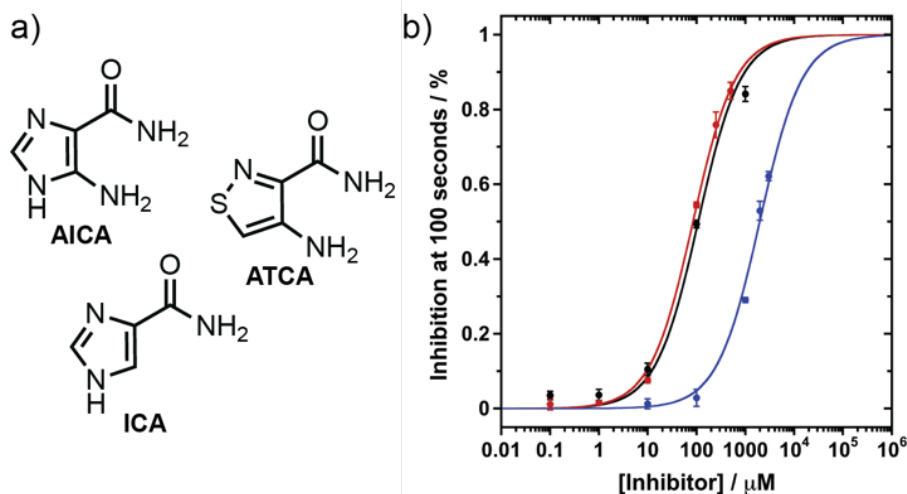


Figure 2.5 Guanine Deaminase Inhibitor Study

a) GDA inhibitor structures of AICA, ATCA, and ICA. b) Overlay of % inhibition at 100 seconds and sigmoidal Hill plot for AICA (black), ATCA (red), and ICA (blue).

2.4 Conclusion

This study set out to assess the utility of two emissive nucleobase analogs, thG_N and ^{tz}G_N, as substrates for the enzymatic reaction of GDA. We demonstrate that isothiazole[4,3-*d*]pyrimidine, ^{tz}G_N, behaves as an isomorphic and isofunctional emissive surrogate for guanine. The interconversion of ^{tz}G_N to ^{tz}X_N can successfully be tracked in real-time as the reaction substrate and product display distinct photophysical properties. The strategic replacement of the GDA substrate with emissive counterparts from both previously published emissive alphabets demonstrate the significance of N7 for GDA substrate recognition. Moreover, this discovery provides a biochemical tool to study the activity of human GDA and offers a spectral window for fabricating real-time high throughput discovery assays of GDA. We illustrate this through a small pilot study of inhibitor effects on GDA activity, which includes one previously reported inhibitor and two new inhibitors.

2.5 Methods

2.5.1 Expression and Purification of GDA

Wild-type human GDA gene, cloned into pET-28B vector (Genescript), was expressed with an N-terminal hexahistidine tag. The construct was sequence-verified (GENEWIZ). The plasmid (4 µg) was dissolved in water to a concentration of 28.8 ng/µL. *E. coli* BL21 (DE3) cells were transformed with the GDA containing plasmid. Overnight starter cultures were grown in Luria Broth (LB) medium at 37 °C with 50 µg/mL of kanamycin. The overnight culture was used to inoculate 1 L of LB medium with 50 µg/mL kanamycin. Cells were grown while shaking at 37 °C until OD₆₀₀ of 0.6 was reached and the culture was down tempered to 18 °C over a period of 1 hour. To induce target protein production, 0.5 mM IPTG was added, and the medium was left to stir at 18 °C overnight. Cells were harvested after overnight growth by centrifugation at 3500 rpm for 35 minutes at 4 °C.

Cells were resuspended in lysis buffer [20 mM HEPES, 500 mM NaCl, 10% glycerol, 0.5 mM TCEP (pH 7.5), supplemented with one tablet of Complete EDTA-free protease inhibitor (Roche Applied Science)] and lysed by sonication. Cell lysate was centrifuged at 10,000 rpm for 1 hour at 4 °C before the supernatant was decanted and filtered through a 0.45 µm syringe filter. GDA was purified by immobilized metal affinity chromatography. IMAC Ni-charged column [2 mL HisPur Ni-NTA Resin (Thermo Scientific)] was equilibrated with lysis buffer to which the lysate was then added. The column was washed with 50 mL of wash buffer supplemented with 20 mM imidazole. The bound protein was eluted from the column with elution buffer (wash buffer supplemented with 200 mM imidazole). Fractions were analyzed by SDS-PAGE and those containing the target protein were pooled, subsequently concentrated and buffer exchanged into

storage buffer [20 mM Tris-HCl buffer (pH 8.0), 10% glycerol, 1 mM DTT] using a centrifugal filter device with a 10 kDa molecular weight cut off. After protein expression and purification, the final protein concentration was 5.3 mg/mL (0.1 mM) in a total volume of 1.7 mL. Protein aliquots were snap-frozen and stored at $-80\text{ }^{\circ}\text{C}$ until further use. Before used in enzymatic reactions the GDA protein stock was diluted 1:100 in sodium phosphate buffer [50 mM (pH 7.4)].

2.5.2 Synthetic Procedures

All synthetic procedures and characterizations of compounds are reported in the supporting information.

2.5.3 Photophysical Properties: General Methods

Absorption spectra were measured on a Shimadzu UV-2450 spectrometer with 0.5 mm resolution and setting the slit at 1 nm. Emission spectra were measured on a Horiba Fluoromax-4 equipped with a cuvette holder and stirring system. Emission measurements were taken with resolution at 1 nm and setting both the excitation and emission slits at 3 nm.

All measurements were carried out in a 10 mm four-sided quartz cuvette from purchased from Helma. All spectra were corrected for the blank. Both instruments were equipped with a thermostat-controlled ethylene glycol-water bath and all measurements were taken at $37\text{ }^{\circ}\text{C}$. Measurements were recorded after a 3-minute temperature equilibration period.

Concentrated stock solutions for xanthine, $^{\text{th}}\text{G}_N$, $^{\text{th}}\text{X}_N$, $^{\text{tz}}\text{G}_N$, and $^{\text{tz}}\text{X}_N$ were prepared in DMSO and stock solution of guanine was prepared in water basified to pH 12 with sodium hydroxide. Samples for experiments were prepared with stock nucleobase diluted to a total sample

volume of 3 mL in deionized water, mixed with a pipette for 10 seconds and placed in the cuvette holder. All samples contain 0.3 v/v % DMSO, except guanine samples.

2.5.4 Quantum Yield Measurements

All sample concentrations were adjusted to optical density lower than 0.1 at the excitation wavelength (λ_{ex}). The fluorescence quantum yield (ϕ) of each nucleobase was evaluated based on 2-aminopurine (0.68 in water, λ_{ex} 320 nm) as an external standard by using the following equation.

$$\phi = \phi_{\text{STD}} \frac{I}{I_{\text{STD}}} \frac{OD_{\text{STD}}}{OD} \frac{n^2}{n_{\text{STD}}^2} \quad (2.1)$$

Where ϕ_{STD} is the fluorescence quantum yield of the standard, I and I_{STD} are the integrated area of the emission band of the sample and the standard respectively, OD and OD_{STD} are the optical density at the excitation wavelength for the sample and standard respectively, and n and n_{STD} are the solvent refractive index of the sample and the standard solutions respectively.

2.5.5 Sensitivity to pH

Sodium phosphate buffers with a final concentration of 50 mM were prepared and adjusted to the desired experimental pH values using HCl or NaOH prior to spectral measurements. Changes in optical density, at 310 and 350 nm, were plotted versus pH. The pK_a values were determined by interpolation of the fitting curves.

2.5.6 Sensitivity to Polarity

Experiments evaluating the effect of polarity were performed in water, dioxane and mixtures of 20, 40, 60, 80 v/v % water in dioxane. The sample $E_T(30)$ values were determined by

dissolving Reichardt's dye in an aliquot of the same solvent used to dilute the nucleobase DMSO sample. The observed wavelength absorption maximum ($\lambda_{\text{abs}}^{\text{max}}$) were then converted to the $E_T(30)$ values (Table 2.S6) using the following equation.

$$E_T(30) = \frac{28591}{\lambda_{\text{abs}}^{\text{max}}} \quad (2.2)$$

2.5.7 Enzymatic Deamination: General Methods

Reaction conditions were the same for all GDA reactions monitored by spectroscopy or chromatography. Concentrated stock solutions for xanthine, $^{\text{th}}\text{G}_N$, $^{\text{th}}\text{X}_N$, $^{\text{tz}}\text{G}_N$, and $^{\text{tz}}\text{X}_N$ were prepared in DMSO and the stock solution of guanine was prepared in water basified to pH 12 with sodium hydroxide. Samples were prepared in a 10.00 mm four-sided quartz cuvette from Helma. Reactions had a total reaction volume of 3 mL with nucleobase and enzyme concentrations of 3 μM and 10 nM in sodium phosphate buffer [50 mM (pH 7.4)]. All measurements were taken at 37 $^{\circ}\text{C}$ and GDA was introduced after a 3-minute temperature equilibration period.

2.5.8 Real-Time Monitoring of GDA via Absorption and Emission

GDA-mediated conversion of guanine and its analogs ($^{\text{th}}\text{G}_N$ and $^{\text{tz}}\text{G}_N$) was monitored by absorption and emission spectroscopy. Absorbance measurements of the enzymatic conversion of guanine (and its analogs) was performed on a Shimadzu UV-2459 spectrometer taking a point every 10 seconds for 600 seconds after the addition of GDA with slit setting 1 nm. The conversion was monitored at 270 nm for guanine to xanthine and at 355 nm for the analogs ($^{\text{th}}\text{G}_N$ and $^{\text{tz}}\text{G}_N$ to $^{\text{tz}}\text{X}_N$). Emission measurements of the conversion of guanine (and analogs) was performed on a

Horiba Fluoromax-4 with cuvette holder and a built-in stirring system with excitation and emission slits set to 3 nm and taking points every 10 seconds for 600 seconds after the addition of GDA.

Emission was monitored at 450 nm with excitation at 360 nm and 328 nm respectively for ${}^{\text{th}}\text{G}_N$ and ${}^{\text{tz}}\text{G}_N$. ${}^{\text{th}}\text{G}_N$ reaction showed no change in absorption or emission intensity in the presence of GDA over 600 seconds. Each experiment was done in triplicate. There is a 6 second lag time after GDA is added to the cuvette after the time 0 measurement.

2.5.9 Steady State Absorption Measurements in the Presence of GDA

Steady state absorption spectra over time were performed on a Shimadzu UV-2450 spectrophotometer setting the slit at 5 nm, using a resolution of 0.5 nm, taking a measurement every 20 seconds. All spectra were corrected for the blank. Smoothing of data was done on spectra for plotting.

2.5.10 HPLC analysis of Enzymatic Conversion of Native G to X and ${}^{\text{tz}}\text{G}_N$ to ${}^{\text{tz}}\text{X}_N$

GDA-mediated conversion was monitored by chromatography. HPLC was carried out with an Agilent 1200 system with a Polaris 5 C18-A 250 x 4.9 mm column. Solutions of 0.1% formic acid (Honeywell Fluka) were prepared by dissolving 1 mL of formic acid in 1 L total volume of acetonitrile (J. T. Baker) or water. Solutions were filtered using Millipore type GNWP 0.2 μm filters before use. Each injection (75 μL) for guanine or ${}^{\text{tz}}\text{G}_N$ experiments was subjected to a linear gradient of 0.5% to 10% acetonitrile in water with 0.1% formic acid for 20 minutes, followed by a flush and equilibration for 10 minutes. ${}^{\text{th}}\text{G}_N$ injections were subjected to a linear gradient of 0.5%

to 10% acetonitrile in water with 0.1% formic acid for 30 minutes, followed by a flush and equilibration for 10 minutes. Each run was monitored at 260, 280, and 320 nm with calibrated reference at 650 nm and slit set at 1 nm.

Concentrated stock solution of guanine, $^{14}\text{C}\text{G}_N$ and $^{15}\text{N}\text{G}_N$ was diluted in phosphate buffer. Solution was warmed to 37 °C for 3 minutes with stirring before addition of GDA stock solution. After the addition of GDA, the enzymatic conversion was quenched in aliquots (after 20, 40, 60, 80, 100, 200 and 500 seconds) by adding formic acid (0.55 M) and placing aliquots on ice. Each 100 μL aliquot was filtered and analyzed by HPLC.

HPLC traces were corrected for the blank and the relative areas plotted as a function of time. Trend lines represent loss of substrate and product apparition over time for a pseudo-first order kinetic reaction.

A set of ordinary differential equations (ODEs) consistent with Michaelis–Menten kinetics (Equations 2.3–6) was solved using the Runge-Kutta method with a method with a variable time step in MatLab (function ode45). Initial concentrations used for enzyme and substrate were 10 nM and 3 μM , respectively. Product and enzyme substrate complex were assumed to have initial concentrations of 0 μM . The resulting fitted curves for each species were optimized by iteratively testing k values that maximized R^2 . This yielded k_1 , k_{-1} , and k_2 values from which K_M and k_2/K_M values were derived.

$$\frac{d[E]}{dt} = -k_1[E][S] + k_{-1}[ES] + k_2[ES] \quad (2.3)$$

$$\frac{d[S]}{dt} = -k_1[E][S] + k_{-1}[ES] \quad (2.4)$$

$$\frac{d[ES]}{dt} = k_1[E][S] - k_{-1} - k_2[ES] \quad (2.5)$$

$$\frac{d[P]}{dt} = k_2[ES] \quad (2.6)$$

2.5.11 Inhibition Studies

Fluorescence real-time monitoring of enzymatic conversion of ${}^t\text{G}_N$ to ${}^t\text{X}_N$ with GDA in the presence of inhibitors was followed by emission spectroscopy by monitoring intensity signal at 450 nm with excitation at 328 nm. 5-aminoimidazole-4-carboxamide (AICA) was tested as an inhibitor in the enzymatic reaction for ${}^t\text{G}_N$ to ${}^t\text{X}_N$ using the same reaction conditions but supplemented with inhibitor concentrations of 0.1, 1, 10, 100, and 1000 μM . 4-aminoisothiazole-3-carboxamide (ATCA) was also tested as an inhibitor in the reaction under the same conditions but supplemented with inhibitor concentrations of 0.1, 1, 10, 100, 250 and 500 μM . 4-imidazolecarboxylic acid (ICA) was also tested as a potential inhibitor under the same reaction conditions with 10, 100, 1000, 2000, and 3000 μM concentrations. IC_{50} values were determined from plots of percent inhibition against respective inhibitor concentration on a logarithmic axis, fitted with sigmoidal Hill curves. All measurements were done in triplicate.

2.5.12 Docking of Guanine, Xanthine, and Analogs in GDA

Docking simulations were performed in Molecular Operating Environment (MOE) 2020 software suite. The crystal structure of Human guanine deaminase (guaD) in complex with zinc and its product Xanthine was obtained from the Protein Data Bank (PDB ID 2UZ9). The crystal structure was chosen because it contains the native product xanthine. The chosen ligands were placed by the Triangle Matcher method and ranked with the London dG values scoring function. A total of 30 poses were refined using the rigid receptor method. Then 5 poses were rescored using a GBVI/WSA dG scoring function. The pose with the ligand most closely aligned with the xanthine ligand was used for comparison and the $\Delta\Delta\text{G}$ value calculated for ${}^t\text{G}_N$ and ${}^h\text{G}_N$ with native

guanine as the reference and for ^{tz}X_N and thX_N with native xanthine as the reference, where ΔG_{ref} is the GBVI/WSA dG scoring of the reference native ligand and ΔG_{lig} is the GBVI/WSA dG scoring of the ligand analogs (Equation 2.7).

$$\Delta\Delta G = \Delta G_{ref} - \Delta G_{lig} \quad (2.7)$$

2.6 Acknowledgements

We thank the National Institutes of Health (through grant no. GM 069773) for generous support, the Chemistry & Biochemistry MS facility, and the UCSD X-ray Crystallography Facility (especially M. Gembicki and C. Moore). We also thank the Burkhardt Lab at UCSD for advice on protein expression and purification and R. Anand for helpful discussions and insight.

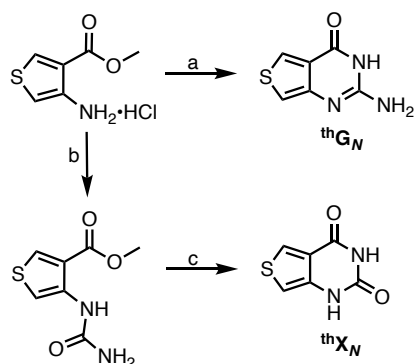
Chapter 2, in full, is a reprint of the material from: Marcela S. Bucardo, You Wu, Paul T. Ludford, Yao Li, Andrea Fin, and Yitzhak Tor. “Real-Time Monitoring of Human Guanine Deaminase Activity by an Emissive Guanine Analog.” *ACS Chem Biol.* **2021**; 16 (7): 1208-1214. doi: 10.1021/acscchembio.1c00232. Permission to use the materials from this manuscript was obtained by the American Chemical Society. The dissertation author was the primary researcher and author of this paper.

2.7 Supporting Information

2.7.1 Synthetic procedures

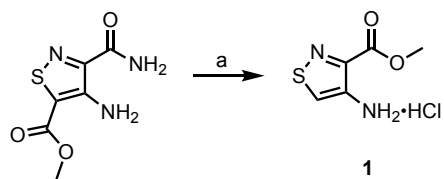
The nucleobase analogs ^{tz}G_N, ^{tz}X_N, thG_N, and thX_N and the starting precursor methyl 4-aminothiazole-3-carboxylate (1) were synthesized based on previously published procedures.¹⁻

4



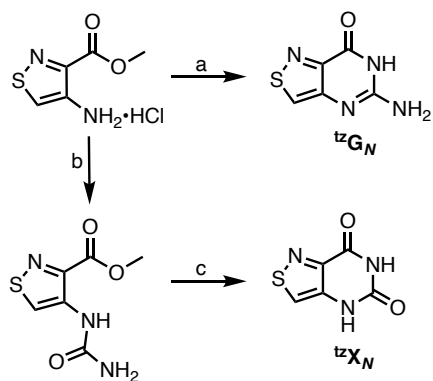
Scheme 2.S1 Synthesis of thienopyrimidine-based analogs, thG_N and thX_N.

(a) Chloroformamidine hydrochloride, DMSO₂, 125 °C, 2.5 h, 77%. (b) KOCN, Acetic acid, water, RT, overnight, 81%. (c) 1 M NaOMe in MeOH, RT, overnight, 70%.



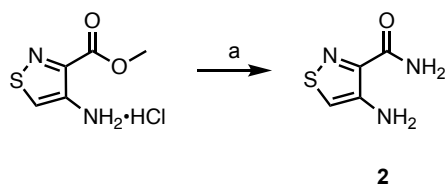
Scheme 2.S2 Synthesis of isothiazolepyrimidine precursor methyl 4-aminothiazole 3-carboxylate hydrochloride (1).

(a) i) HCl, 120 °C, 1.5 h. ii) H₂SO₄, MeOH, 65 °C, overnight, 66% over 2 steps.



Scheme 2.S3 Synthesis of isothiazolo-pyrimidine-based analogs, t^zG_N and t^zX_N , from precursor **4**.

(a) Chloroformamidine hydrochloride, DMSO, 125 °C, 2.5 h, 85%. (b) KOCN, Acetic acid, water, RT, overnight, 85%. (c) 1 M NaOMe in MeOH, RT, overnight, 82%.



Scheme 2.S4 Synthesis of 4-aminoisothiazole-3-carboxamide **2**, (ATCA).

(a) MeOH, NH₃, 60 °C, overnight, 87%.

4-aminoisothiazole 3-carboxamide (**2**)

Solid **1** (0.2 g, 0.1 mmol) is dissolved in cold anhydrous methanol (7 mL) in a 15 mL reaction vial with stir bar. Gaseous ammonia was bubbled through for 15 minutes and the vial was capped and left to stir overnight at 60 °C. The reaction was then evaporated to dryness and subjected to purification by column chromatography (0% MeOH to 5% MeOH in DCM) to yield a yellow powder (0.13 g, 87%). R_f: 0.33 (5% methanol in DCM). ¹H NMR (500MHz, DMSO-d₆): δ 7.84 (s, 1H), 7.61 (s, 1H), 7.46 (s, 1H), 5.73 (s 2H). ¹³C NMR (125MHz, DMSO-d₆): δ 164.86, 148.49, 147.02, 123.72. ESI-HRMS calculated for [C₄H₆N₃OS]⁺ 144.0226, found 144.0225.

2.7.2 X-Ray Crystal structures

2.1. Experimental summary

The single crystal x-ray diffraction studies were carried out on a Bruker Kappa APEX-II CCD diffractometer quipped with Cu K_{α} radiation ($\lambda = 1.5478$) or Mo K_{α} radiation ($\lambda = 0.71073$) at the UCSD Chemistry & Biochemistry Small Molecule X-ray facility. Crystal blocks were mounted on a Cryoloop with Paratone oil. Data were collected in a nitrogen gas stream at 100(2) K using ϕ and ω scans. The data were integrated using the Bruker SAINT software program and scaled using SADABS software program. Solution by direct methods (SHELXT) produced a complete phasing model system consistent with the proposed structure. All nonhydrogen atoms were refined anisotropically by full-matrix least-squares (SHELLXL-2014). All carbon bonded hydrogens were placed using a rigid model. Their positions were constrained relative to their parent atom using the appropriate HFIX command SHELLXL-2014. All other hydrogen atoms (H-bonding) were located in the difference map. Their relative positions were restrained using DFIX commands and their thermals freely refined.

Deposition numbers: 2073101, 2073102, 2073062, and 2073063.

Table 2.S1 Crystal Data and structure refinement for **thG_N**

Report date	2018-03-21	
Identification code	thG	
Empirical formula	C ₆ H ₅ N ₃ O S	
Molecular formula	C ₆ H ₅ N ₃ O S	
Formula weight	167.19	
Temperature	100.0 K	
Wavelength	1.54178 Å	
Crystal system	Monoclinic	
Space group	P 1 21/c 1	
Unit cell dimensions	a = 7.2425(6) Å	α = 90°.
	b = 14.8279(12) Å	β = 94.751(3)°.
	c = 12.8685(11) Å	γ = 90°.
Volume	1377.2(2) Å ³	
Z	8	
Density (calculated)	1.613 Mg/m ³	
Absorption coefficient	3.680 mm ⁻¹	
F(000)	688	
Crystal size	0.231 x 0.157 x 0.084 mm ³	
Crystal color, habit	Colorless Block	
Theta range for data collection	4.558 to 68.321°.	
Index ranges	-8 ≤ h ≤ 8, -17 ≤ k ≤ 17, -15 ≤ l ≤ 14	
Reflections collected	25913	
Independent reflections	2519 [R(int) = 0.0310, R(sigma) = 0.0171]	
Completeness to theta = 68.000°	99.8 %	
Absorption correction	Semi-empirical from equivalents	
Max. and min. transmission	0.3201 and 0.2149	
Refinement method	Full-matrix least-squares on F ²	
Data / restraints / parameters	2519 / 6 / 223	
Goodness-of-fit on F ²	1.062	
Final R indices [I > 2σ(I)]	R1 = 0.0301, wR2 = 0.0833	
R indices (all data)	R1 = 0.0319, wR2 = 0.0849	
Extinction coefficient	n/a	
Largest diff. peak and hole	0.256 and -0.267 e.Å ⁻³	

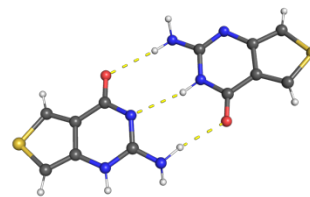


Table 2.S2 Crystal data and structure refinement for thX_N

Report date	2018-04-04
Identification code	THX01
Empirical formula	C ₆ H ₄ N ₂ O ₂ S
Molecular formula	C ₆ H ₄ N ₂ O ₂ S
Formula weight	168.17
Temperature	100.0 K
Wavelength	0.71073 Å
Crystal system	Monoclinic
Space group	P 1 21/c 1
Unit cell dimensions	a = 10.1968(16) Å α = 90°. b = 5.3149(8) Å β = 102.119(4)°. c = 12.257(2) Å γ = 90°.
Volume	649.48(18) Å ³
Z	4
Density (calculated)	1.720 Mg/m ³
Absorption coefficient	0.436 mm ⁻¹
F(000)	344
Crystal size	0.271 x 0.117 x 0.093 mm ³
Crystal color, habit	Colorless Block
Theta range for data collection	2.043 to 28.278°.
Index ranges	-13 ≤ h ≤ 13, -6 ≤ k ≤ 7, -16 ≤ l ≤ 13
Reflections collected	8784
Independent reflections	1596 [R(int) = 0.0582, R(sigma) = 0.0463]
Completeness to theta = 25.000°	100.0 %
Absorption correction	Semi-empirical from equivalents
Max. and min. transmission	0.2482 and 0.2096
Refinement method	Full-matrix least-squares on F ²
Data / restraints / parameters	1596 / 2 / 108
Goodness-of-fit on F ²	1.075
Final R indices [I > 2σ(I)]	R1 = 0.0376, wR2 = 0.0963
R indices (all data)	R1 = 0.0435, wR2 = 0.1004
Extinction coefficient	n/a
Largest diff. peak and hole	0.361 and -0.331 e.Å ⁻³

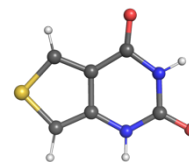


Table 2.S3 Crystal Data and structure refinement for ${}^{12}\text{G}_N$

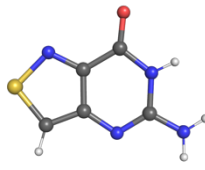
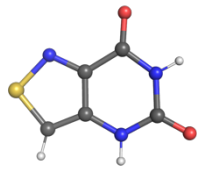
Report date	2018-07-10	
Identification code	tor119	
Empirical formula	C ₅ H ₄ N ₄ O S	
Molecular formula	C ₅ H ₄ N ₄ O S	
Formula weight	168.18	
Temperature	100.0 K	
Wavelength	0.71073 Å	
Crystal system	Monoclinic	
Space group	P 1 21/c 1	
Unit cell dimensions	a = 3.6599(2) Å b = 11.2567(5) Å c = 15.0364(7) Å	$\alpha = 90^\circ$. $\beta = 96.825(2)^\circ$. $\gamma = 90^\circ$.
Volume	615.09(5) Å ³	
Z	4	
Density (calculated)	1.816 Mg/m ³	
Absorption coefficient	0.457 mm ⁻¹	
F(000)	344	
Crystal size	0.03 x 0.005 x 0.005 mm ³	
Crystal color, habit	light yellow needle	
Theta range for data collection	2.266 to 26.720°.	
Index ranges	-4 ≤ h ≤ 4, -13 ≤ k ≤ 14, -18 ≤ l ≤ 18	
Reflections collected	9691	
Independent reflections	1303 [R(int) = 0.0555]	
Completeness to theta = 25.242°	100.0 %	
Absorption correction	Semi-empirical from equivalents	
Max. and min. transmission	0.7455 and 0.6591	
Refinement method	Full-matrix least-squares on F ²	
Data / restraints / parameters	1303 / 0 / 100	
Goodness-of-fit on F ²	1.046	
Final R indices [I > 2σ(I)]	R1 = 0.0337, wR2 = 0.0733	
R indices (all data)	R1 = 0.0471, wR2 = 0.0784	
Largest diff. peak and hole	0.332 and -0.314 e.Å ⁻³	

Table 2.S4 Crystal data and structure refinement for $^{12}\text{X}_N$

Report date	2018-07-11	
Identification code	tor120	
Empirical formula	C ₅ H ₃ N ₃ O ₂ S	
Molecular formula	C ₅ H ₃ N ₃ O ₂ S	
Formula weight	169.16	
Temperature	100.0 K	
Wavelength	0.71073 Å	
Crystal system	Monoclinic	
Space group	P 1 21/c 1	
Unit cell dimensions	a = 6.9522(10) Å b = 12.2384(17) Å c = 6.9021(10) Å	$\alpha = 90^\circ$. $\beta = 93.431(3)^\circ$. $\gamma = 90^\circ$.
Volume	586.20(14) Å ³	
Z	4	
Density (calculated)	1.917 Mg/m ³	
Absorption coefficient	0.488 mm ⁻¹	
F(000)	344	
Crystal size	0.12 x 0.08 x 0.04 mm ³	
Crystal color, habit	colorless block	
Theta range for data collection	2.935 to 26.736°.	
Index ranges	-8 ≤ h ≤ 8, 0 ≤ k ≤ 15, 0 ≤ l ≤ 8	
Reflections collected	1244	
Independent reflections	1244 [R(int) = 0.0362]	
Completeness to theta = 25.242°	100.0 %	
Absorption correction	Semi-empirical from equivalents	
Max. and min. transmission	0.491 and 0.402	
Refinement method	Full-matrix least-squares on F ²	
Data / restraints / parameters	1244 / 0 / 101	
Goodness-of-fit on F ²	1.036	
Final R indices [I > 2σ(I)]	R1 = 0.0362, wR2 = 0.0873	
R indices (all data)	R1 = 0.0456, wR2 = 0.0927	
Largest diff. peak and hole	0.409 and -0.459 e.Å ⁻³	

2.7.3 Absorption and emission spectroscopy

Table 2.S5 Complete photophysical properties of nucleobases

	solvent	λ_{abs}^a (ϵ^b)	λ_{em}^a (Φ)	Φ_{ϵ}	Stokes Shift ^c	Polarity sensitivity	pK_a (abs)
^{tz} G _N	water	320 (5.4±0.1)	446 (0.068±0.004)	351	8.88	125.3	3.28, 8.96
	dioxane	336 (5.1±0.1)	419 (0.026±0.001)	129	5.90		
^{tz} X _N	water	315 (6.1±0.1)	394 (0.018±0.001)	116	6.42	53.1	8.8
	dioxane	315 (6.4±0.01)	375 (0.001±0.001)	11	5.08		
th G _N	water	315 (3.0±0.1)	439 (0.40±0.04)	1179	8.97	137.4	4.41, 10.19
	dioxane	325 (3.0±0.1)	423 (0.40±0.05)	1182	7.18		
th X _N	water	308 (3.2±0.1)	420 (0.46±0.05)	1406	8.66	71.9	9.92
	dioxane	303 (3.6±0.1)	383 (0.065±0.002)	242	6.95		

^a λ_{abs} , max and λ_{em} , max are in nm. ^b ϵ is in $10^3 \text{ M}^{-1} \text{ cm}^{-1}$. ^c Stokes Shifts is in 10^3 cm^{-1} . Experiments done in triplicate.

Table 2.S6 E_T(30) experimental values for water:dioxane mixtures

water:dioxane	Reported E _T (30) (kcal mol ⁻¹)	Experimental E _T (30) th G _N and ^{tz} G _N , th X _N and ^{tz} X _N (kcal mol ⁻¹)
1:0	63.1	-
4:1	57.5	57.9, 57.5
3:2	55	54.8, 54.9
2:3	51.6	51.7, 51.6
1:4	48.3	47.7, 48.1
0:1	36.4	35.8, 36.5

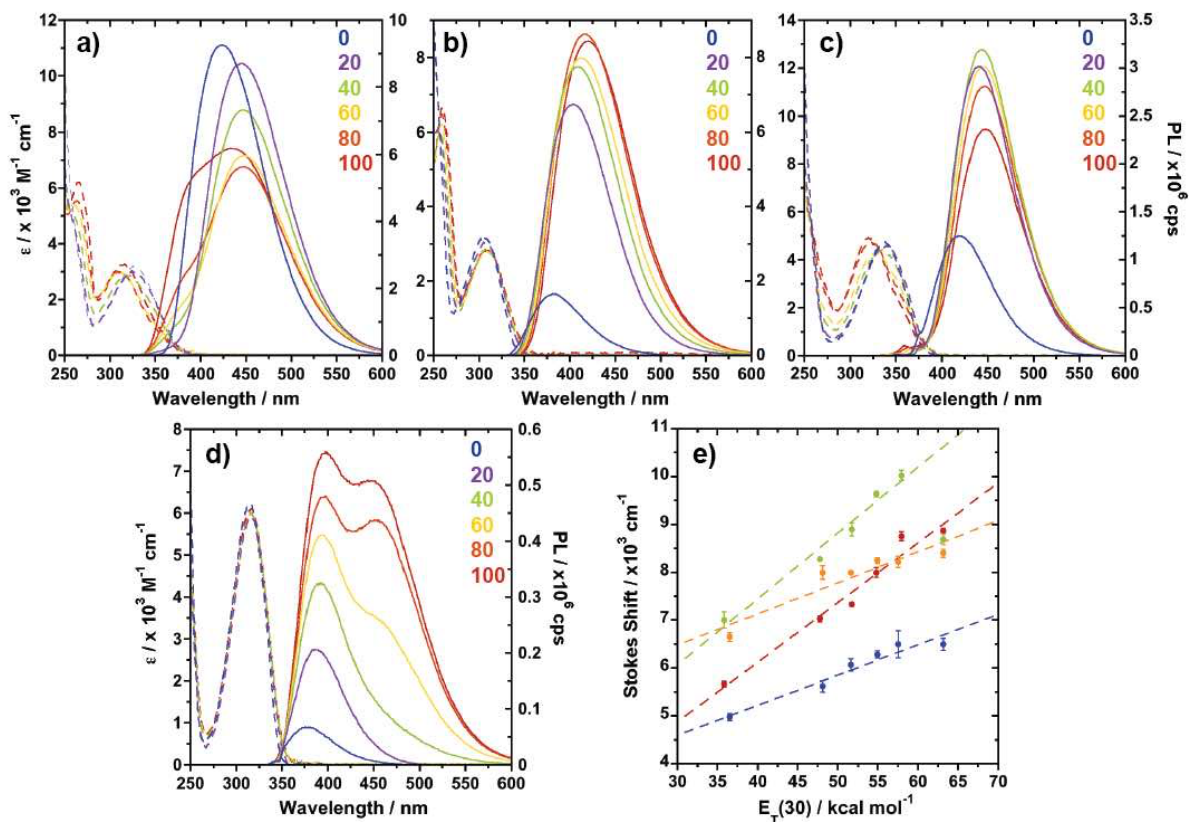


Figure 2.S1 Nucleobase absorption and emission traces in water:dioxane mixtures

Absorption (dashed lines) and emission (solid lines) traces in water/dioxane mixtures from 0 to 100% water for (a) ${}^{\text{th}}\text{G}_N$, (b) ${}^{\text{th}}\text{X}_N$, (c) ${}^{\text{tz}}\text{G}_N$, and (d) ${}^{\text{tz}}\text{X}_N$. (e) Stokes shift correlation versus solvent polarity [$E_{\text{T}}(30)$] of water/dioxane mixtures for ${}^{\text{th}}\text{G}_N$ (green), ${}^{\text{th}}\text{X}_N$ (red), ${}^{\text{tz}}\text{G}_N$ (blue), and ${}^{\text{tz}}\text{X}_N$ (orange)].).

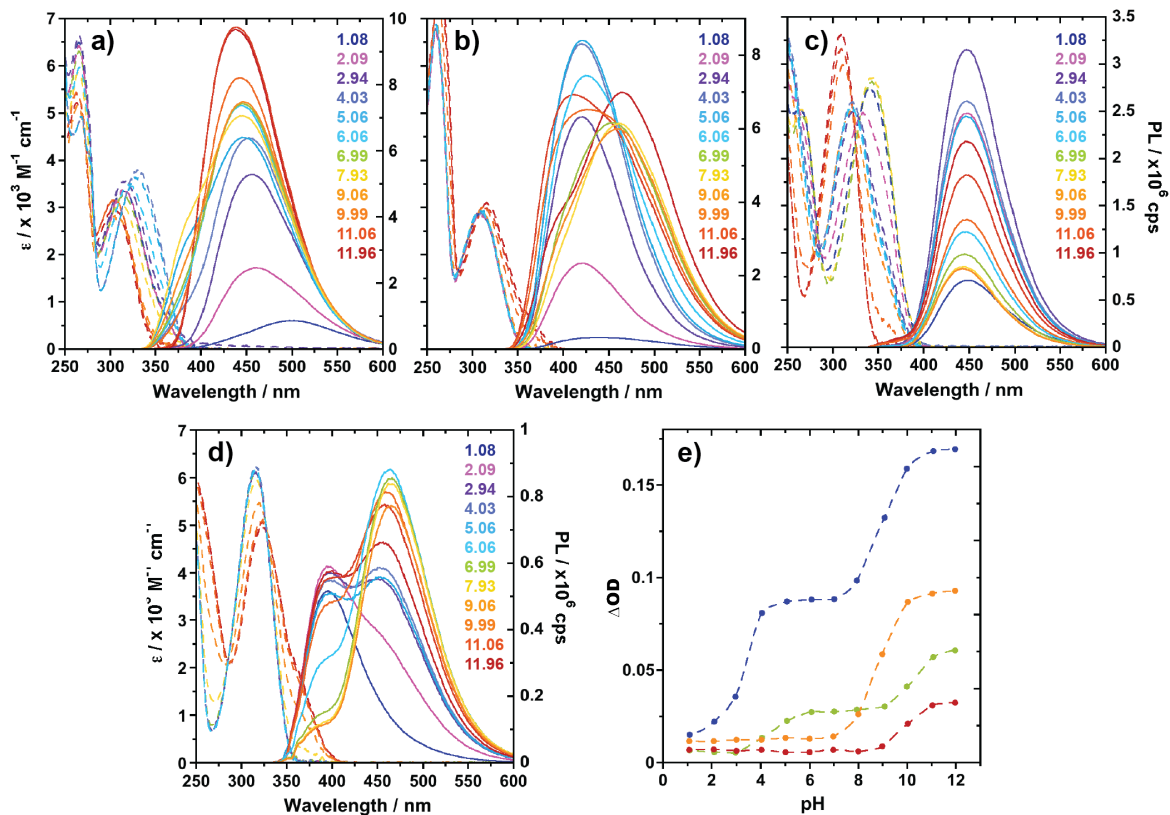


Figure 2.S2 Nucleobase absorption and emission traces in buffer solution at varying pH

Absorption (dashed lines) and emission (solid lines) traces in buffer solution of varying pH for (a) ${}^{\text{th}}\text{G}_N$, (b) ${}^{\text{th}}\text{X}_N$, (c) ${}^{\text{tz}}\text{G}_N$, (d) ${}^{\text{tz}}\text{X}_N$. (e) Change in optical density versus pH for ${}^{\text{th}}\text{G}_N$ (green), ${}^{\text{th}}\text{X}_N$ (red), ${}^{\text{tz}}\text{G}_N$ (blue), and ${}^{\text{tz}}\text{X}_N$ (orange).

2.7.4 Real-time monitoring of GDA reactions

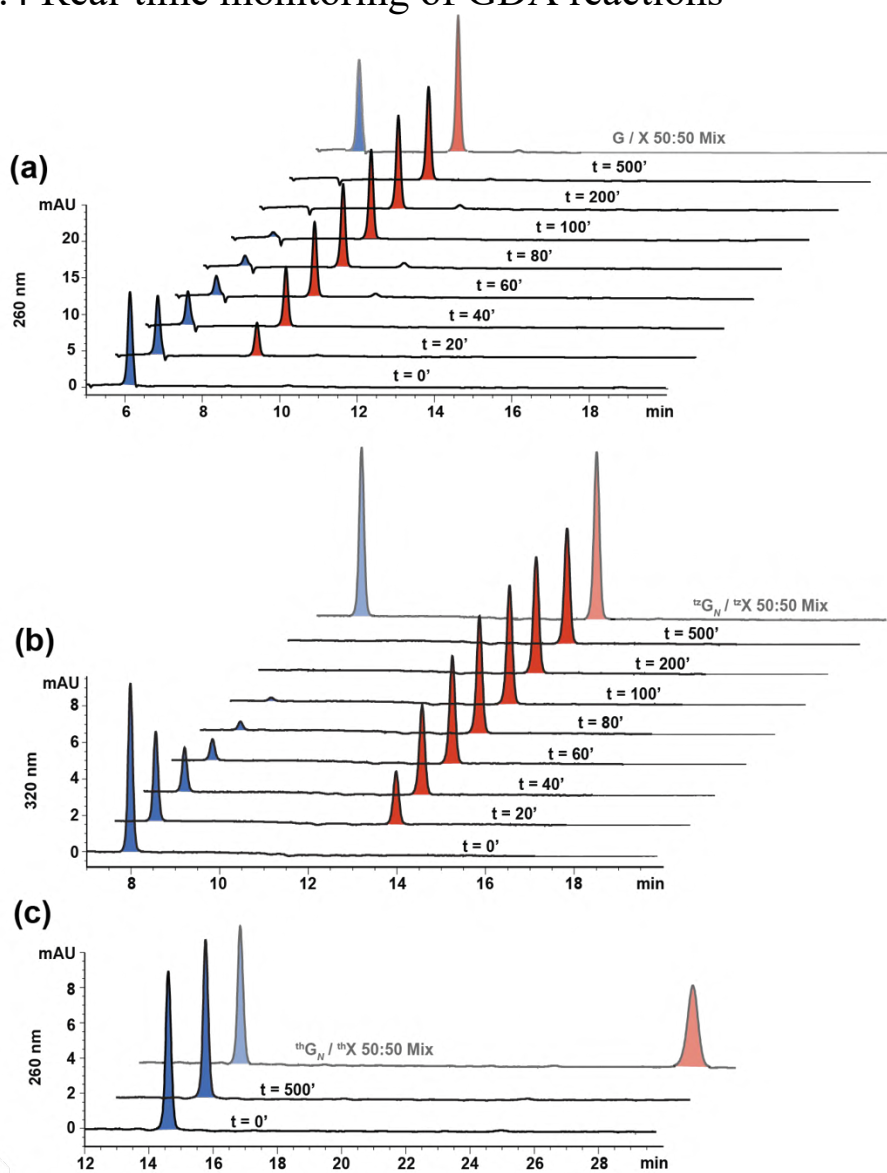


Figure 2.S3 GDA-mediated deamination analysis by HPLC

(a) Chromatogram shows enzymatic conversion of native guanine (blue) to xanthine (red) monitored at 260 nm. (b) Enzymatic conversion of $^{12}\text{G}_N$ (blue) to $^{12}\text{X}_N$ (red) monitored at 320 nm. (c) No enzymatic conversion of $^{13}\text{G}_N$ (blue) to $^{13}\text{X}_N$ (red) observed. Each data set shows a standard isomolar mixture of the starting material and product (transparent trace).

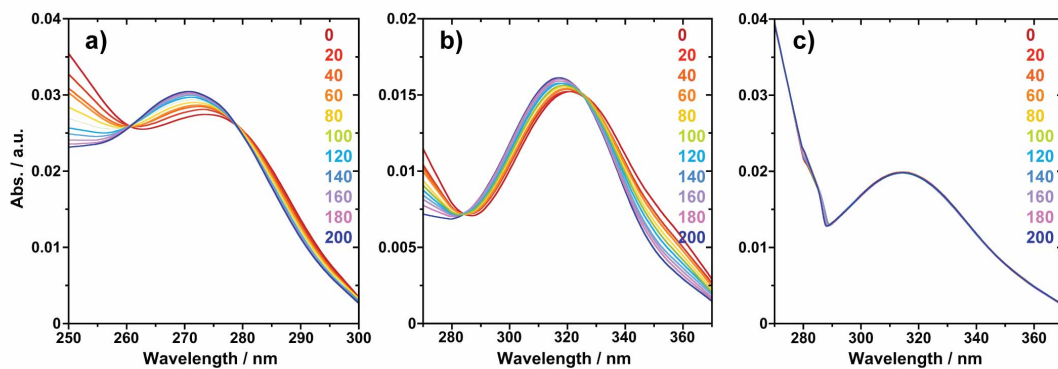


Figure 2.S4 Steady state absorption of guanine and analogs by GDA

Steady state absorption traces of enzymatic conversion of (a) guanine to xanthine, (b) $^{12}\text{G}_N$ to $^{12}\text{X}_N$, and (c) $^{13}\text{G}_N$, over time from 0 (red) to 200 seconds (blue) with measurements made every 20 seconds.

2.7.5 MOE docking results

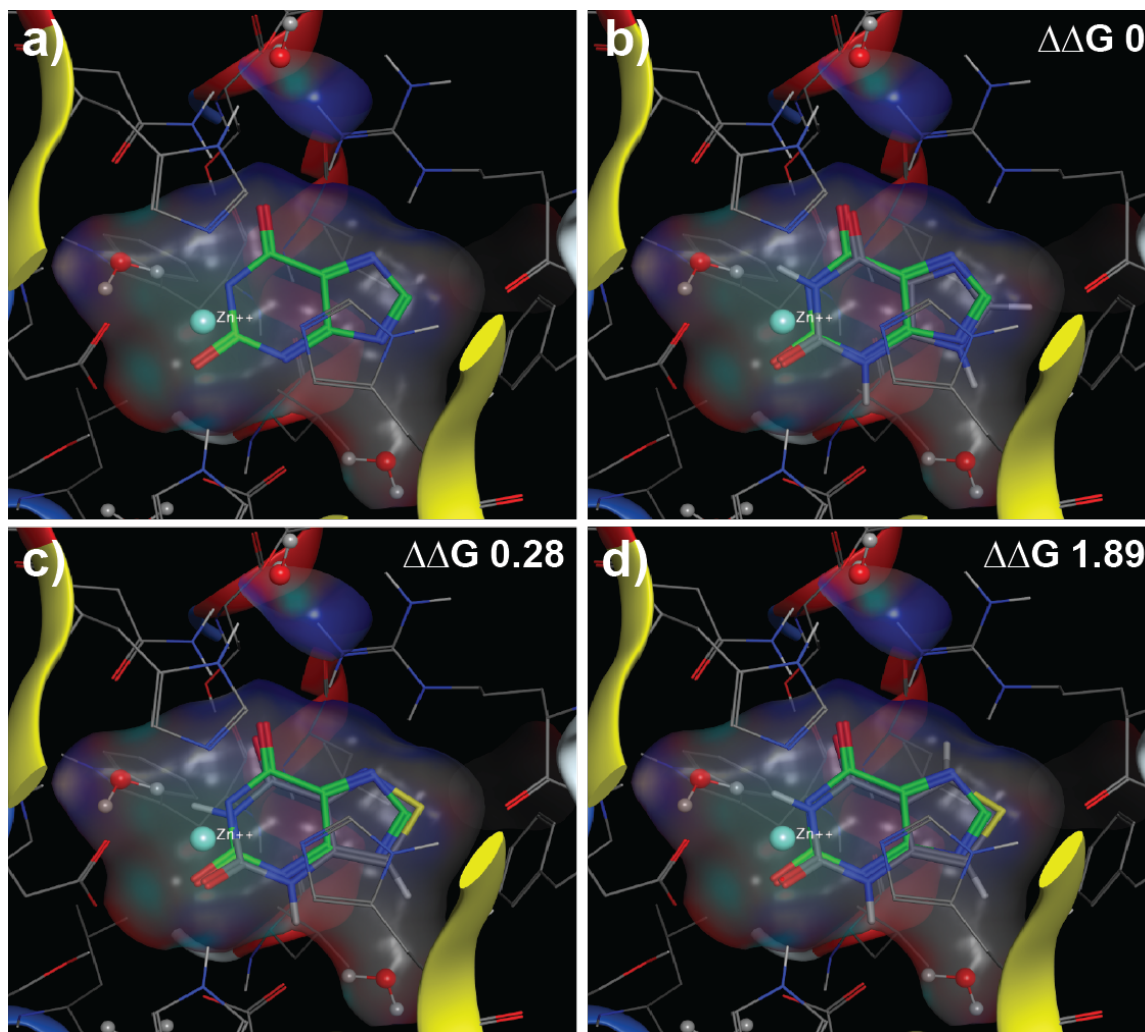


Figure 2.S5 MOE docking of xanthine and analogs in GDA active site

MOE docking images of xanthine and analogs in GDA active site (PDB 2UZ9) with calculated $\Delta\Delta G$ of docking (see methods) with xanthine as a reference. (a) Crystal structure active site with xanthine bound, (b) docking of native guanine, (c) docking of ${}^t\mathbf{X}_N$ with $\Delta\Delta G$ of 0.28, (d) and docking of ${}^{th}\mathbf{X}_N$ with more positive $\Delta\Delta G$ of 1.89 when compared to ${}^t\mathbf{X}_N$. ${}^{th}\mathbf{X}_N$ docking shows nucleobase analog structure deformation as well as steric hindrance at the position equivalent to the xanthine crystal substrate N7. The N7 moiety of ${}^t\mathbf{X}_N$ will likely hydrogen bond to Arg235, whereas the CH group of ${}^{th}\mathbf{X}_N$ is sterically hindered in the active site.

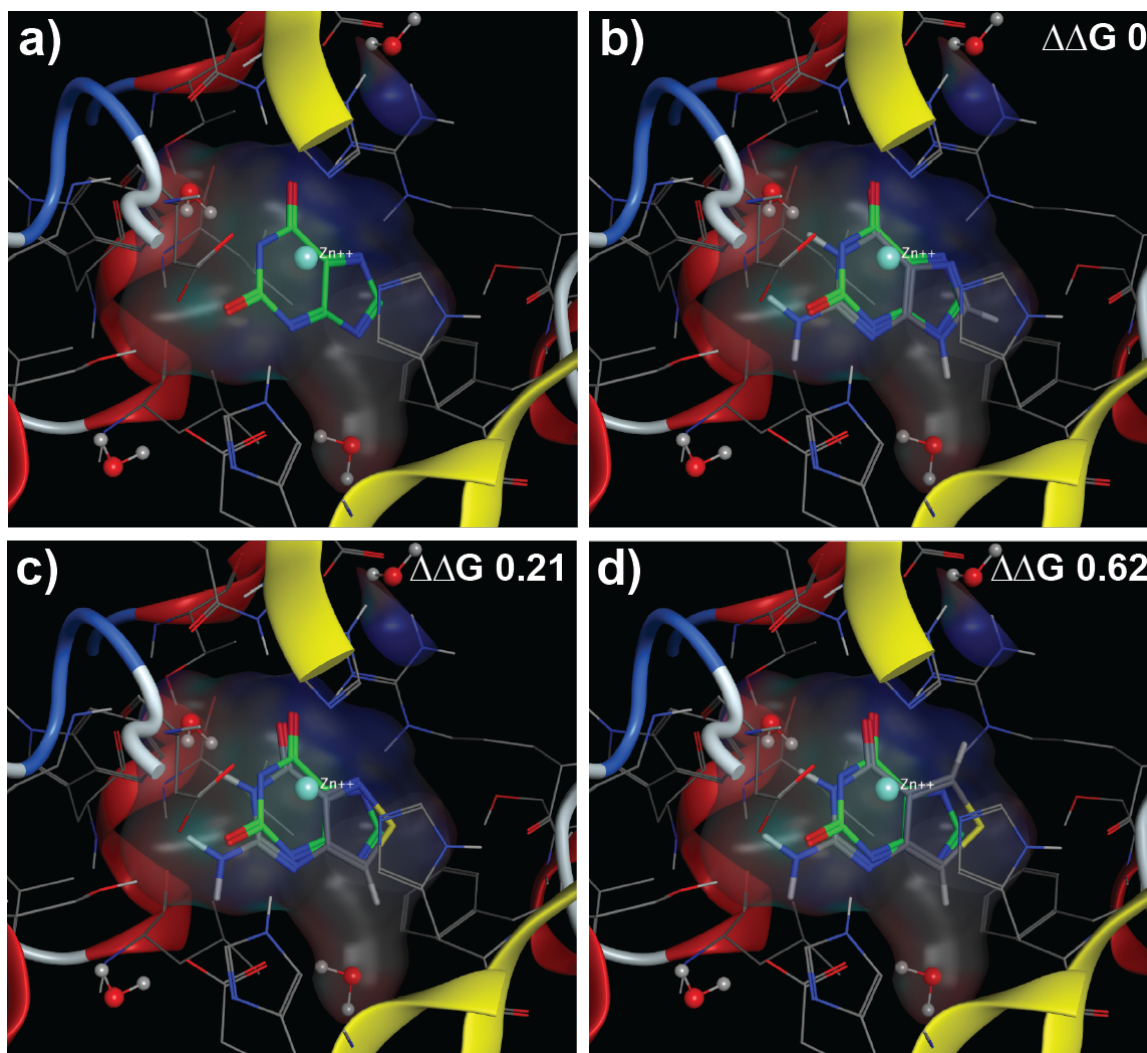


Figure 2.S6 MOE docking of guanine and analogs in GDA active site

MOE docking images of guanine and analogs in GDA active site (PDB ID 2UZ9) with calculated $\Delta\Delta G$ (see methods) of docking with guanine as a reference. (a) Crystal structure active site with xanthine bound, (b) docking of native guanine, (c) docking of ${}^{\text{t}z}\text{G}_N$ with $\Delta\Delta G$ of 0.21, and (d) docking of ${}^{\text{t}h}\text{G}_N$ with more positive $\Delta\Delta G$ of 0.62 when compared to ${}^{\text{t}z}\text{G}_N$. ${}^{\text{t}h}\text{G}_N$ docking shows nucleobase analog structure deformation as well as steric hindrance at the position equivalent to the xanthine crystal substrate N7, where the CH group of ${}^{\text{t}h}\text{G}_N$ is sterically hindered by Arg235 in the active site. Arg235 likely provides a basic site that favors the N7 moiety in ${}^{\text{t}z}\text{G}_N$ for substrate recognition.

2.7.6 Real-time monitoring of GDA and tzG with inhibitors

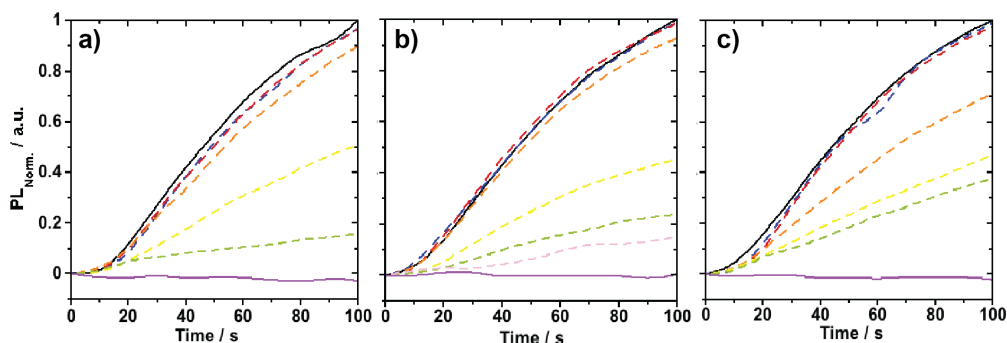


Figure 2.S7 Kinetics of AICA, ATCA, and ICA as GDA inhibitors

(a) Conversion of ${}^{\text{tz}}\text{G}_N$ to ${}^{\text{tz}}\text{X}_N$ by GDA in the presence of AICA at 0 (solid black), 0.1 (dashed blue), 1 (dashed red), 10 (dashed orange), 100 (dashed yellow), 1000 μM (green dashed), and finally 1000 μM without GDA (solid purple). (b) Conversion of ${}^{\text{tz}}\text{G}_N$ to ${}^{\text{tz}}\text{X}_N$ by GDA in the presence of ATCA at 0 (solid black), 0.1 (dashed blue), 1 (dashed red), 10 (dashed orange), 100 (dashed yellow), 250 (dashed green), 500 μM (dashed pink), and lastly 500 μM without GDA (solid purple). (c) Conversion of ${}^{\text{tz}}\text{G}_N$ to ${}^{\text{tz}}\text{X}_N$ by GDA in the presence of ICA at 0 (solid black), 10 (dashed blue), 100 (dashed red), 1000 (dashed orange), 2000 (dashed yellow), 3000 μM (dashed green), and lastly 3000 μM without GDA.

2.7.8 Supplementary references

- 1) Shin, D.; Sinkeldam, R. W.; Tor, Y. Emissive RNA Alphabet. *J. Am. Chem. Soc.* **2011**, *133* (38), 14912–14915.
- 2) Rovira, A. R.; Fin, A.; Tor, Y. Chemical Mutagenesis of an Emissive RNA Alphabet. *J. Am. Chem. Soc.* **2015**, *137* (46), 14602–14605.
- 3) Srivatsan, S. G.; Weizman, H.; Tor, Y. A Highly Fluorescent Nucleoside Analog Based on Thieno[3,4-d]Pyrimidine Senses Mismatched Pairing. *Org. Biomol. Chem.* **2008**, *6* (8), 1334–1338.
- 4) Rovira, A. R.; Fin, A.; Tor, Y. Expanding a Fluorescent RNA Alphabet: Synthesis, Photophysics and Utility of Isothiazole-Derived Purine Nucleoside Surrogates. *Chem. Sci.* **2017**, *8* (4), 2983–2993.

2.8 References

- (1) Gaded, V.; Anand, R. Nucleobase Deaminases: A Potential Enzyme System for New Therapies. *RSC Adv.* **2018**, *8* (42), 23567–23577.
- (2) Wang, J.; Bing, T.; Zhang, N.; Shen, L.; He, J.; Liu, X.; Wang, L.; Shangguan, D. The Mechanism of the Selective Antiproliferation Effect of Guanine-Based Biomolecules and Its Compensation. *ACS Chem. Biol.* **2019**, *14* (6), 1164–1173.
- (3) Slater, P. G.; Cammarata, G. M.; Monahan, C.; Bowers, J. T.; Yan, O.; Lee, S.; Lowery, L. A. Characterization of *Xenopus Laevis* Guanine Deaminase Reveals New Insights for Its Expression and Function in the Embryonic Kidney. *Dev. Dyn.* **2019**, *248* (4), 296–305.
- (4) Jung, J. M.; Noh, T. K.; Jo, S. Y.; Kim, S. Y.; Song, Y.; Kim, Y.-H.; Chang, S. E. Guanine Deaminase in Human Epidermal Keratinocytes Contributes to Skin Pigmentation. *Molecules* **2020**, *25* (11).
- (5) Paletzki, R. F. Cloning and Characterization of Guanine Deaminase from Mouse and Rat Brain. *Neuroscience* **2002**, *109* (1), 15–26.
- (6) Shek, R.; Hilaire, T.; Sim, J.; French, J. B. Structural Determinants for Substrate Selectivity in Guanine Deaminase Enzymes of the Amidohydrolase Superfamily. *Biochemistry* **2019**, *58* (30), 3280–3292.
- (7) Akum, B. F.; Chen, M.; Gunderson, S. I.; Riefler, G. M.; Scerri-Hansen, M. M.; Firestein, B. L. Cypin Regulates Dendrite Patterning in Hippocampal Neurons by Promoting Microtubule Assembly. *Nat. Neurosci.* **2004**, *7* (2), 145–152.
- (8) Rodríguez, A. R.; O’Neill, K. M.; Swiatkowski, P.; Patel, M. V.; Firestein, B. L. Overexpression of Cypin Alters Dendrite Morphology, Single Neuron Activity, and Network Properties via Distinct Mechanisms. *J. Neural Eng.* **2018**, *15* (1), 016020.
- (9) Swiatkowski, P.; Sewell, E.; Sweet, E. S.; Dickson, S.; Swanson, R. A.; McEwan, S. A.; Cuccolo, N.; McDonnell, M. E.; Patel, M. V.; Varghese, N.; Morrison, B.; Reitz, A. B.; Meaney, D. F.; Firestein, B. L. Cypin: A Novel Target for Traumatic Brain Injury. *Neurobiol. Dis.* **2018**, *119*, 13–25.
- (10) Zuccarini, M.; Giuliani, P.; Frinchi, M.; Mudò, G.; Serio, R. M.; Belluardo, N.; Buccella, S.; Carluccio, M.; Condorelli, D. F.; Caciagli, F.; Ciccarelli, R.; Di Iorio, P. Uncovering the Signaling Pathway behind Extracellular Guanine-Induced Activation of NO System: New Perspectives in Memory-Related Disorders. *Front. Pharmacol.* **2018**, *9*.
- (11) Wilson, D. K.; Rudolph, F. B.; Quijcho, F. A. Atomic Structure of Adenosine Deaminase Complexed with a Transition-State Analog: Understanding Catalysis and Immunodeficiency Mutations. *Science* **1991**, *252* (5010), 1278–1284.

- (12) Kinoshita, T.; Nakanishi, I.; Terasaka, T.; Kuno, M.; Seki, N.; Warizaya, M.; Matsumura, H.; Inoue, T.; Takano, K.; Adachi, H.; Mori, Y.; Fujii, T. Structural Basis of Compound Recognition by Adenosine Deaminase. *Biochemistry* **2005**, *44* (31), 10562–10569.
- (13) Bitra, A.; Biswas, A.; Anand, R. Structural Basis of the Substrate Specificity of Cytidine Deaminase Superfamily Guanine Deaminase. *Biochemistry* **2013**, *52* (45), 8106–8114.
- (14) Egeblad, L.; Welin, M.; Flodin, S.; Gräslund, S.; Wang, L.; Balzarini, J.; Eriksson, S.; Nordlund, P. Pan-Pathway Based Interaction Profiling of FDA-Approved Nucleoside and Nucleobase Analogs with Enzymes of the Human Nucleotide Metabolism. *PLOS ONE* **2012**, *7* (5), e37724.
- (15) Wojczewski, C.; Stolze, K.; Engels, J. W. Fluorescent Oligonucleotides - Versatile Tools as Probes and Primers for DNA and RNA Analysis. *Synlett* **1999**, *1999* (10), 1667–1678.
- (16) Hawkins, M. Fluorescent Pteridine Nucleoside Analogs: A Window on DNA Interactions. *Cell Biochem. Biophys.* **2001**, No. 34, 257–281.
- (17) Rist, M. J.; Marino, J. P. Fluorescent Nucleotide Base Analogs as Probes of Nucleic Acid Structure, Dynamics and Interactions. *Curr. Org. Chem.* **2002**, *6* (9), 775–793.
- (18) Millar, D. P. Fluorescence Studies of DNA and RNA Structure and Dynamics. *Curr. Opin. Struct. Biol.* **1996**, *6* (3), 322–326.
- (19) Okamoto, A.; Saito, Y.; Saito, I. Design of Base-Discriminating Fluorescent Nucleosides. *J. Photochem. Photobiol. C Photochem. Rev.* **2005**, *6*, 108–122.
- (20) Ranasinghe, R. T.; Brown, T. Fluorescence Based Strategies for Genetic Analysis. *Chem. Commun. Camb. Engl.* **2005**, No. 44, 5487–5502.
- (21) Silverman, A. P.; Kool, E. T. Detecting RNA and DNA with Templated Chemical Reactions. *Chem. Rev.* **2006**, *106* (9), 3775–3789.
- (22) Wilson, J. N.; Kool, E. T. Fluorescent DNA Base Replacements: Reporters and Sensors of Biological Systems. *Org. Biomol. Chem.* **2006**, *4* (23), 4265–4274.
- (23) Dodd, D.; Hudson, R. Intrinsically Fluorescent Base-Discriminating Nucleoside Analogs. *Mini-Rev. Org. Chem.* **2009**, *6*, 378–391.
- (24) Wilhelmsson, L. M. Fluorescent Nucleic Acid Base Analogues. *Q. Rev. Biophys.* **2010**, *43* (2), 159–183.
- (25) Wierzchowski, J.; Antosiewicz, J. M.; Shugar, D. 8-Azapurines as Isosteric Purine Fluorescent Probes for Nucleic Acid and Enzymatic Research. *Mol. Biosyst.* **2014**, *10* (11), 2756–2774.

- (26) Jones, A. C.; Neely, R. K. 2-Aminopurine as a Fluorescent Probe of DNA Conformation and the DNA-Enzyme Interface. *Q. Rev. Biophys.* **2015**, *48* (2), 244–279.
- (27) Wilhelmsson, M. *Fluorescent Analogs of Biomolecular Building Blocks: Design and Applications*; 2016.
- (28) Xu, W.; Chan, K. M.; Kool, E. T. Fluorescent Nucleobases as Tools for Studying DNA and RNA. *Nat. Chem.* **2017**, *9* (11), 1043–1055.
- (29) Saito, Y.; Hudson, R. H. E. Base-Modified Fluorescent Purine Nucleosides and Nucleotides for Use in Oligonucleotide Probes. *J. Photochem. Photobiol. C Photochem. Rev.* **2018**, *36*, 48–73.
- (30) Shin, D.; Sinkeldam, R. W.; Tor, Y. Emissive RNA Alphabet. *J. Am. Chem. Soc.* **2011**, *133* (38), 14912–14915.
- (31) Rovira, A. R.; Fin, A.; Tor, Y. Chemical Mutagenesis of an Emissive RNA Alphabet. *J. Am. Chem. Soc.* **2015**, *137* (46), 14602–14605.
- (32) Sinkeldam, R. W.; McCoy, L. S.; Shin, D.; Tor, Y. Enzymatic Interconversion of Isomorphic Fluorescent Nucleosides: Adenosine Deaminase Transforms an Adenosine Analogue into an Inosine Analogue. *Angew. Chem. Int. Ed.* **2013**, *52* (52), 14026–14030.
- (33) Ludford, P. T.; Rovira, A. R.; Fin, A.; Tor, Y. Fluorescing Isofunctional Ribonucleosides: Assessing Adenosine Deaminase Activity and Inhibition. *ChemBioChem* **2019**, *20* (5), 718–726.
- (34) Adamek, R. N.; Ludford, P.; Duggan, S. M.; Tor, Y.; Cohen, S. M. Identification of Adenosine Deaminase Inhibitors by Metal-Binding Pharmacophore Screening. *ChemMedChem* **2020**, *15* (22), 2151–2156.
- (35) Srivatsan, S. G.; Weizman, H.; Tor, Y. A Highly Fluorescent Nucleoside Analog Based on Thieno[3,4-d]Pyrimidine Senses Mismatched Pairing. *Org. Biomol. Chem.* **2008**, *6* (8), 1334–1338.
- (36) Rovira, A. R.; Fin, A.; Tor, Y. Expanding a Fluorescent RNA Alphabet: Synthesis, Photophysics and Utility of Isothiazole-Derived Purine Nucleoside Surrogates. *Chem. Sci.* **2017**, *8* (4), 2983–2993.
- (37) Gewald, K.; Bellmann, P. Synthese und Reaktionen von 4-Aminoisothiazolen. *Liebigs Ann. Chem.* **1979**, *1979* (10), 1534–1546.
- (38) Rogstad, K. N.; Jang, Y. H.; Sowers, L. C.; Goddard, W. A. First Principles Calculations of the PKa Values and Tautomers of Isoguanine and Xanthine. *Chem. Res. Toxicol.* **2003**, *16* (11), 1455–1462.

- (39) Didier, P.; Kuchlyan, J.; Martinez-Fernandez, L.; Gosset, P.; Léonard, J.; Tor, Y.; Improta, R.; Mély, Y. Deciphering the PH-Dependence of Ground- and Excited-State Equilibria of Thienoguanine. *Phys. Chem. Chem. Phys.* **2020**, *22* (14), 7381–7391.
- (40) Lewis, A. S.; Glantz, M. D. Rabbit Liver Guanine Deaminase. Chemical, Physical, and Kinetic Properties. *J. Biol. Chem.* **1974**, *249* (12), 3862–3866.
- (41) Bergstrom, J. D.; Bieber, A. L. Characterization of Purified Guanine Aminohydrolase. *Arch. Biochem. Biophys.* **1979**, *194* (1), 107–116.
- (42) Chakraborty, S.; Shah, N. H.; Fishbein, J. C.; Hosmane, R. S. A Novel Transition State Analogue Inhibitor of Guanase Based on Azepinomycin Ring Structure: Synthesis and Biochemical Assessment of Enzyme Inhibition. *Bioorg. Med. Chem. Lett.* **2011**, *21* (2), 756–759.

CHAPTER 3: Fluorescent Probes for O^6 -Alkylguanine-DNA-

Transferase Activity and Microscopy in Living Cells

3.1 Abstract

Human O^6 -Alkylguanine-DNA-transferase (hAGT) is a repair protein that provides protection from mutagenic events caused by O^6 -alkylguanine lesions. In a single step, an active site nucleophilic cysteine residue displaces the O^6 -alkyl group and restores guanine. As this stoichiometric activity is tissue specific, indicative of tumor status, and correlated to chemotherapeutic success, tracking activity of hAGT could prove informative for disease diagnosis and therapy. Herein, we explore two families of emissive O^6 -methyl- and O^6 -benzylguanine analogs based on our previously described ${}^{\text{th}}\text{G}_N$ and ${}^{\text{tz}}\text{G}_N$, a thieno- and isothiazolo-guanine surrogates, respectively, as potential reporters. We establish that **O^6 -Bn ${}^{\text{th}}\text{G}_N$** and **O^6 -Bn ${}^{\text{tz}}\text{G}_N$** provide a spectral window to optically monitor hAGT activity, can be used as substrates for the widely used SNAP-Tag delivery system, and are sufficiently bright for visualization in mammalian cells using fluorescence microscopy.

3.2 Introduction

DNA alkylation can be caused by both endogenous and exogenous agents. Cellular repair mechanisms exist to evade the potentially mutagenic outcomes from such nucleobase modifications thus maintaining genome integrity.¹⁻³ Human O^6 -Alkylguanine-DNA-transferase (hAGT) is a repair protein that protects DNA from O^6 -alkylguanine lesions.⁴⁻⁵ Mechanistically, hAGT acts by irreversibly transferring an alkyl group at the O^6 position of the damaged guanine nucleobase to a cysteine residue in the protein active site to form a stable thioester and restore the

native purine.⁶ hAGT thus is a *kamikaze* or suicide protein, meaning that each repair event tags the protein for degradation. Although *O6* alkylation of guanine is not the most common guanine modification, hAGT's stoichiometric reaction suggests a highly important protective activity.⁷

The cellular activity of hAGT has been associated with disease progression and therapeutic susceptibility of various cancers.⁸ Classical chemotherapeutic agents alkylate DNA, causing cytotoxicity, implying potential resistance if hAGT activity is upregulated. Glioblastoma, for example, the most common type of malignant brain tumors, is treated with temozolomide, a methylating agent. Its efficacy is diminished, however, with elevated hAGT activity. As hAGT activity is tissue-dependent and varies with disease progression, having a simple and real time fluorogenic detection to measure its activity could prove useful.⁹ Furthermore, hAGT was engineered to function as a highly specific protein self-labeling tag, coined SNAP-Tag. By adorning the benzyl moiety of guanine with an emissive dye, for example, the SNAP-Tag and a genetically fused protein can be labeled for diverse biotechnological applications.¹⁰⁻¹²

Our lab has developed two fluorescent RNA alphabets based on the thieno[3,4-*d*]pyrimidine (thN) and isothiazolo[4,3-*d*]pyrimidine (^{tz}N) heterocyclic cores (Figure 3.1a).¹³⁻¹⁴ Their isomorphic character provides biochemically active nucleoside surrogates, which are endowed with useful photophysical features, absent in their native counterparts. These compounds have served as powerful biophysical tools for exploring cellular processes involving nucleosides, nucleotide cofactors, and secondary messengers.¹⁵⁻²⁷ The nucleobase heterocycles were utilized for the first time to monitor the activity of human guanine deaminase.²⁸ Rewardingly, guanine deaminase deaminates ^{tz}G_N, the guanine surrogate, to the corresponding xanthine analog, ^{tz}X_N, with reaction rates corresponding to the native substrates (Figure 3.1b). The enzymatic deamination of ^{tz}G_N could be tracked via emission change as the substrate and product display

distinct spectroscopic signatures. Similarly, we set to investigate the substrate recognition of hAGT with the thieno, **O⁶-BnthG_N** and **O⁶-MethG_N**, and isothiazolo, **O⁶-Bn^{tz}G_N** and **O⁶-Me^{tz}G_N**, *O*6 alkyl guanine analogs (Figure 3.1c). We began by establishing synthetic methods to activate the previously published thG_N and ^{tz}G_N at their respective *O*6 positions, analyzed the photophysical signatures of the new compounds, and assessed the tolerance of hAGT active site to the alkyl guanine surrogates. To further exemplify the utility of these analogs we tested them with the SNAP-Tag and evaluated their utility for live-cell imaging in mammalian cells. We observed that both benzylated nucleobases **O⁶-BnthG_N** and **O⁶-Bn^{tz}G_N** provide a spectral window to optically monitor hAGT activity and can be used as substrates for the widely used SNAP-Tag delivery system. Additionally, both benzylated derivatives show uptake by mammalian cells and are sufficiently bright for visualization by fluorescence microscopy.

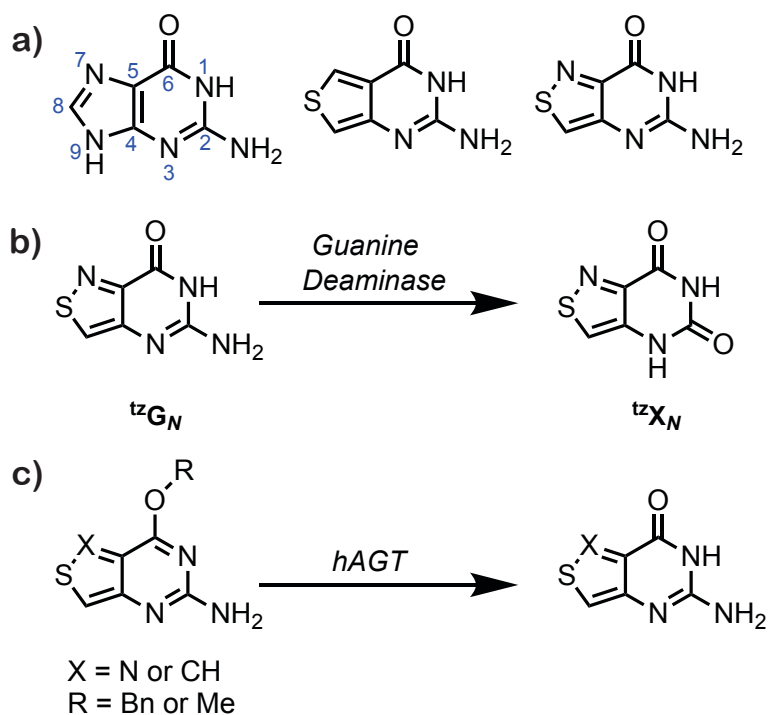


Figure 3.1 Structures of guanine, ${}^{\text{th}}\mathbf{G}_N$, and ${}^{\text{tz}}\mathbf{G}_N$. GDA and hAGT reactions

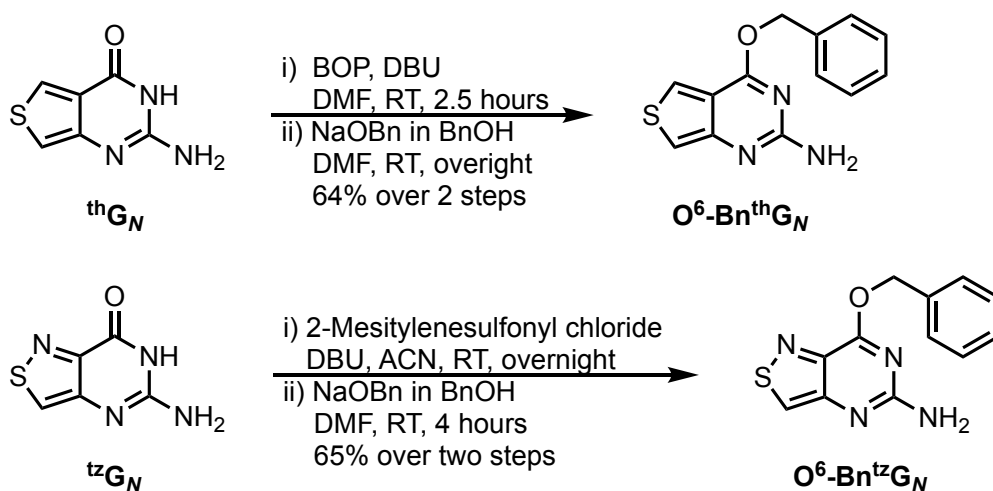
Structures of native guanine (displaying the conventional purine numbering system), as well as ${}^{\text{th}}\mathbf{G}_N$, and ${}^{\text{tz}}\mathbf{G}_N$. b) Guanine deaminase converts ${}^{\text{tz}}\mathbf{G}_N$ to ${}^{\text{tz}}\mathbf{X}_N$. c) Potential conversion of O^6 -benzylguanine analogs ($O^6\text{-Bn}{}^{\text{th}}\mathbf{G}_N$ and $O^6\text{-Me}{}^{\text{th}}\mathbf{G}_N$ or $O^6\text{-Bn}{}^{\text{tz}}\mathbf{G}_N$ and $O^6\text{-Me}{}^{\text{tz}}\mathbf{G}_N$) to the respective guanine analogs (${}^{\text{th}}\mathbf{G}_N$ or ${}^{\text{tz}}\mathbf{G}_N$) by hAGT.

3.3 Results and Discussion

Emissive guanine analogs containing either a thienopyrimidine-core, ${}^{\text{th}}\mathbf{G}_N$, or an isothiazolepyrimidine-core, ${}^{\text{tz}}\mathbf{G}_N$, were prepared according to previously reported procedures.^{13–14} Briefly, either the commercially available methyl 4-aminothiophene 3-carboxylate hydrochloride or synthesized 4-aminoisothiazole-3-carboxamide hydrochloride²⁹ were cyclized with chloroformamide hydrochloride in DMSO_2 at 125°C to yield ${}^{\text{th}}\mathbf{G}_N$, or ${}^{\text{tz}}\mathbf{G}_N$, respectively. These core structures served as the starting materials for synthesizing the O^6 -alkylated guanine analogs.

The alkylated guanine surrogates of interest were the O^6 -benzyl derivative, as it is most favorable substrate for hAGT and the specific substrate engineered for the SNAP-Tag protein, and the O^6 -methyl derivative, as it is the most biologically relevant alkylated guanine. Classically,

such derivatives have been prepared via a Mitsunobu reaction. In the case of our thienopyrimidine and isothiazolopyrimidine heterocycles, however, Mitsunobu reactions yielded mixtures of *N*1-, *exo N*2- and only traces of *O*6 alkylated products, or only *N*1- and *exo N*2- alkylated products, respectively (note, for simplicity, the conventional numbering of the purine system is used as shown in Figure 3.1a). Alternative reported methods were thus employed as summarized for the *O*6-benzyl derivatives in Scheme 1 and *O*6-methyl derivatives in Scheme S3.1. To activate thG_N at its carbonyl, benzotriazole-1-yloxytris(dimethylamino)phosphonium hexafluorophosphate (BOP) and DBU were used followed by the addition of 0.5 M sodium benzyloxide in benzyl alcohol or 1 M sodium methoxide in methanol to afford **O⁶-BnthG_N** and **O⁶-MethG_N** in 64% and 86% yields, respectively.³⁰ To produce the isothiazolopyrimidine derivatives, ^{tz}G_N was activated by producing a DMAP-^{tz}G_N salt using DMAP, 2-mesitylenesulfonyl, and DBU and then exposing the activated salt to 0.5 M sodium benzyloxide in benzyl alcohol or 1 M sodium methoxide in methanol, to yield **O⁶-Bn^{tz}G_N** and **O⁶-Me^{tz}G_N** in 65% and 75% yields, respectively (Scheme 3.1).³¹



Scheme 3.1 Synthesis of *O*6-benzyl thieno- and isothiazolo-guanine analogs

To evaluate whether the alkylated (i.e., the enzyme substrate) and the corresponding parent heterocycle (i.e., the product) (Figure 3.2a) are photophysically distinguishable, their spectroscopic properties were evaluated in water. As seen in Figure 2b-c and summarized in Table 1, the absorption and emission spectra of the two families of heterocycles show substantial shifts when alkylated and offer means to distinguish substrates from reaction products. The guanine analogs, thG_N and ^{tz}G_N, were previously shown to have bathochromic-shifted absorption and emission maxima when compared to their native counterparts in water (λ_{max} 315 and 320 nm, $\lambda_{\text{em,max}}$ 439 and 446 nm, respectively).²⁸ The *O*-alkylation caused additional red-shifting for both heterocyclic families, showing absorption maxima at 337, 338, 350, and 349 nm for **O⁶-BnthG_N**, **O⁶-MethG_N**, **O⁶-Bn^{tz}G_N**, and **O⁶-Me^{tz}G_N**, respectively. Similarly, fluorescence spectroscopy shows substantial changes that provide different photophysical fingerprints for each derivative, with emission maxima at 460, 465, 460, and 459 nm, for **O⁶-BnthG_N**, **O⁶-MethG_N**, **O⁶-Bn^{tz}G_N**, and **O⁶-Me^{tz}G_N**, respectively.

Table 3.1 Photophysical data of nucleobase analogs in water

	$\lambda_{\text{abs,max}}^{\text{a}}$	ϵ^{b}	$\lambda_{\text{em,max}}^{\text{a}}$	ϕ	$\epsilon\phi$
th G _N ^c	315	3.0 ± 0.1	439	0.40 ± 0.04	1200
O⁶-BnthG_N	337	3.2 ± 0.02	460	0.42 ± 0.01	1344
O⁶-MethG_N	338	3.1 ± 0.03	465	0.85 ± 0.01	2635
^{tz} G _N ^c	320	5.4 ± 0.1	446	0.07 ± 0.01	378
O⁶-Bn^{tz}G_N	350	5.8 ± 0.02	460	0.83 ± 0.01	4814
O⁶-Me^{tz}G_N	349	5.6 ± 0.03	459	0.83 ± 0.01	4648

^a $\lambda_{\text{abs,max}}$ and $\lambda_{\text{em,max}}$ are in nm. ^b ϵ is in 10³ M⁻¹ cm⁻¹. Measured in triplicate in water. ^cPreviously reported values.

All derivatives, excluding thG_N, exhibit classically shaped emission bands (Figure 3.1b). In contrast, the thiophenopyrimidine thG_N analog populates two tautomeric forms in H-bonding-capable solvents, such as water, and displays a blue-shifted shoulder. Spectral deconvolution of

the absorption and emission spectra previously showed that each tautomer can be selectively excited. The long and short emitting tautomer forms have been attributed to the keto-amino tautomers ${}^{\text{th}}\text{G}_N\text{-1H}$ and ${}^{\text{th}}\text{G}_N\text{-3H}$, respectively (Figure 3.1a).³²⁻³³ Once ${}^{\text{th}}\text{G}_N$ is alkylated at the O6 position, the structure is locked into one favorable tautomeric form thus displaying only the red-shifted emission band. All alkylated products showed a higher emission quantum yield compared to the parent non-alkylated heterocycles. $\text{O}^6\text{-Bn}{}^{\text{th}}\text{G}_N$ displayed a modest increase to 0.42 from the non-alkylated precursor ${}^{\text{th}}\text{G}_N$ at 0.40, while $\text{O}^6\text{-Me}{}^{\text{th}}\text{G}_N$ showed a substantial increase to 0.85. Both $\text{O}^6\text{-Bn}{}^{\text{tz}}\text{G}_N$ and $\text{O}^6\text{-Me}{}^{\text{tz}}\text{G}_N$ showed much higher emission quantum yield compared to the non-alkylated precursor ${}^{\text{tz}}\text{G}_N$ ($\phi = 0.83$ and 0.07 , respectively). The alkylated derivatives portray comparable molar absorptivity to the non-alkylated parent molecule; however, the increase in emission quantum yield observed for $\text{O}^6\text{-Me}{}^{\text{th}}\text{G}_N$, $\text{O}^6\text{-Bn}{}^{\text{tz}}\text{G}_N$, and $\text{O}^6\text{-Me}{}^{\text{tz}}\text{G}_N$, consequently produces a substantial relative increase in apparent brightness. The apparent brightness increases over two-fold for $\text{O}^6\text{-Me}{}^{\text{th}}\text{G}_N$ compared to ${}^{\text{th}}\text{G}_N$ and over four-fold for $\text{O}^6\text{-Bn}{}^{\text{tz}}\text{G}_N$, and $\text{O}^6\text{-Me}{}^{\text{tz}}\text{G}_N$ compared to ${}^{\text{tz}}\text{G}_N$.

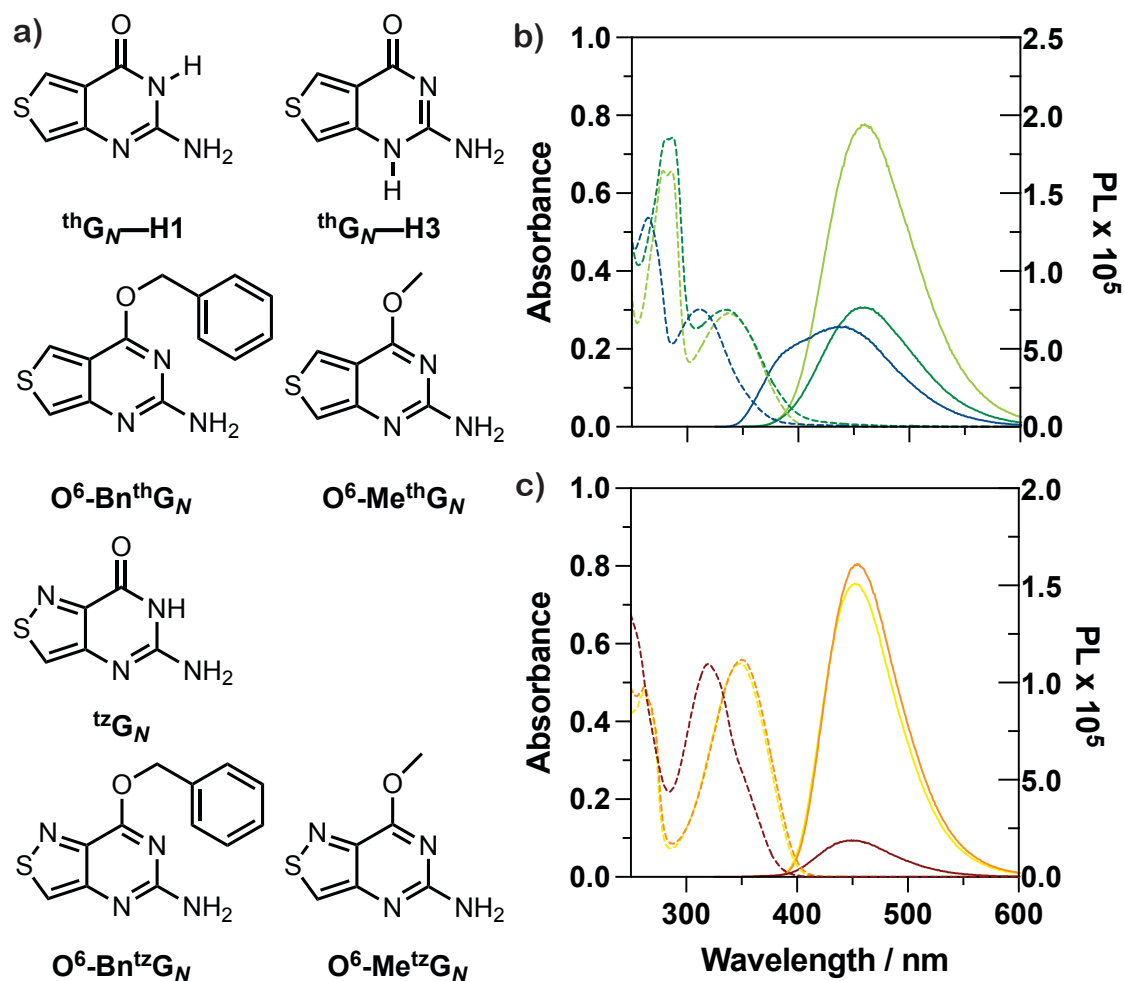


Figure 3.2 ${}^{\text{th}}\text{G}_N$, ${}^{\text{tz}}\text{G}_N$, and alkylated derivative structures and spectra

a) Structures of ${}^{\text{th}}\text{G}_N\text{-H1}$, ${}^{\text{th}}\text{G}_N\text{-H3}$, $\text{O}^6\text{-Bn}{}^{\text{th}}\text{G}_N$, $\text{O}^6\text{-Me}{}^{\text{th}}\text{G}_N$, ${}^{\text{tz}}\text{G}_N$, $\text{O}^6\text{-Bn}{}^{\text{tz}}\text{G}_N$, and $\text{O}^6\text{-Me}{}^{\text{tz}}\text{G}_N$ nucleobase analogs. b) Absorption (dashed lines) and emission (solid lines) of ${}^{\text{th}}\text{G}_N$ (blue), $\text{O}^6\text{-Bn}{}^{\text{th}}\text{G}_N$ (dark green), $\text{O}^6\text{-Me}{}^{\text{th}}\text{G}_N$ (lime). c) Absorption (dashed lines) and emission (solid lines) of ${}^{\text{tz}}\text{G}_N$ (red), $\text{O}^6\text{-Bn}{}^{\text{tz}}\text{G}_N$ (orange), and $\text{O}^6\text{-Me}{}^{\text{tz}}\text{G}_N$ (yellow).

To test the alkylated derivatives as hAGT and SNAP-tag substrates and assess their utility to track dealkylation reactions, they were subjected to the corresponding commercially available recombinant proteins (see Procedures). The reactions were run in DPBS buffer at 37 °C and monitored by fluorescence spectroscopy via excitation at the isosbestic point of each pair of compounds under the same conditions. Given the different spectroscopic characteristics of the

alkylated vs. the non-alkylated parent heterocycles, tracking of the substrate to product conversion should show a time-dependent change in emission.

Rewardingly, **O⁶-BnthG_N** and **O⁶-Bn^{tz}G_N** show a change in emission intensity at a single wavelength when exposed to hAGT. An increase in emission at 400 nm is seen for **O⁶-BnthG_N**. This increase is consistent with its transformation to thG_N, and the emission signal associated with the short emitting tautomer unavailable to the locked reaction substrate. A decrease in emission at 450 nm is seen for **O⁶-Bn^{tz}G_N**, consistent with transformation to the less bright ^{tz}G_N. No emission changes were observed for **O⁶-MethG_N** and **O⁶-Me^{tz}G_N** (Figure 3.3). Reaction *t*_{1/2} values were calculated assuming a pseudo-first order reaction kinetics for the dealkylation of both benzylated analogs to the corresponding “repaired” thiophenopyrimidine or isothiazolepyrimidine nucleobase (*t*_{1/2} = 173 and 50 s for **O⁶-BnthG_N**; and **O⁶-Bn^{tz}G_N**, respectively, Table 3.2).

Table 3.2 AGT and SNAP-Tag reaction rates

	$\lambda_{\text{exc}}^{\text{a}} / \lambda_{\text{mnt}}^{\text{a}}$	AGT		SNAP-Tag	
		$k_{\text{app}}^{\text{b}}$	<i>t</i> _{1/2} ^c	$k_{\text{app}}^{\text{b}}$	<i>t</i> _{1/2} ^c
O⁶-BnthG_N to th G _N	321 / 400	0.004	173	0.011	63
O⁶-MethG_N to th G _N	325 / 400	NR	NR	NR	NR
O⁶-Bn^{tz}G_N to ^{tz} G _N	334 / 450	0.014	50	0.005	139
O⁶-Me^{tz}G_N to ^{tz} G _N	334 / 450	NR	NR	NR	NR

^a λ_{exc} and λ_{mnt} reported in nm and represent the wavelength for excitation and wavelength monitored, respectively. ^b k_{app} pseudo-first order rate constant. ^cReaction half-life calculated assuming pseudo-first-order kinetics. Experiments done in triplicate.

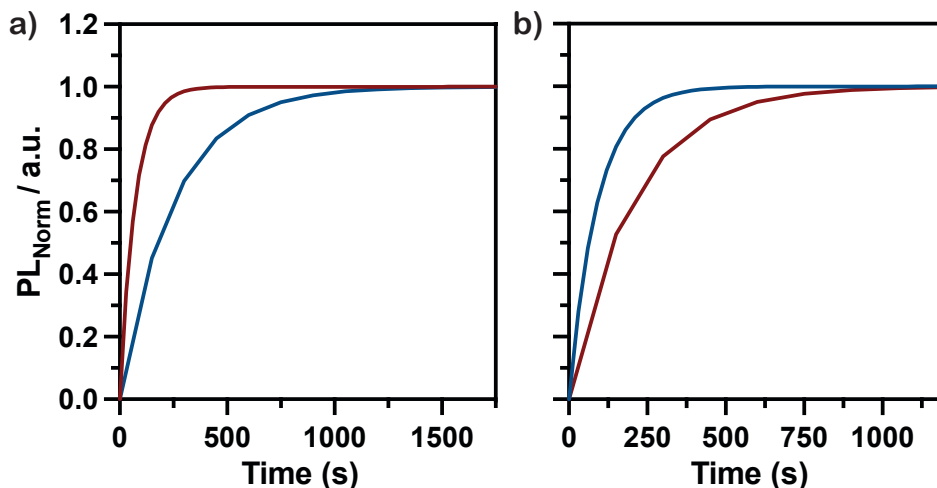


Figure 3.3 Tracking hAGT and SNAP-Tag reactions via emission change

a) Fluorescence changes upon dealkylation of $\text{O}^6\text{-Bn}^{\text{th}}\text{G}_N$ to $^{\text{th}}\text{G}_N$ at 400 nm (blue) and $\text{O}^6\text{-Bn}^{\text{tz}}\text{G}_N$ to $^{\text{tz}}\text{G}_N$ at 450 nm (red) by hAGT. b) Fluorescence changes upon dealkylation of $\text{O}^6\text{-Bn}^{\text{th}}\text{G}_N$ to $^{\text{th}}\text{G}_N$ at 400 nm (blue) and $\text{O}^6\text{-Bn}^{\text{tz}}\text{G}_N$ to $^{\text{tz}}\text{G}_N$ at 450 nm (red) by SNAP-Tag.

To preliminary demonstrate the utility of the alkylated analogs in the context of real-time protein fluorescent labeling or cargo delivery using the SNAP-Tag technology, emission intensity was monitored using the same protocol as for hAGT but with the commercially available SNAP-Tag purified protein. Similar to reactions with hAGT, the resulting photophysical data showed that reactions of $\text{O}^6\text{-Bn}^{\text{th}}\text{G}_N$ and $\text{O}^6\text{-Bn}^{\text{tz}}\text{G}_N$ are accompanied by a detectable change in emission intensity (Figure 3.3b). Reactions of $\text{O}^6\text{-Me}^{\text{th}}\text{G}_N$ and $\text{O}^6\text{-Me}^{\text{tz}}\text{G}_N$ do not show a change in emission signal. Reaction $t_{1/2}$ values were calculated for the reactions (Table 3.2) with the SNAP-Tag protein ($t_{1/2} = 63$ and 139 s for $\text{O}^6\text{-Bn}^{\text{th}}\text{G}_N$ and $\text{O}^6\text{-Bn}^{\text{tz}}\text{G}_N$, respectively).

The changes in emission intensity observed with $\text{O}^6\text{-Bn}^{\text{th}}\text{G}_N$ and $\text{O}^6\text{-Bn}^{\text{tz}}\text{G}_N$ are consistent with the dealkylation reaction of these substrates with both hAGT and SNAP-Tag. In these reactions, the restored guanine surrogate is less bright than the O6 alkyl substrate, so a drop in fluorescence is tracked. Notably, $\text{O}^6\text{-Bn}^{\text{tz}}\text{G}_N$ displays a faster reaction with hAGT than $\text{O}^6\text{-Bn}^{\text{th}}\text{G}_N$, showcasing the increased isofunctionality of the isothiazolopyrimidine analogs, which

possesses a nitrogen atom in the position equivalent to the N7 position in native nucleobases and nucleosides. Previous explorations using either crystal structures or AGT mutants have shown interactions with the nucleobase's N7, O6, N3 and its exocyclic amine, while substitutions at the C8 and N9 positions are tolerated.³⁴⁻³⁷ The necessary protein/nucleobase interactions are retained in the isothiazolo guanine analog.

Intriguingly, the relative reaction kinetics was reversed for **O⁶-BnthG_N** compared to **O⁶-Bn^{tz}G_N** with the SNAP-Tag protein. This is likely due to the engineering of the SNAP-Tag protein. From the library of hAGT mutants tested for increased activity and selectivity for benzylated guanosine derivatives protein mutants containing S159E showed increased efficiency. In hAGT, Ser159 hydrogen bonds to the basic N7 site. In the SNAP-Tag protein it is mutated to glutamic acid, which is deprotonated, and the reactive substrate is tautomerized to N7-H instead of the N9-H.³⁸ Such tautomerization is not possible for the thiopheno and isothiazolo analogs. However, the hydrogen at the thiophene C7 position can potentially be better accommodated by the deprotonated glutamic acid residue.³⁴ Additionally, we note that the higher reactivity of the benzylated analogs react efficiently while the methyl alkylated do not for both hAGT and the SNAP-Tag. This consistent with previous data regarding nucleobase reactivity.³⁴

Following the evaluation of substrate recognition by hAGT and SNAP-Tag via fluorescence kinetics experiments, **O⁶-BnthG_N**, **O⁶-MethG_N**, **O⁶-Bn^{tz}G_N**, and **O⁶-Me^{tz}G_N** were incubated with human embryonic kidney (HEK293T) cells to assess whether the chromophoric properties of these compounds could be utilized for cellular imaging and if hAGT activity could be determined in cells. Following a one-hour incubation period with 100 μM of the thiophene substrates and 500 μM of the isothiazole substrates, HEK293T cells were visualized. Fluorescence signal was observed in the cytosol for cells incubated with **O⁶-BnthG_N** and **O⁶-Bn^{tz}G_N**, suggesting

that cells uptake the benzyl alkylated derivatives. No fluorescence signal was detected with **O⁶-MethG_N** or **O⁶-Me^{tz}G_N** (Figure 3.4a). To further ascertain the effect of these compounds, fluorescence change was measured over 30 minutes after an initial 10-minute incubation period in both HEK293T and CHO-K1 cells. HEK293T cells express hAGT localized in the cytosol, whereas CHO-K1 cells are AGT deficient.³⁹ A decrease in fluorescence intensity was observed from time 0 to 1020 seconds for both **O⁶-BnthG_N** and **O⁶-Bn^{tz}G_N** in HEK293T cells as shown in Figure 3.4b and c, consistent with the conversion of alkyl compounds to non-alkylated guanine derivatives. No change in fluorescence is observed in CHO-K1 cells for either of the benzyl compounds. The changes in fluorescence are further quantified in 10 regions of interest (ROI) over time and a decrease in fluorescence is seen in HEK293T cells and not in CHO-K1 cells (Figure 3.5). These results taken together suggest that hAGT activity can be monitored using **O⁶-BnthG_N** and **O⁶-Bn^{tz}G_N** for live cell imaging purposes.

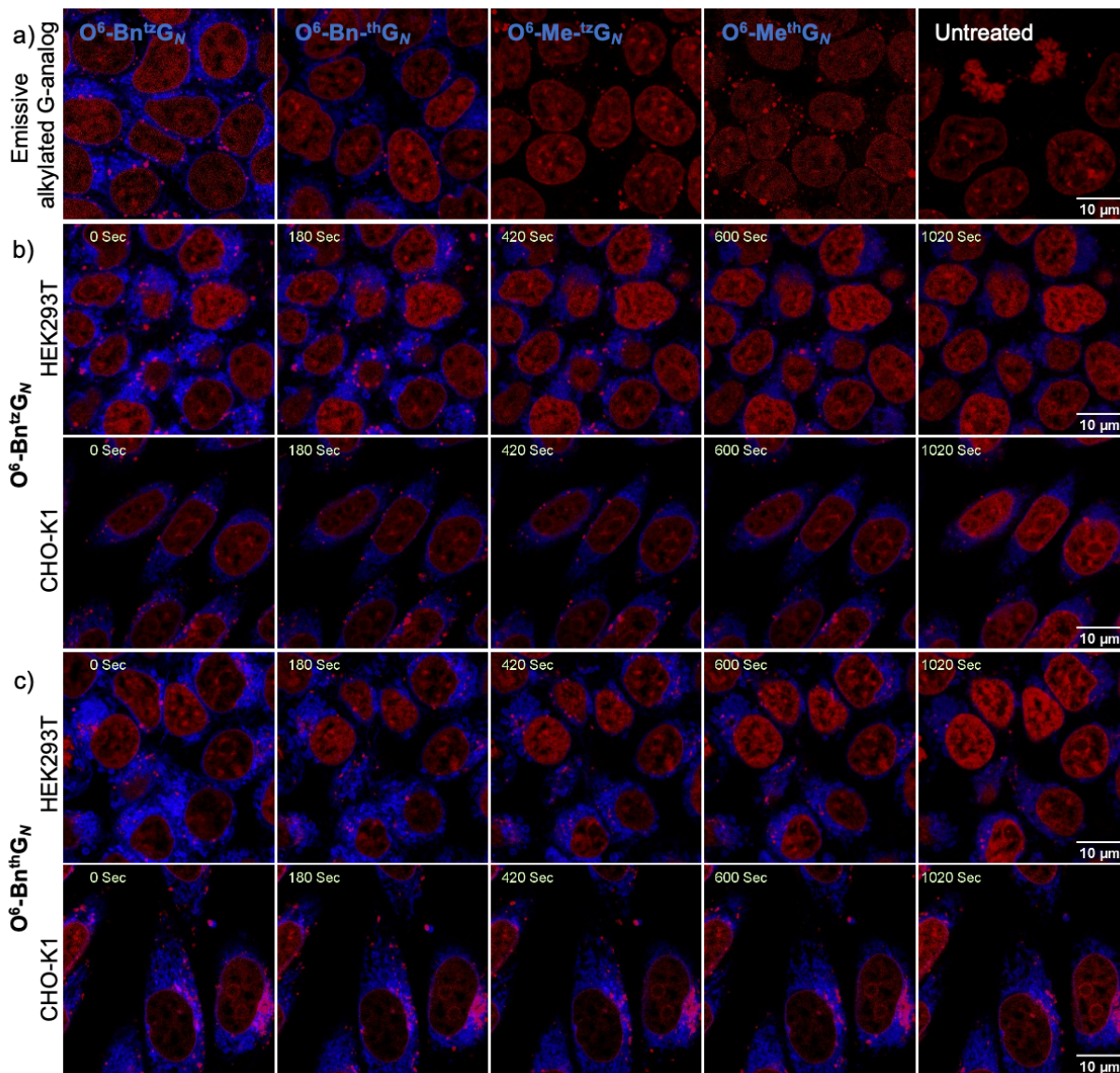


Figure 3.4 Live Cell Imaging of O^6 - $Bn^{th}G_N$, O^6 - $Me^{th}G_N$, O^6 - $Bn^{tz}G_N$, and O^6 - $Me^{tz}G_N$

a) Live-cell imaging of a) O^6 - $Bn^{th}G_N$, O^6 - $Me^{th}G_N$, O^6 - $Bn^{tz}G_N$, and O^6 - $Me^{tz}G_N$ in HEK293T cells after 1 hour incubation versus untreated cells. b) Fluorescence images of HEK293T cells and CHO-K1 cells incubated with 500 μ M O^6 - $Me^{tz}G_N$ and c) 100 μ M O^6 - $Bn^{th}G_N$ at indicated times.

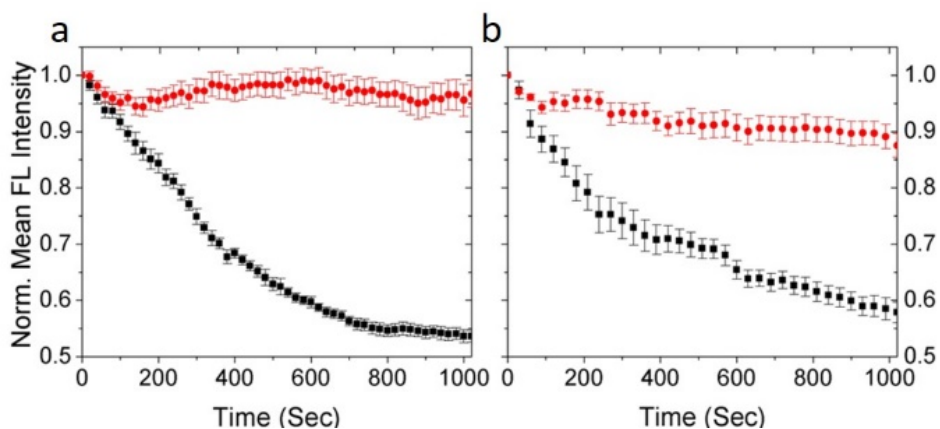


Figure 3.5 Real-time fluorescence monitoring of $O^6\text{-Bn}^{\text{tr}}\text{G}_N$ and $O^6\text{-Bn}^{\text{th}}\text{G}_N$ in live cells

Real-time fluorescence monitoring of $O^6\text{-Bn}^{\text{tr}}\text{G}_N$ (a) and $O^6\text{-Bn}^{\text{th}}\text{G}_N$ (b) in live HEK293T (black) and CHO-K1 (red) cells. Data points are averages of at least 10 ROIs.

3.4 Conclusion

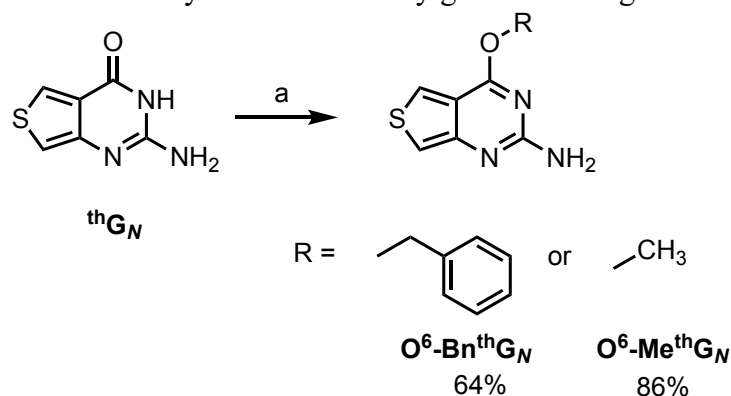
This study set out to assess the utility of two emissive nucleobase analog families, $^{\text{th}}\text{N}$ and $^{\text{tr}}\text{N}$, as substrates for the reaction monitoring of hAGT. We demonstrate that $O^6\text{-Bn}^{\text{th}}\text{G}_N$ and $O^6\text{-Bn}^{\text{tr}}\text{G}_N$ behave as an isomeric, emissive surrogates for O^6 -alkylguanine as hAGT substrates. The conversion of $O^6\text{-Bn}^{\text{th}}\text{G}_N$ or $O^6\text{-Bn}^{\text{tr}}\text{G}_N$ to $^{\text{th}}\text{G}_N$ or $^{\text{tr}}\text{G}_N$, respectively, can successfully be tracked in real-time as the reaction substrate and product will display distinct photophysical properties. Moreover, this discovery provides a biophysical tool to study the activity of hAGT. Further, we exemplify the utility of these analogs as substrates for the SNAP-Tag self-labeling system protein and measured their uptake and cellular fluorescence. Both benzylated derivatives show uptake by cells, are sufficiently bright for visualization by fluorescence microscopy, and fluorescence change corresponding to protein activity is suggested by live cell microscopy experiments.

3.5 Methods

3.5.1 Synthetic Procedures

Nucleobase analogs ${}^{\text{th}}\text{G}_N$ and ${}^{\text{tz}}\text{G}_N$ were synthesized based previously reported procedures.

Scheme 3.2 Synthesis of O^6 -alkylguanine analogs $\text{O}^6\text{-Bn}{}^{\text{th}}\text{G}_N$ and $\text{O}^6\text{-Me}{}^{\text{th}}\text{G}_N$ ^a



^a*Reagents and conditions:* (a) i) DBU, BOP, DMF, 2.5 h, RT; ii) 1 M NaOBn in BnOH, RT, overnight, 64% or 0.5 NaOMe in MeOH, RT, overnight, 86%.

4-(benzyloxy)thieno[3,4-*d*]pyrimidin-2-amine ($\text{O}^6\text{-Bn}{}^{\text{th}}\text{G}_N$)

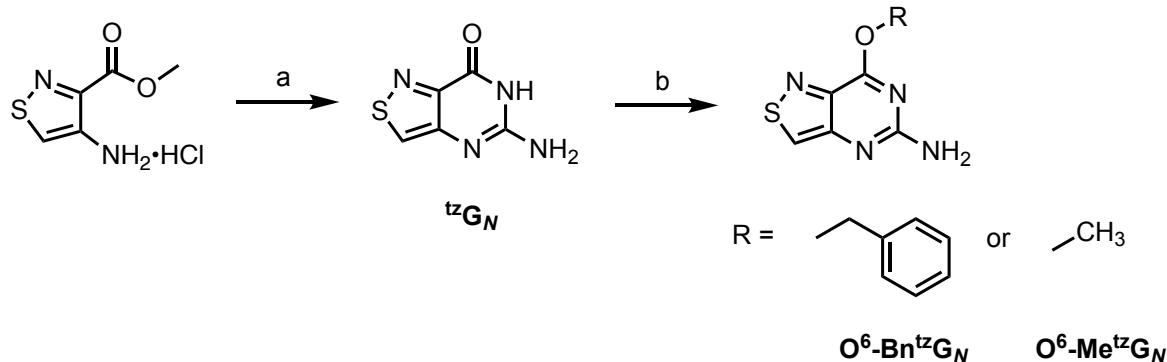
To a flame dried flask purged with argon, solid ${}^{\text{th}}\text{G}_N$ (0.040 g, 0.24 mmol) was added and dissolved in anhydrous DMF (3 mL). DBU (0.054 mL, 0.36 mmol) was then added dropwise followed by BOP (0.138 g, 0.31 mmol). The solution was allowed to stir at room temperature for 2.5 hours and then 1 M NaOBn in BnOH (0.72 mL) was introduced dropwise. The reaction was allowed to stir overnight at room temperature and was then partitioned between DCM and water. The organic extract was washed twice with water and once with brine. The solution was then dried over sodium sulfate and evaporated to dryness. The resulting residue was subjected to column chromatography with a gradient of 0–5% MeOH in DCM to yield an off-white powder (0.040 g, 64%). ¹H NMR (400MHz, DMSO-*d*₆): δ 5.53 (s, 2H), 6.44 (s, 2H), 7.08 (s, 1H), 7.35–7.46 (m, 3H), 7.53–7.59 (m, 2H), 8.19 (s, 1H). ¹³C NMR (100MHz, DMSO-*d*₆): δ 66.53, 106.72, 117.63,

123.40, 128.11, 128.25, 128.29, 135.75, 148.73, 153.64, 159.37, 164.47. ESI-HRMS calculated for $[C_{13}H_{12}N_3OS]^+$ 258.0696, found 258.0697.

4-methoxythieno[3,4-*d*]pyrimidin-2-amine (O^6 -MethG_N)

Solid thG_N (0.040g, 0.240 mmol) was placed in a flame dried flask and dissolved in anhydrous DMF (3 mL). DBU (0.054 mL, 0.36 mmol) was then added dropwise followed by the solid BOP (0.138 g, 0.311 mmol). The solution stirred at room temperature for 2.5 hours before 0.5 M NaOMe in MeOH (1.44 mL) was added dropwise. The reaction was left to stir at room temperature overnight. The following day the solution was evaporated to dryness and subjected to column chromatography with a gradient of 0–10% MeOH in DCM, yielding an off-white powder (0.037 g, 86%). ¹H NMR (400MHz, DMSO-*d*₆): δ 3.96 (s, 3H), 6.38 (s, 2H), 7.04 (s, 1H), 8.12 (s, 1H). ¹³C NMR (100MHz, DMSO-*d*₆): δ 54.01, 107.66, 118.24, 122.61, 153.71, 159.67, 164.31. ESI-HRMS calculated for $[C_7H_8N_3OS]^+$ 182.0383, found 182.0383.

Scheme 3.3 Synthesis ^{tz}G_N and O^6 -alkylguanine analogs O^6 -Bn^{tz}G_N and O^6 -Me^{tz}G_N^a



^aReagents and conditions: (a) Chloroformamidinium hydrochloride, DMSO₂, 125°C, 2.5 h, 85%. (b) i) DMAP, 2-Mesitylenesulfonyl chloride, DBU, ACN, RT, overnight; ii) 0.5 M NaOMe in MeOH, DMF, RT, 30 min, 75% or 1 M NaOBn in BnOH, DMF, RT, 4 hours, 65%.

5-aminoisothiazolo[4,3-*d*]pyrimidin-7(6*H*)-one (¹³G_N)

Updated work up for previously published reaction:

Solid DMSO₂ (6g, 9.25 mmol) was added to a flame-dried flask and heated to 125°C. A homogeneous mixture of 4-aminoisothiazole-3-carboxamide hydrochloride salt (0.300 g, 1.54 mmol) and chloroformamidine hydrochloride (0.266 g, 2.31 mmol) was added in 2 batches, 15 minutes apart, to the liquid DMSO₂. The reaction was left to stir for 1.5 hours and then cooled to room temperature. The solidified reaction mixture was then resuspended in a minimal amount of water, basified with concentrated ammonium hydroxide, and stirred vigorously for 1 hour. The solution was then evaporated to dryness, resuspended in a minimal amount of DCM, filtered and was then thoroughly washed with DCM. The remaining yellow solid was then dissolved in MeOH and evaporated to afford a light-yellow solid.

7-methoxyisothiazolo[4,3-*d*]pyrimidin-5-amine (O⁶-Me¹³G_N)

To a flame dried flask purged with argon, solids ¹³G_N (0.122 g, 0.725 mmol), DMAP (0.106 g, 0.870 mmol), and 2-mesitylenesulfonyl chloride (0.178 g, 1.09 mmol) were added and subsequently dissolved in anhydrous ACN (10 mL). DBU (0.16 mL, 1.09 mmol) was introduced dropwise, and the reaction mixture was left to stir overnight at room temperature. The suspension was filtered and the solid washed with ACN and diethyl ether. The orange-red solid was then dried under high vacuum for 2 hours, and then argon purged. The solid was dissolved in anhydrous DMF (10 mL) and 0.5 M NaOMe in MeOH (4.36 mL) was added dropwise. After 30 minutes the solution was partitioned between EtOAc and water. Brine was added to the aqueous phase and extracted with EtOAc twice more. The organic phases were combined, dried over sodium sulfate, and evaporated. The remaining residue was subjected to column chromatography with a gradient of 0–

5% MeOH in DCM to afford a yellow solid (0.099 g, 75% yield). ¹H NMR (400MHz, DMSO-d₆): δ 4.04 (s, 3H), 6.72 (s, 2H), 8.79 (s, 1H). ¹³C NMR (100MHz, DMSO-d₆): δ 54.46, 136.49, 143.42, 153.39, 159.94, 162.11. ESI-HRMS calculated for [C₆H₇N₄OS]⁺ 183.0335, found 183.0338.

7-(benzyloxy)isothiazolo[4,3-*d*]pyrimidin-5-amine (O⁶-Bn¹²G_N)

Solids ¹²G_N (0.052 g, 0.201 mmol), DMAP (0.030 g, 0.241 mmol), and 2-mesitylenesulfonyl chloride (0.066 g, mmol 0.30) were added to a flame dried flask purged with argon. The solids were then dissolved in anhydrous ACN (5 mL) and DBU (0.05 mL, 0.302 mmol) was dropwise introduced. The reaction mixture was left to stir overnight at room temperature. The resulting suspension was filtered, and the filtrate washed with acetonitrile and diethyl ether. The solid was then dried under high vacuum for 2 hours, purged with argon, and dissolved in anhydrous DMF (5 mL). 1 M NaOBn in BnOH (0.60 mL) was added dropwise to the solution. After 4 hours, the solution was partitioned between DCM and water and the aqueous layer extracted with DCM twice more. The organic phases were combined and dried over sodium sulfate and evaporated. The resulting residue was subjected to column chromatography with a gradient of 0–5%MeOH in DCM to afford a light-yellow solid (got 34 mg, 65%). ¹H NMR (400MHz, DMSO-d₆): δ 5.54 (s, 2H), 6.76 (s, 2H), 7.35–7.45 (m, 3H), 7.54–7.58 (m, 2H), 8.80 (s, 1H). ¹³C NMR (100MHz, DMSO-d₆): δ 68.39, 128.93, 129.05, 129.41, 136.28, 136.64, 143.32, 153.58, 159.86, 161.42. ESI-HRMS calculated for [C₁₂H₁N₄OS]⁺ 259.0648, found 259.0644.

3.5.2 Photophysical Properties: General Methods

Absorption spectra were measured on a Shimadzu UV-2450 spectrometer setting the slit at 1 nm and with 0.5 nm resolution. Emission spectra were measured on a Horiba Fluoromax-4 and measurements were taken with a 1 nm resolution and setting the slits to 1 nm. Emission intensities were corrected to reflect an optical density of 0.1 at the excitation wavelength. All measurements were carried out in a 3 mL 10 mm four-sided quartz cuvette purchased from Helma. Both instruments were equipped with a thermostat-controlled ethylene glycol-water bath, and all measurements were taken at $37.0 \pm 0.1^\circ\text{C}$. Measurements were recorded after a 3-minute temperature equilibration period. All spectra were corrected for the blank.

Highly concentrated stocks solutions of ${}^{\text{th}}\text{G}_N$, $\text{O}^6\text{-Bn}{}^{\text{th}}\text{G}_N$, $\text{O}^6\text{-Me}{}^{\text{th}}\text{G}_N$, ${}^{\text{tz}}\text{G}_N$, $\text{O}^6\text{-Bn}{}^{\text{tz}}\text{G}_N$ and $\text{O}^6\text{-Me}{}^{\text{tz}}\text{G}_N$ were prepared in DMSO. Samples were prepared from the stock nucleobase solutions diluted to a total volume of 3 mL in deionized water or DPBS buffer, mixed with a pipet for 10 seconds, and placed in the cuvette holder to equilibrate for 3 minutes. All samples contain 0.3 v/v % DMSO. All measurements were done in triplicate.

3.5.3 Quantum Yield Measurements

Fluorescence quantum yields were measured on a Horiba Fluoromax-4 with (1 nm resolution, excitation slit at 1 nm and emission slit at 3 nm). All sample concentrations were adjusted to have an optical density lower than 0.1 at the excitation wavelength. All measurements were done in triplicate. The fluorescence quantum yields were measured relative to 2-aminopurine (0.68 in water, λ_{ex} 320 nm) as an external standard by using the following equation:

$$\phi = \phi_{STD} \frac{I}{I_{STD}} \frac{OD_{STD}}{OD} \frac{n^2}{n_{STD}^2}$$

Where ϕ_{STD} is the fluorescence quantum yield of the standard, I and I_{STD} are the integrated area of the emission band of the sample and the standard respectively, OD and OD_{STD} are the optical density at the excitation wavelength for the sample and standard respectively, and n and n_{STD} are the solvent refractive index of the sample and the standard solutions respectively.

3.5.4 Protein Reaction: Real-Time monitoring of hAGT and SNAP-Tag reactions via Emission

Recombinant hAGT protein with a His-Tag terminus (MGMT; O-6-methylguanine-DNA methyltransferase) was purchased from BPS Bioscience and SNAP-Tag purified protein with a C-terminal DDT moiety was purchased from New England Biolabs.

Reaction conditions were the same for all hAGT and SNAP-Tag reactions monitored by emission spectroscopy. Concentrated stocks were prepared in DMSO. Samples were prepared in a 125 μ L 10.00 mm four-sided quartz cuvette from Helma. Reactions had a total volume of 125 μ L with a nucleobase concentration of 0.5 μ M and protein (either hAGT or SNAP-Tag) concentration of 2.5 μ M in DPBS1x buffer. All measurements were taken at $37.0 \pm 0.1^\circ\text{C}$ and the protein was introduced after a 3-minute temperature equilibration period. All samples contain 0.01 v/v% DMSO.

Protein mediated conversion of emissive O6-alkylguanine analogs was monitored by emission spectroscopy. Emission measurements were performed on a Horiba Fluoromax-4, collecting data at varying time increments and appropriate durations (see table). Real-time

monitoring of the conversions was done upon excitation at the isosbestic point (see table) for each pair of compounds in DPBS buffer. The conversions of **O⁶-BnthG_N** and **O⁶-MethG_N** to **thG_N** were followed at 400 nm, setting the excitation slit to 5 nm and the emission slit at 10 nm. The conversions of **O⁶-Bn^{tz}G_N** and **O⁶-Me^{tz}G_N** to **^{tz}G_N** were followed at 450 nm, setting the excitation slit at 1 nm and the emission slit at 10 nm. Each experiment was done in triplicate. Note, there is a 6 second lag time after protein addition after time 0 measurement.

3.5.5 Mammalian cell culture

HEK293T cells were grown in DMEM, CHO-K1 were grown in DMEM/F12, both media were supplemented with 10% FCS and 1% penicillin-streptomycin. All cells were grown in a humidified chamber of 95% air, and 5% CO₂ at 37 °C.

3.5.6 Live Cell Imaging

96-well microtiter plates and Fluorodish wells used were coated with PDL before use according to the following procedure:

Wells were covered with PDL solution (0.1 mg/mL, 100 or 120 µl per well for 96 well-plate or fluorodish-well respectively), and incubated for 3 h at RT. The PDL solution was then removed by aspiration, and wells were re-sterilized under UV light for 20 min and further dried for an additional 1.5h. Finally, wells were washed with PBS twice (100 or 120 µl per well).

3.5.7 Working concentrations determination

HEK293T Cells were plated into PDL-coated 96-well microtiter plates (30 x 10³ cells per well) and allowed to adhere for 24 h. The Media was aspirated and solutions of tested compounds

in growth media (100 μ L) were added at final concentrations of: 100, 50, and 1 μ M for **O⁶-MethG_N** and **O⁶-BnthG_N**, and 500, 100, 50, and 1 μ M for **O⁶-Me^{tz}G_N** and **O⁶-Bn^{tz}G_N**. Cultures were then incubated for 1.5 h in a humidified chamber of 95% air, and 5% CO₂ at 37 °C. Cells were then washed twice with PBS buffer containing Ca and Mg ions and were visualized in this buffer using an EVOS widefield fluorescence microscope.

3.5.8 Confocal microscopy

HEK293T cells were Plated into PDL-coated Fluorodish wells 10 mm diameter with cover glass bottom (wpi), fit for live cell imaging and compatible with oil objectives, (100 x 10³ cells per well) and allowed to adhere for 24 h. The Media was aspirated and solutions of tested compounds in growth media (100 μ L) were added at final concentrations of 500 μ M of **O⁶-Me^{tz}G_N** and **O⁶-Bn^{tz}G_N** and 100 μ M of **O⁶-MethG_N** and **O⁶-BnthG_N**. Cultures were incubated for 1h. During this incubation time the nuclear stain NucRedTM Live 647, was added 5 μ l to 100 μ l culture and incubated for 30 mins. Wells were then washed with PBS containing Ca, Mg, and 1 mM HEPES and were visualized in this buffer using Beethoven 100X. All images were taken at the same microscope settings.

3.5.9 Fluorescence Real-time monitoring of **O⁶-Bn^{tz}G_N** and **O⁶-BnthG_N** in live cells

HEK293T or CHO-K1 cells were Plated into PDL-coated Fluorodish wells (100 x 10³ or 40 x 10³ respectively) and allowed to adhere for 24 h. NucRed was added (5 μ l to 100 μ l) and incubated for 20 mins. The Media was then aspirated and solutions containing tested compounds and NucRed (5 μ l) in media were added at final concentrations of 250 μ M of **O⁶-Bn^{tz}G_N** and 100

μM of $\text{O}^6\text{-Bn}^{\text{th}}\text{G}_N$ and were incubated for 10 minutes. Wells were then aspirated and washed with Fluorobrite supplemented with 10% FCS and were visualized in this buffer using Beethoven 100X. Timelapse images were taken every 20 and 30 seconds for $\text{O}^6\text{-Bn}^{\text{tz}}\text{G}_N$ and $\text{O}^6\text{-Bn}^{\text{th}}\text{G}_N$ respectively for 30 mins. All images were taken at the same microscope settings. Mean fluorescence intensities of at least 10 different ROIs selected from the images as well as mean fluorescence intensities of the whole images were measured over time using ImageJ.

3.6 Acknowledgements

We thank the National Institutes of Health (through grant no. GM139407) for generous support, the Chemistry & Biochemistry MS facility, and the UCSD X-ray Crystallography Facility (especially M. Gembicki) and the UCSD NMR Facility.

Chapter 3, in part, is adapted from work currently being prepared for submission of the material: “Fluorescent Probes for O^6 -Alkylguanine-DNA-Transferase Activity and Microscopy in Living Cells” *in preparation*. Permission to use materials from the manuscript was also obtained from co-authors, Kfir Steinbuch and Yitzhak Tor. The dissertation author was the primary researcher and author of this paper.

3.7 Supplemental Information

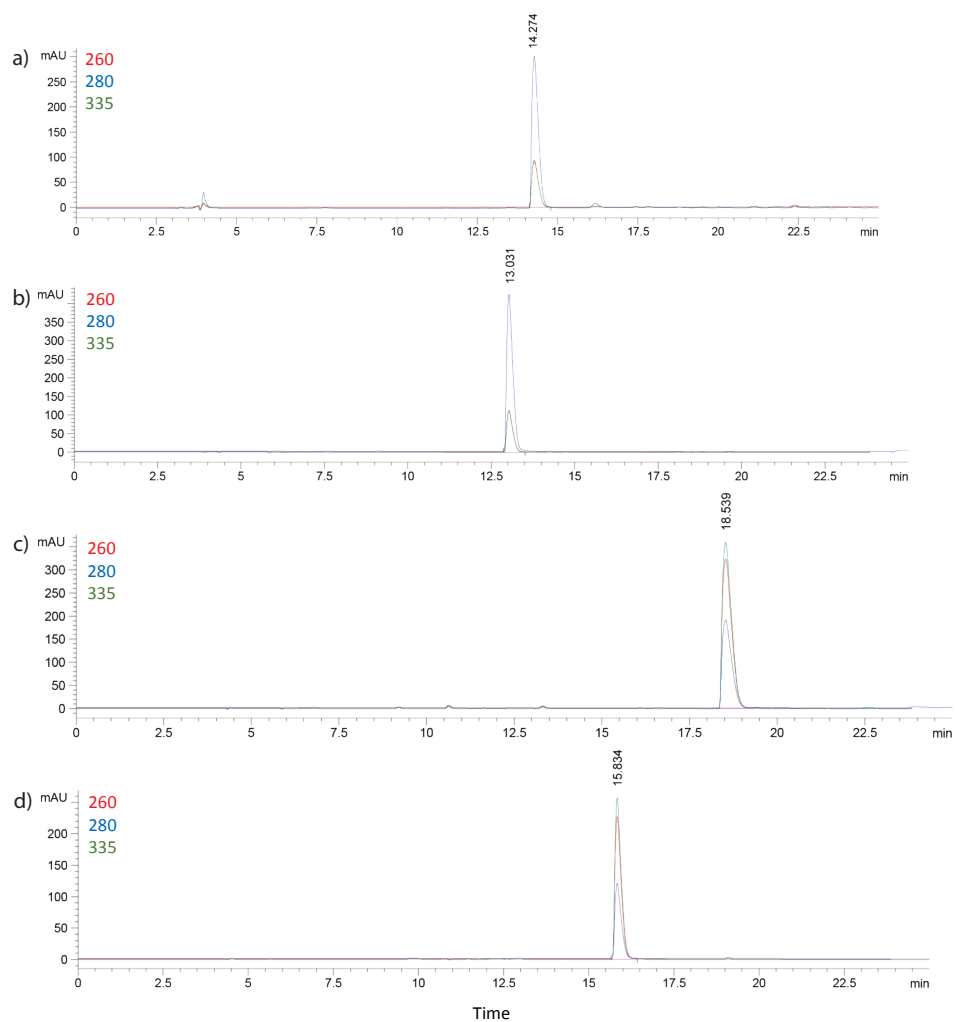


Figure 3.S1 HPLC traces of stock solutions for compounds

Raw HPLC traces of stock solutions for compounds a) O^6 - $Bn^{th}G_N$, b) O^6 - $Me^{th}G_N$, c) O^6 - $Bn^{tz}G_N$, d) O^6 - $Me^{tz}G_N$.

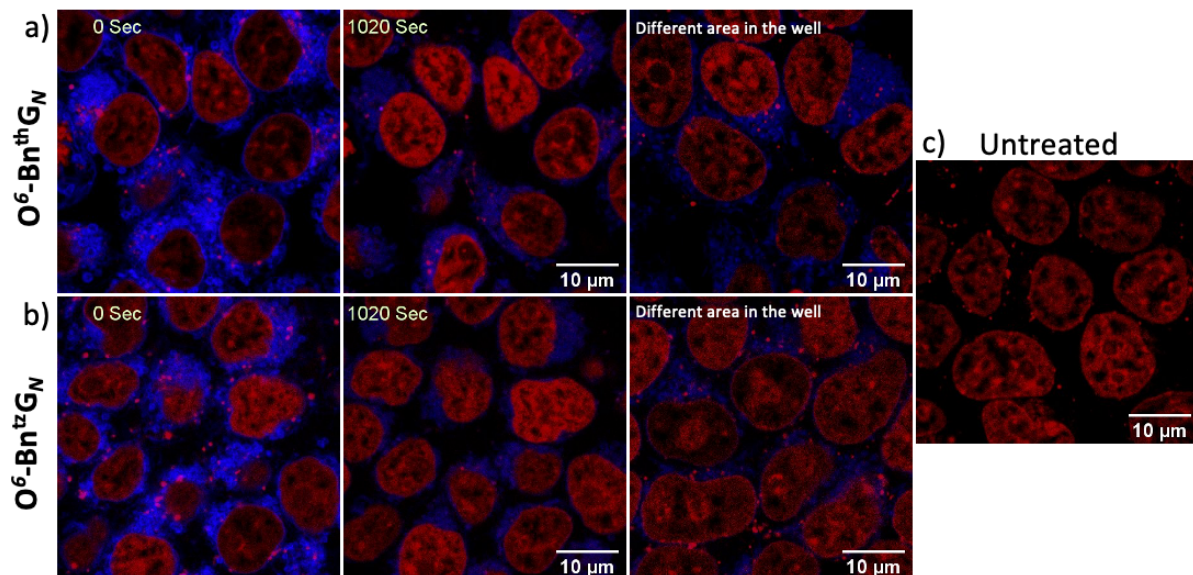


Figure 3.S2 Fluorescence change control for microscopy experiments

Fluorescence change control for microscopy experiments for a) $O^6\text{-Bn}^{\text{th}}G_N$, b) $O^6\text{-Bn}^{\text{tz}}G_N$, c) and untreated cells suggests decrease in fluorescence is due to protein activity and not photobleaching.

3.8 References

1. DeBont, R. Larebeke, N. Endogenous DNA damage in humans: a review of quantitative data. *Mutagenesis*. **2004**, *19* (3), 169–185.
2. Mingard, C.; Wu, J.; McKeague, M.; Strula, S. J. Next-generation DNA damage sequencing. *Chem. Soc. Rev.* **2020**, *49*, 7354–7377.
3. Shrivastav, N.; Li, D.; Essigmann, J. M. Chemical biology of mutagenesis and DNA repair. *Carcinogenesis*. **2010**, *31* (1), 59–70.
4. Pegg, A. Enzymatic removal of O⁶-methylguanine from DNA by mammalian cell extracts. *Biochem. and Biophys. Res. Commun.* **1978**, *48* (1) 166–173.
5. Yarosh, D. B.; Rice, M.; Rufus, S. D.; Foote, R. S.; Mitra, S. O⁶-Methylguanine-DNA methyltransferase in human cells. *Mutat. Res. DNA Repair Rep.* **1984**, *131* (1), 27–36.
6. Pegg, A. E.; Boosalis, M.; Smason, L.; Moschel, R. C.; Byer, T. L.; Swenn, K.; Dolan, M. E. Mechanism of inactivation of human O⁶-alkylguanine-DNA alkyltransferase by O⁶-benzylguanine. *Biochemistry*. **1993**, *32* (35), 11998–12006.
7. Xu-Welliver, M.; Pegg, A. E. Degradation of the alkylated form of the DNA repair protein, O⁶-alkylguanine-DNA alkyltransferase. *Carcinogenesis*. **2002**, *23* (5), 823–830.
8. Wickstrom, M.; Dyberg, C. Milosevic, J.; Einvik, C.; Calero, R.; Sveinbjornsson, B.; Sanden, E.; Darabi, A.; Siesjo, P.; Kool, M.; Kogner, P. Baryawno, N.; Johnsen, J. I. Wnt/B-catenin pathway regulated MGMT gene expression in cancer and inhibition of Wnt signaling prevents chemoresistance. *Nat. Commun.* **2015**, *6*, 8904.
9. Singh, N.; Miner, A.; Hennis, L.; Mittal, S. Mechanisms of temozolomide resistance in glioblastoma-a comprehensive review. *Cancer Drug. Resist.* **2021**, *4* (1), 17–43.
10. Juillerat, A.; Gronemeyer, T.; Keppler, A.; Gendreizig, S.; Pick, H.; Vogel, H.; Johnsson, K. Directed evolution of O⁶-alkylguanine-DNA alkyltransferase for efficient labeling of fusion proteins with small molecules in vivo. *Chem. Biol.* **2003**, *10* (4), 313-317.
11. Keppler, A.; Pick, H.; Arrivoli, C.; Vogel, H.; Johnsson, K. Labeling of fusion proteins with synthetic fluorophores in live cells. *Proc. Natl. Acad. Sci. USA.* **2004**, *101* (27), 9955–9959.
12. Juillerat, A.; Heinis, C.; Sielaff, I.; Barnikow, J.; Jaccard, H.; Kunz, B.; Terskikh, A.; Johnsson, K. Engineering Substrate Specificity of O⁶-alkylguanine-DNA Alkyltransferase for Specific Protein Labeling in Living Cells. *Chembiochem.* **2005**, *6* (7), 1263–1269.

13. Shin, D.; Sinkeldam, R. W.; Tor, Y. Emissive RNA Alphabet. *J. Am. Chem. Soc.* **2011**, *133* (38), 14912–14915.
14. Rovira, A. R.; Fin, A.; Tor, Y. Chemical Mutagenesis of an Emissive RNA Alphabet. *J. Am. Chem. Soc.* **2015**, *137* (46), 14602–14605.
15. Liu, W.; Shin, D.; Tor, Y. Monitoring translation with modified mRNAs strategically labeled with isomorphous fluorescent guanosine mimetics. *ACS Chem. Biol.* **2013**, *8* (9), 2017–2023.
16. Sinkeldam, R. W.; McCoy, L. S.; Shin, D.; Tor, Y. Enzymatic Interconversion of Isomorphous Fluorescent Nucleosides: Adenosine Deaminase Transforms thA to thI, Two Distinct Fluorophores. *Angew. Chem. Int. Ed.* **2013**, *52*, 14026–14030.
17. Mizrahi, R. A.; Shin, D.; Sinkeldam, R. W.; Phelps, K. J.; Fin, A.; Tantillo, D. J.; Tor, Y.; Beal, P. A. A Fluorescent Adenosine Analogue as a Substrate for A-to-I RNA Editing Enzyme. *Angew. Chem. Int. Ed.* **2015**, *54*, 8713–8716.
18. Vranken, C.; Fin, A.; Tufar, P.; Hofkens, J.; Burkhart, M.; Tor, Y. Chemoenzymatic Synthesis and Utilization of a SAM Analog with an Isomorphous Nucleobase. *J. Org. Chem.* **2016**, *81*, 4530–4539.
19. Li, Y.; Fin, A.; McCoy, L. S.; Tor, Y. Polymerase-Mediated Site-Specific Incorporation of a Synthetic Fluorescent Isomorphous G Surrogate into RNA. *Angew. Chem. Int. Ed.* **2017**, *56*, 1303–1307.
20. Rovira, A. R.; Fin, A.; Tor, Y. Emissive Synthetic Cofactors: An Isomorphous, Isofunctional, and Responsive NAD⁺ Analogue. *J. Am. Chem. Soc.* **2017**, *139*, 15556–15559.
21. Halle, F.; Fin, A.; Rovira, A. R.; Tor, Y. Emissive synthetic cofactors interconversions of ^{tz}A analogues of ATP, NAD⁺, NADH, NADP⁺, AND NADPH. *Angew. Chem. Int. Ed.* **2017**, *57*, 1087–1090.
22. Li, Y.; Ludford, P. T.; Fin, A.; Rovira, A. R.; Tor, Y. Enzymatic Synthesis and Applications of Fluorescent Cyclic Dinucleotides. *Chem. Euro. J.* **2020**, *26*, 6076–6084.
23. Li, Y.; Fin, A.; Rovira, A. R.; Su, Y.; Dippel, A. B.; Valderrama, J. A.; Riestra, A.; Nizet, V.; Hammond, M. C.; Tor, Y. Tuning the innate immune response to cyclic dinucleotides using atomic mutagenesis. *ChemBioChem* **2020**, *21* (18), 2595–2598.
24. Adamek, R. N.; Ludford, P. T.; Duggan, S. M.; Tor, Y.; Cohen, S. M. Identification of Adenosine Deaminase Inhibitors by Metal-binding Pharmacophore Screening. *ChemMedChem* **2020**, *22*, 2151–2156.

25. Ludford, P. T.; Li, Y.; Yang, S.; Tor, Y. Cytidine deaminase can deaminate fused pyrimidine ribonucleosides. *Org. Biol. Chem.* **2021**, *19*, 6237–6243.
26. Cong, D.; Li, Y.; Ludford, P. T.; Tor, Y. Isomorphic Fluorescent Nucleosides Facilitate Real-Time Monitoring of RNA Depurination by Ribosome Inactivating Proteins. *Chem. Euro. J.* **2022**, *28*, e202200994.
27. Hadidi, K. Steinbuch, K. B.; Dozier, L. E.; Patrick, G. N.; Tor, Y. Inherently Emissive Puromycin Analogues for Live Cell Labelling. *Angew. Chem. Int. Ed. Engl.* **2023**, *62* (23), e202216784.
28. Bucardo, M. S.; Wu, Y.; Ludford, P. T.; Li, Y.; Fin, A.; Tor, Y. Real-Time Monitoring of human Guanine Deaminase Activity by an Emissive Guanine Analog. *ACS Chem. Biol.* **2021**, *16* (7), 1208–1214.
29. Gewald, K., Bellmann, P. Synthese und Reaktionen von 4-Aminoisothiazolen. *Liebigs Ann. Chem.* **1979**, *10*, 1534–1546.
30. Frank, J.; Laskhman, M. K. A simple method for C-6 modification of guanine nucleosides. *Org. Biomol. Chem.* **2009**, *7* (14), 2933–2940.
31. Fillion, A.; Franco, Pinto, J.; Granzhan, A. Harnessing an emissive guanine surrogate to design small-molecule fluorescent chemosensors of O⁶-methylguanine-DNA-methyltransferase (MGMT). *Org. Biomol. Chem.* **2022**, *20* (9), 1888–1892.
32. Sholokh, M.; Improta, R.; Mori, M.; Sharma, R.; Kenfack, C.; Shin, D.; Voltz, K.; Stote, R. H.; Zaporozhets, O. A.; Botta, M.; Tor, Y.; Mély, Y. Tautomers of a Fluorescent G Surrogate and Their Distinct Photophysics Provide Additional Information Channels. *Angew. Chem. Int. Ed.* **2016**, *55*, 7974–7978.
33. Didier, P.; Kuchlyan, J.; Martinez-Fernandez, L.; Gosset, P.; Leonard, J.; Tor, Y.; Improta, R.; Mely, Y. What Makes Thienoguanosine an Outstanding Fluorescent DNA Probe? *Phys. Chem. Chem. Phys.* **2020**, *22*, 7381–7391.
34. Daniels, D. S.; Tainer, J. A.; Conserved structural motifs governing the stoichiometric repair of alkylated DNA by O⁶-alkylguanine-DNA alkyltransferase. *Mutat. Res.* **2000**, *460* (4), 151–63.
35. Wibley, J. E. A.; Pegg, A. E.; Moody, P. C. E. Crystal structure of the human O⁶-alkylguanine-DNA alkyltransferase. *Nucleic Acids Res.* **2000**, *28*, 393–401.
36. Goodtzova, K.; Kanugula, S.; Edara, S.; Pegg, A. E. Investigation of the role of tyrosine-114 in the activity of human O⁶-alkylguanine-DNA alkyltransferase. *Biochemistry.* **1998**, *37*, 12489–12495.

37. Vora, R. A.; Pegg, A. E.; Ealick, S. E. A new model for how O⁶-methylguanine-DNA methyltransferase binds DNA. *Proteins*. **1998**, *32*, 3–6.
38. Imal, Y.; Oda, H.; Nakatsuru, Y.; Ishikawa, T. A polymorphism at codon 160 of human O⁶-methylguanine-DNA methyltransferase gene in young patients with adult type cancers and functional assay. *Carcinogenesis*. **1995**, *16* (10), 2441–2445.
39. Yu, W.; Wu, T.; Huang, C.; Chen, I.; Tan, K. Protein sensing in living cells by molecular rotor-based fluorescence-switchable chemical probes. *Chem. Sci.* **2016**, *7*, 301–307.

CHAPTER 4: Reflections and Future Directions

4.1 Reflections and Dissertation Summary

The Tor lab has designed a series of isomorphous nucleobase analogs, implemented in the previously published emissive RNA alphabets. The two notable families are based on either a thieno[3,4-*d*]pyrimidine core¹ (thN) or isothiazole[4,3-*d*]pyrimidine core (^{tz}N).² One area that remained largely unexplored was the use of the unglycosylated heterocycles as nucleobase surrogates.

In the work described here, we employed guanine-based emissive analogs, thG_N and ^{tz}G_N, for the evaluation of metabolic and epigenetic cellular modifications. We established that the nucleobase analogs were susceptible to cellular pathways. Our emissive nucleobases were recognized as substrates as they retained the morphology of their native counterparts and retained critical molecular contacts. Guanine deaminase can deaminate ^{tz}G_N to ^{tz}X_N at rates corresponding to the native reaction. The findings from this investigation showcased the functionality of the ^{tz}N core versus the thN core, as thG_N does not act as a substrate as N7 recognition is vital for reaction.³ Finally, we showcased the potential of this fluorescent nucleobase surrogate to provide a visible spectral window for a real-time study of guanine deaminase and its inhibition.

Equally important, both human *O*⁶-alkylguanine-DNA-transferase (hAGT) and SNAP-Tag proteins dealkylate *O*⁶-benzylated thG_N and ^{tz}G_N derivatives. Using **O⁶-BnthG_N** and **O⁶-Bn^{tz}G_N** as substrates can offer a means through which to visualize the activity of these proteins. Most importantly, both benzylated derivatives are sufficiently bright for visualization by fluorescence microscopy in live mammalian cells and fluorescence intensity (FI) change suggesting protein activity was observed.

4.2 Future synthetic directions and activity investigation of hAGT

4.2.1 Project shortcomings and further possible experimentation

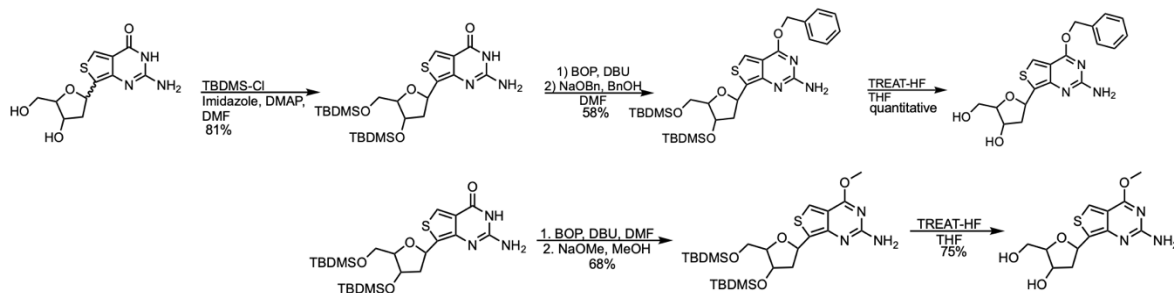
Chapter 3 is adapted from work currently being prepared for submission. Additional investigation of hAGT protein activity and proof-of-concept can be achieved via additional experimentation. The transformation of **O⁶-BnthG_N** or **O⁶-Bn^{tz}G_N** to the respective dealkylated products, thG_N or ^{tz}G_N, by hAGT is currently being assessed using HPLC analysis as kinetic evaluation of protein activity is classically done using HPLC and can be compared to rates derived via fluorescence intensity (FI) change.

For the first time, the nucleobase probes designed by the Tor lab were visualized in cells. The brightness of the new alkylated nucleobase analogs can provide a means for tracking protein activity in cells. The potential to visualize AGT activity has been evaluated in HEK293T cells, expressing hAGT, and CHO-K1 cells, not expressing AGT. A change in FI was observed in HEK293T cells but not in CHO cells, as expected, and suggests hAGT protein activity. To expand on these results, additional cell lines can be explored. HeLa cells express greater quantities of hAGT than HEK cells.⁴ Using our probes to track FI change in HeLa cells would expand the working range of AGT activity observed in cells.

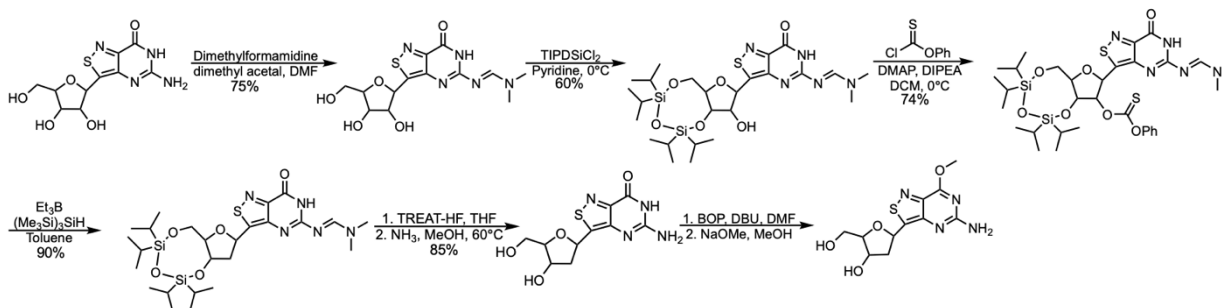
Progenitor cancer cells, which are typically used to study hAGT activity in glioblastoma, can be used to assess the cellular dealkylation activity of hAGT.⁵ Additionally, protein activity could be localization. As hAGT protein expression is tissue dependent and variable with disease progression, an assay of hAGT activity could provide a real-time, non-invasive method for measuring hAGT in cancer cells, deciphering tumorigenic potential of cells, and ultimately provide a tool for the clinical evaluation of combination regimens for treatment.

4.2.2 Synthesis of O⁶-alkyl dthG_N and d^{tz}G_N nucleosides

As the dealkylation of the nucleobase analogs can be tracked via FI change, the same could be achieved for the nucleoside equivalents. Using previously described methods for the synthesis of dthG the O⁶ position can be alkylated as described in chapter 3 and presented in Scheme 4.1.⁶ The synthesis of d^{tz}G can be achieved via pseudo-Barton-McCombie deoxygenation followed by alkylation at the O⁶ position as shown in Scheme 4.2.⁷



Scheme 4.1 Synthesis of O⁶-BndthG and O⁶-MedthG.



Scheme 4.2 Synthesis of O⁶-Med^{tz}G.

4.2.3 Preliminary data of O⁶-alkyl dthG_N with SNAP-Tag protein reactions

The preliminary reaction of alkylated deoxy-thiophenoguanosine derivatives was tested with SNAP-Tag protein. As expected, from nucleobase reactivity, the benzyl derivative showed a change in FI while the methyl did not (Figure 4.1).

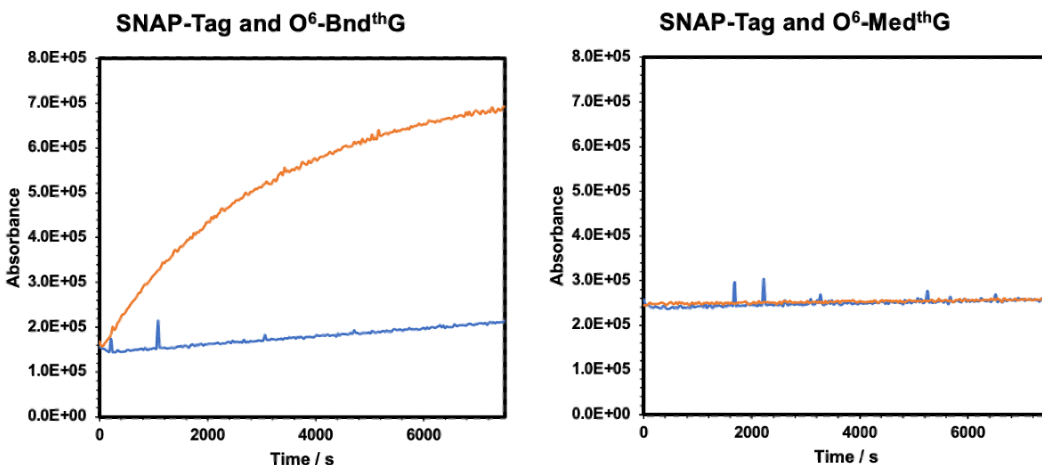


Figure 4.1 Preliminary data for fluorescence intensity change tracked for O⁶-BndthG and O⁶-MedthG reaction with SNAP-Tag protein.

4.3 Future of nucleobase-based probes

Emissive nucleobase probes have come a long way. Their evolution described in Chapter 1 has led to the current isomorphous nucleobase analogs the Tor Lab has published. Although the pursuit of increased functionality may have come to its peak with the described ¹²N core, improved photophysical properties of these small molecules could prove to be useful in continuing imaging endeavors in live mammalian cells. The evolution of the pyrimidine core could continue as shown in Figure 4.2 to the design of isoxazolepyrimidine derivatives.

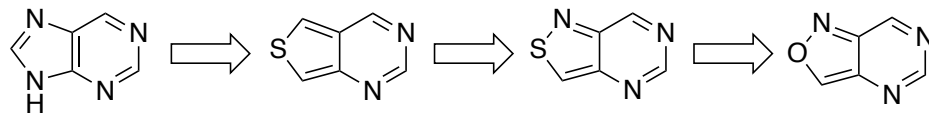


Figure 4.2 Theoretical further evolution of emissive nucleobase analogs

4.4 References

1. Shin, D.; Sinkeldam, R. W.; Tor, Y. Emissive RNA Alphabet. *J. Am. Chem. Soc.* **2011**, *133* (38), 14912–14915.
2. Rovira, A. R.; Fin, A.; Tor, Y. Chemical Mutagenesis of an Emissive RNA Alphabet. *J. Am. Chem. Soc.* **2015**, *137* (46), 14602–14605.
3. Bucardo, M. S.; Wu, Y.; Ludford, P. T.; Li, Y.; Fin, A.; Tor, Y. Real-Time Monitoring of human Guanine Deaminase Activity by an Emissive Guanine Analog. *ACS Chem. Biol.* **2021**, *16* (7), 1208–1214.
4. Yu, W.; Wu, T.; Huang, C.; Chen, I.; Tan, K. Protein sensing in living cells by molecular rotor-based fluorescence-switchable chemical probes. *Chem. Sci.* **2016**, *7*, 301–307.
5. Hotta, T.; Saito, Y.; Fujita, H.; Mikami, T.; Kurisu, K.; Kiya, K.; Uozumi, T.; Isowa, G.; Ishizaki, K.; Ikenaga, M. *J. of Neuro-Onco.* **1994**, *21*, 135–140.
6. Park, S.; Otomo, H.; Zheng, L.; Sugiyama, H. Highly emissive deoxyguanosine analogue capable of direct visualization of B-Z transition. *Chem. Comm.* **2014**, *50*, 1573–1575.
7. Barton, D. H. R.; McCombie, S. W. A new method for the deoxygenation of secondary alcohols. *J. Chem. Soc., Perkin Trans.* **1975**, *16*, 1574–1595.